

**Immuno-Isolation Strategies for Islet Transplantation
into Rodent and Non-Human Primate Models**

BY

MATTHEW A. BOCHENEK
B.S., University of Illinois at Urbana/Champaign, 2009

THESIS

Submitted as partial fulfillment of the requirements
for the degree of Doctor of Philosophy in Bioengineering
in the Graduate College of the
University of Illinois at Chicago, 2015

Chicago, Illinois

Doctoral Committee:

Jose Oberholzer, Chair and Advisor
David Eddington
Yong Wang
Richard Gemeinhart , Biopharmaceutical Sciences
Berit Strand, Norwegian University of Science and Technology

DEDICATION

This thesis is dedicated to my parents, family, and loved ones who provided encouragement and compassion as well as sustenance and much-needed distraction during this journey.

ACKNOWLEDGMENTS

First, I would like to acknowledge Dr. Oberholzer for his continued support and dedication to the field of Type I Diabetes. He has been inspirational and provided invaluable opportunities to work with talented researchers from around the world during my PhD. I would also like to thank Dr. Wang for always helping fine-tune my writing and ideas, our conversations and arguments about what is the best way to do things. You provided a great deal of mentoring, especially once Dr. Qi got a new position, and I am forever thankful. I would also like to thank Dr. Qi for the mentoring provided. Almost all the techniques dealing with islets I learned from you.

Thank you Berit for always answering my questions about encapsulation and providing feedback on directions I should take during Skype calls of my progress reports. These were very helpful and always enjoyable conversations. Thanks to Dr. Lacik as well for the expertise instilled in me with encapsulation and listening to my progress reports with the comfort of an ale. Your comedy always made talks fun while still coming up with great ideas and plans for the future. Also, thank you Anne Marie for the feedback given on manuscripts and the warm hospitality during our stay in Norway. I still remember the delicious fish!

Dr. Gemeinhart, I can't thank you enough for writing so many letters of recommendation for me. They may have been painful but it did pay off with awards, which you helped me achieve. Also, thank you for your tutelage in the beginning of grad school when I was young and naïve. You led me in great directions, showed me the essence of stellar grant proposals, and that polymers are strange and don't always behave as we'd think. I will always remember this. Thank you Dr. Eddington for letting me know it's acceptable to not know something, and the importance of *in vitro* analysis instead of just seeing if something works *in vivo*. I will try to continue this practice in my future career as a scientist.

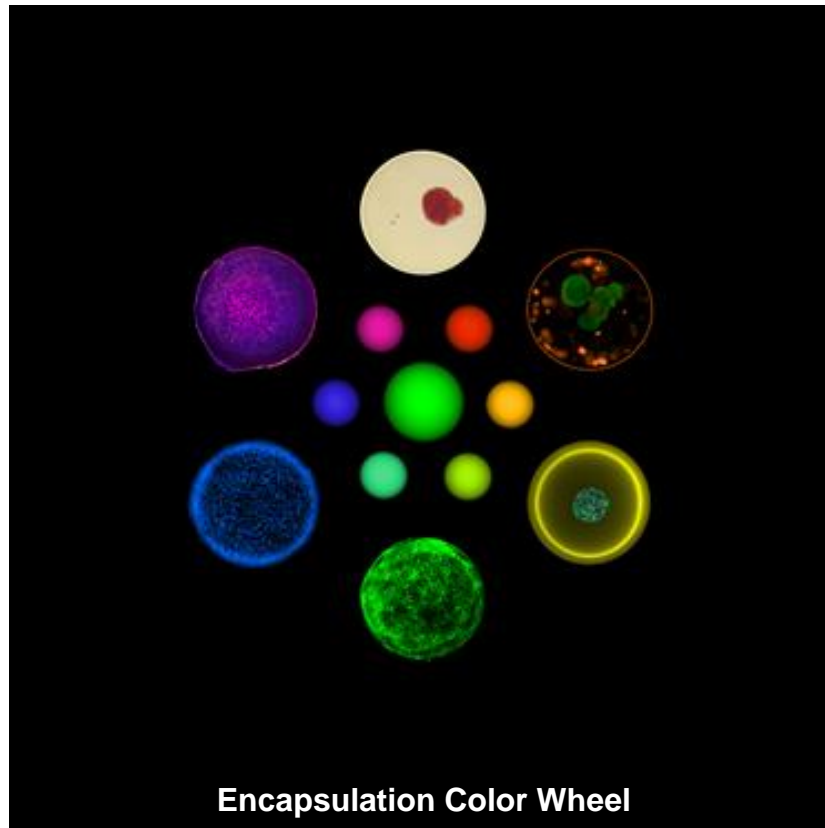
ACKNOWLEDGMENTS (continued)

I would also like to thank Dr. Anderson and his team members at MIT. Omid, Josh, Arturo, and Dan are incredible scientists, and I was very privileged to be able to work with such talented individuals. Their materials and findings have contributed greatly to the field of encapsulation and I am honored to be a part of these projects. Also, thanks to Nicolai Suter from Nisco Engineering in Switzerland for all the hard work put into the design of the encapsulator. This vision of a new encapsulation system would not have been possible without your expertise and suggestions.

Also, thanks to Enza for being my backbone and honorary mom in the lab. Also, learning the convoluted language of my brain when working with me was a great feat! You provided much scientific mentoring in this journey especially the importance of data organization. James thanks for being my right-hand man, tackling work together, and always being there if I needed assistance. Also, thank you to others in the lab that helped with experiments: Josh, Augusta, Mohammad, Mustafa, Diana, Maureen, Ben, Barabara, Kirstie, and Lingjia. This work would not have been possible without your help, and we are a great team.

I would also like to thank my family, friends and significant others for putting up with me during grad school. Thanks for understanding if I had to miss events because of an all-night human isolation or other experiments that kept me busy. You kept me sane, and I am indebted to you for your compassion, understanding, and motivation to complete this journey. I love you all.

PREFACE



R: Encapsulated human islet stained red with dithizone (DTZ). Islets are cell clusters of 1,000-2,000 cells that control blood glucose levels within the body. Islet transplantation can functionally cure Type I diabetes and islet encapsulation represents a strategy for transplantation without immunosuppression.

O: Encapsulated human islets stained with viability dyes to determine how many cells are alive or dead within the islets. This is important to show if islets are alive within the encapsulation material.

Y: Cross-section of an islet stained with fluorescent markers to for the five types of cells that make up islets. The islet is placed in an empty polymethylene co-guanidine (PMCG) capsule, which has unique material properties that interact with the viability dyes.

G: Adsorption of complement protein C3 to the surface of capsules (AnneMarie Rosktad). Encapsulated islets can reverse diabetes in mice; however, these results do not translate well in large animals or humans. In higher order species, the immune system identifies the material as foreign and surrounds it in cellular overgrowth. This results in decreased nutrition to the islets and their ultimate death. How the overgrowth is initiated is still unknown, yet some researchers hypothesize that it is due to protein adsorption on the capsule surface.

B: DAPI nuclear staining of the cells composing the overgrowth.

V: Histology staining of overgrowth covering a microbead. The completely colored capsule shows how this dense network of cells impedes nutrient diffusion and suffocates the islets to cause their death.

Center Tertiary: Chemically modified capsules. Prevention of pericapsular overgrowth must be solved before islet encapsulation can become implemented in the clinic. We are investigating if chemical modifications to current encapsulation materials can alter the microbead surface properties so the immune system cannot recognize the microbead and detrimental overgrowth is never formed.

CONTRIBUTION OF AUTHORS

Chapter 1 reviews the literature and highlights the research of my dissertation in the larger context of the field of islet transplantation and immune-isolation strategies for islet transplantation.

Chapter 3 represents a recently submitted unpublished manuscript for which I am the primary author and major contributor of the design and execution of experiments. Dr. Berit Strand and Dr. Gudmund Skjak-Brak are the inventors of the microcapsule system ($\text{Ca}^{2+}/\text{Ba}^{2+}$ - 1.8% wt/vol alginate) used in the study. Enza Marchese and Maureen Davis contributed to histology images (Figure 3.2:C, 3.3:D-F, 3.4:C, 3.5:A-D). Dr. Meirigeng Qi instructed during rodent islet isolation and intramuscular transplantations.

Chapter 4 represents a collaborative effort between researchers at MIT: Dr. Dan Anderson, Dr. Robert Langer, Dr. Arturo Vegas, Dr. Omid Veisheh, and Dr. Joshua Doloff, and team members working in the clinical islet transplantation program at UIC: Matthew Bochenek, Dr. Jose Oberholzer, Dr. James McGarrigle, Dr. Mustafa Omami, and Enza Marchese. Results section 4.1: insulin secretion kinetics of medium and large encapsulated islets was published in the manuscript (Veisheh, O., et al., *Size- and shape-dependent foreign body immune response to materials implanted in rodents and non-human primates*. Nature Materials, 2015. 14(6): p. 643-51.). The microfluidic perfusion data was obtained by Joshua Mendoza Elias. I performed the encapsulations, insulin ELISA, data organization, and statistical analysis. Results section 4.2: *in vitro* and *in vivo* functionality of large 1.5 mm Ba^{2+} alginate encapsulated cyno represents a series of my own experiments directed at investigating how the size of encapsulation material may affect cyno islet functionality. These experiments were performed in order to prepare for future experiments using a diabetic NHP allogeneic transplant model. Results section 4.3: protective capacity of chemically modified alginates using a NHP allogeneic transplant model was conducted in close collaboration with the members previously mentioned at MIT and UIC.

CONTRIBUTION OF AUTHORS (continued)

Dr Arturo Vegas is the principal inventor of the chemically modified alginate system under Dr. Dan Anderson and Dr. Robert Langer at MIT. This collaborative research project between UIC and MIT will continue and ultimately be published as part of a co-authored manuscript.

Chapter 5 discusses a novel encapsulator that was designed in collaboration with Nicolai Suter from Nisco Engineering in Switzerland and Igor Lacik in Slovakia. I will be the primary author of this manuscript once experimental characterization of the device has been completed. The encapsulator is intended to arrive November 5, 2015.

TABLE OF CONTENTS

1	PROBLEM STATEMENT	1
1.1	Immuno-isolation strategies for islet transplantation	1
2	MATERIALS AND METHODS	4
2.1	Animals (Rodents).....	4
2.1.1	Animal care	4
2.1.2	Rodent strains for diabetic studies.....	4
2.1.3	Rat islet isolation and culture	5
2.1.4	Diabetes induction via streptozotocin (STZ).....	5
2.1.5	Animal monitoring	6
2.2	Microencapsulation of islets.....	7
2.2.1	NTNU, Trondheim, Norway method: $\text{Ca}^{2+}/\text{Ba}^{2+}$ - alginate encapsulation (0.5 mm).....	7
2.2.2	UIC, Chicago, USA method: Ba^{2+} -alginate encapsulation (1.5 mm)	7
2.2.3	MIT, Boston, USA method: Ba^{2+} -chemically modified alginate encapsulation (1.5 mm)	8
2.3	<i>In vitro</i> islet assessments	9
2.3.1	Islet counting	9
2.3.2	Viability.....	10
2.3.3	Dithizone (DTZ) staining	11
2.3.4	Insulin ELISA.....	11
2.4	<i>In vivo</i> transplantation procedures and assessments.....	12
2.4.1	Naked islet kidney capsule transplantation (Mice)	12
2.4.2	Encapsulated islet intraperitoneal transplantation (Rodent).....	13
2.4.3	Oral glucose tolerance test (OGTT)	14
2.4.4	Retrieval of encapsulated islets (Rodent).....	14
2.4.5	Encapsulated islet intramuscular transplantation (Rat)	15
2.4.6	Laparoscopic encapsulated islet transplantation and retrieval of IP space (NHP)..	15

TABLE OF CONTENTS (continued)

3 SKELETAL MUSCLE TISSUE AS A POTENTIAL TRANSPLANTATION SITE FOR PANCREATIC ISLETS ENCAPSULATED IN Ca²⁺/Ba²⁺-ALGINATE MICROBEADS	18
3.1 Introduction	18
3.2 Methods	20
3.2.1 Study design	20
3.2.2 Intramuscular retrieval of alginate microbeads	20
3.2.3 Fibrotic overgrowth of retrieved microbeads	20
3.2.4 Histological analysis of retrieved freely floating microbeads	21
3.2.5 Histology of microbead grafts embedded in whole leg muscle	21
3.2.6 Statistical analysis	22
3.3 Results:	23
3.3.1 Encapsulation and intramuscular transplantation	23
3.3.2 Empty microbeads in the intramuscular space after 8 weeks	24
3.3.3 Encapsulated isogeneic islets in the intramuscular space after 8 weeks	25
3.3.4 Encapsulated allogeneic islets in the intramuscular space after 8 weeks	27
3.3.5 Fibrotic tissue overgrowth of retrieved microbeads	29
3.3.6 Immune cells involved in rejection of allogeneic encapsulated islets	29
3.4 Discussion:	30
3.5 Conclusion:	34
4 ANTI-FIBROTIC STRATEGIES FOR IMMUNE-ISOLATION DEVICES: LARGE SIZED 1.5 mm ENCAPSULATED ISLETS FOR THE TREATMENT OF DIABETES	35
4.1 Introduction:	35
4.2 Methods:	36
4.2.1 Real-time fluorescence imaging of islet intracellular calcium	36
4.2.2 Intracellular calcium [Ca ²⁺] _i stimulation kinetics	37
4.2.3 Insulin secretion kinetics	37
4.2.4 Glucose static insulin secretion (GSIS) assay	38

TABLE OF CONTENTS (continued)

4.3 Results and discussion:.....	39
4.3.1 Insulin secretion kinetics of naked and encapsulated rat islets within medium 0.5 mm and large 1.5 mm Ba ²⁺ alginate capsules.....	39
4.3.2 In vitro and in vivo characterization of cynomolgus monkey islet functionality within large 1.5 mm Ba ²⁺ alginate capsules using diabetic rodent models	46
4.3.3 In vitro and in vivo characterization of cynomolgus monkey islet functionality within large 1.5 mm Ba ²⁺ chemically modified alginates using an allogeneic NHP transplantation model.....	73
4.4 Conclusion: Large 1.5 mm encapsulated islets	96
5 A NOVEL ENCAPSULATOR FOR THE CONTINUOUS PRODUCTION OF CAPSULES WITH CONTROLLED SIZE AND GELATION TIME.....	98
5.1 Introduction	98
5.1.1 Physics behind encapsulation droplet formation.....	99
5.1.2 Apparatuses available for islet encapsulation and current limitations	105
5.1.3 Key technologies to implement into a clinically relevant islet encapsulator	112
5.1.4 Design criteria for novel encapsulator.....	113
5.2 Apparatus Design: Electrostatic with integrated Loop Reactor (ELR) Encapsulator for continuous production of spherical polymer hydrogels with controlled gelation time	114
5.3 Conclusion:.....	125
6 CITED LITERATURE	126
7 APPENDIX.....	138
8 VITA	139

LIST OF TABLES

Table I: Microbead characteristics pre-transplant and post 8 week retrieval	25
Table II: Percentage of microbeads with surface area covered by tissue overgrowth.....	29
Table III: DTZ staining of encapsulated cyno islets prior to allogeneic transplantation.....	75
Table IV: Brightfield and DTZ staining of retrieved encapsulated cyno islets following 4 weeks of allogeneic transplantation (Low islet seeding density).....	77
Table V: DTZ staining of encapsulated cyno islets prior to allogeneic transplantation.....	86
Table VI: Brightfield and DTZ staining of retrieved encapsulated cyno islets following 4 weeks of allogeneic transplantation (High islet seeding density).	90
Table VII: Polymer characteristics that affect size of droplet formation during encapsulation	101
Table VIII: Encapsulator characteristics that affect size of droplet formation during encapsulation	104

LIST OF FIGURES

Figure 3-1: DTZ and viability staining of rat islets pre- and post-encapsulation	24
Figure 3-2: 8 week retrieval of empty microbeads transplanted intramuscularly.	25
Figure 3-3: 8 week retrieval of encapsulated isogeneic islets transplanted intramuscularly.	27
Figure 3-4: 8 week retrieval of encapsulated allogeneic islets transplanted intramuscularly (n = 6).....	28
Figure 3-5: H&E/IHC staining for specific immune cell type and localization within allo-clump.....	30
Figure 4-1: Intracellular calcium responses of naked and encapsulated rat islets in response to insulin secretagogues.	41
Figure 4-2: Insulin secretion of naked and encapsulated rat islets in response to insulin secretagogues.	43
Figure 4-3: Size-dependent insulin secretion kinetics per 10 minutes	45
Figure 4-4: Dithizone (DTZ) staining of cynomolgus islets post-isolation, post 1 day culture/pre-encapsulation, and post-encapsulation within 1.5 mm Ba ²⁺ alginate beads.	48
Figure 4-5: Viability of cynomolgus islets 1 day post isolation/pre-encapsulation and 1 day culture post-encapsulation/pre-transplantation into STZ induced diabetic nude mice.	49
Figure 4-6: <i>In vivo</i> functionality of 1.5 mm alginate encapsulated cyno islets transplanted IP compared to naked cyno islets transplanted into the kidney capsule of immune-compromised STZ diabetic nude mice.....	51
Figure 4-7: <i>In vivo</i> functionality of 1.5 mm encapsulated cynomolgus islets in immune-competent STZ induced diabetic C57b/6 mice.....	53
Figure 4-8: Glucose Stimulated Insulin Secretion (GSIS) under low glucose (2 mM) and high glucose (18 mM) of naked and 1.5 mm Ba ²⁺ encapsulated cynomolgus islets over time.	56
Figure 4-9: <i>In vivo</i> functionality of short-term cultured 1.5 mm encapsulated cynomolgus islets in immune-compromised STZ diabetic nude mice.	61
Figure 4-10: Dithizone (DTZ) staining of 1.5 mm Ba ²⁺ encapsulated cynomolgus islets retrieved from STZ diabetic nude mice 30 days post-transplantation.	63
Figure 4-11: Viability of 1.5 mm Ba ²⁺ alginate encapsulated cynomolgus islets retrieved from STZ diabetic nude mice 30 days post transplantation.....	64
Figure 4-12: GSIS of 1.5 mm Ba ²⁺ alginate encapsulated cynomolgus islets that were retrieved from cured STZ diabetic nude mice	65
Figure 4-13: GSIS of encapsulated cyno islets performed immediately post retrieval from STZ nude mice and after over-night culture (1.5 mm Ba ²⁺ alginate encapsulated cyno islets).	66

LIST OF FIGURES (continued)

Figure 4-14: Representative intracellular calcium influx [ΔCa^{2+}] _i , and mitochondrial potential changes ($\Delta\Psi_m$) in response to insulin secretagogues of single encapsulated cyno islets performed immediately post-retrieval from mice and after 5 hour culture. (0.5 mm $\text{Ca}^{2+}/\text{Ba}^{2+}$ alginate encapsulated cyno islets)	67
Figure 4-15: Intracellular calcium [Ca^{2+}] _i , mitochondrial potential (Ψ_m), and insulin secretion profiles of naked (pre-transplantation) and retrieved encapsulated cyno islets (STZ nude mice) in response to insulin secretagogues using a microfluidic-based perfusion assay.....	68
Figure 4-16: Intracellular calcium levels of 1.5 mm Ba^{2+} alginate encapsulated islets performed pre-transplantation (n = 2 runs; 50 encapsulated islets per run).....	70
Figure 4-17: Viability and glucose stimulated insulin secretion (GSIS) of encapsulated cyno islets prior to allo-transplantation into non-diabetic recipients (Low islet seeding density).	76
Figure 4-18: DTZ staining of RZA15-chemically modified alginate encapsulated cyno islets retrieved 4 months post-transplantation in non-diabetic cynomolgus recipient (n = 1).....	80
Figure 4-19: Peripheral degeneration of cells for encapsulated cyno islets after 30 day retrieval from nude mice (RZA15 and SLG20) and long-term cultured encapsulated islets (SLG20).	81
Figure 4-20: Viability and glucose stimulated insulin secretion (GSIS) of encapsulated cyno islets post 4 week retrieval from cynomolgus monkey recipients (Low islet seeding density).....	82
Figure 4-21: Average GSIS of retrieved encapsulated cyno islets from STZ nude mice (SLG20) and Cyno NHP (RZA15)	84
Figure 4-22: Viability and glucose stimulated insulin secretion (GSIS) of encapsulated cyno islets prior to allo-transplantation into non-diabetic recipients (High islet seeding density).	87
Figure 4-23: GSIS of encapsulated cyno islets at the high seeding density using 4 purification protocols	89
Figure 4-24: Viability and glucose stimulated insulin secretion (GSIS) of encapsulated cyno islets post 4 week retrieval from cynomolgus monkey recipients (High islet seeding density).....	91
Figure 4-25: Encapsulated human islets within chemically modified RZA15 alginate 1.5 mm Ba^{2+} at low, medium, and high islet seeding densities.....	95
Figure 5-1: Competitive forces regulating droplet size during encapsulation and spherical hydrogel formation.....	100
Figure 5-2: Types of encapsulation apparatuses currently available and the downward forces employed to control droplet sizes	103
Figure 5-3: Buchi Encapsulator B395 Pro™ testing with PMCG polymer system.	107
Figure 5-4: Current encapsulation apparatuses available for islet transplantation	109

LIST OF FIGURES (continued)

Figure 5-5: Loop reactor for continuous production of hydrogel spheres with controlled gelation time.	110
Figure 5-6: Size of $\text{Ca}^{2+}/\text{Ba}^{2+}$ alginate microbeads in response to voltage variation.....	112
Figure 5-7: General diagram of ELR encapsulation	116
Figure 5-8: 3D rendering of the ELR Encapsulator with integrated Loop Reactor.....	117
Figure 5-9: Top and side view of Ring Electrode Accelerator	118
Figure 5-10: Diagram of the internal housing unit of the ELR Encapsulator.....	121
Figure 5-11: Encapsulation Circuit for Continuous Production of Spherical Hydrogels	123

LIST OF ABBREVIATIONS

ANOVA	Analysis of variance
ATP	Adenosine Triphosphate
BALB/C	Bagg Albino C inbred mouse strain
BID	Bi-daily
BSA	Bovine serum albumin
C57b/6	C57 black 6J inbred mouse strain
CIPRO	Ciprofloxacin
CIT	Consortium for Islet Transplantation
CMRL	Connaught Medical Research Laboratories
CS	Cellulose sulfate
DI	De-ionized
DMSO	Dimethyl sulfoxide
DNA	Deoxyribonucleic acid
DTZ	Dithizone
ECM	Extracellular matrix
EDTA	Ethylenediaminetetraacetic acid
ELISA	Enzyme-linked immunosorbent assay
EtOH	Ethyl alcohol
FBS	Fetal bovine serum
FDA	Fluorescein diacetate
G	Guluronic acid
GLUT2	Glucose transporter 2
GSIS	Glucose-stimulated insulin secretion
HBSS	Hank's buffered salt solution

LIST OF ABBREVIATIONS (continued)

HEPES	4-(2-hydroxyethyl)-1-piperazineethanesulfonic acid
HMGB1	High mobility group box 1
IEQ	Islet equivalence
IL	Interleukin
IM	Intramuscular
INF- γ	Interferon gamma
IP	Intraperitoneal
ITS	Insulin-transferrin-selenium
K _{ATP}	ATP-sensitive potassium ion channel
KCl	Potassium chloride
M	Manuronic acid
MCP-1	Monocyte chemoattractant protein-1
MIT	Massachusetts Institute of Technology
mmHg	Millimeter of mercury
MOPS	3-(<i>N</i> -morpholino)propanesulfonic acid
PEEK	Polyether ether ketone
PI	Propidium iodide
PFO	Peri-capsular fibrotic overgrowth
PLL	Poly-L-lysine
PLO	Poly-L-ornithine
PMCG	Polymethylethe co-guanadine
PS	Penicillin/streptomycin
RPMI	Roswell Park Memorial Institute media
SC	Sub-cutaneous

LIST OF ABBREVIATIONS (continued)

STZ	Streptozotocin
TBS	Tris-buffered saline
T1DM	Type one diabetes mellitus
TNF- α	Tumor necrosis factor alpha
UPLVG	Ultra-pure-low-viscosity-high-guluronic
VDCC	Voltage-dependent calcium channel

SUMMARY

Human pancreatic islet transplantation into the liver of patients with Type 1 Diabetes Mellitus (T1DM) can restore physiological glycemic control. However, this therapy requires immunosuppression with potential health risks. To universally apply this therapy, immuno-isolation technologies are needed to protect transplanted islets from rejection without immunosuppression.

Achieving proper oxygenation of immune-isolated islets after transplantation is one of the leading obstacles to future clinical application of these technologies. Investigators are researching diverse strategies to achieve proper oxygenation and function of immune-isolated islets. Many strategies have attempted to modulate the transplanted islets to be less immunogenic (immune modulation), less susceptible to debilitating effects of hypoxia on islet functionality, or insulintropic agents to augment insulin secretion. Immune modulation strategies of immune-isolated islets has included material-based research [1, 2], co-encapsulation of islets with immune-modulatory cell types such as MSCs or Sertoli cells [3, 4], and co-encapsulation with immune modulatory molecules [5]. To combat islet hypoxia post-transplantation, others have investigated methods to increase oxygenation using spontaneous oxygen generation or external oxygen provisions to name a few [6-8]. To increase immune-isolated islet function, researchers have investigated methods to co-encapsulate islets with insulintropic molecules such as GLP-1 [9], or cells that actively secrete insulintropic molecules such as IGF-II secreting cells [10].

The focus of this thesis was to explore strategies to achieve better oxygenation and functionality of immune-isolated islets by investigating an alternative site of transplantation for immune-isolated islets. Also, material and size based strategies were investigated as a strategy to provide immune modulation of immune-isolated islets via fibrosis resistive strategies. Fibrosis of immune-isolation materials can

SUMMARY (continued)

restrict oxygenation to the islets within the material and leads to islet graft failure [11-13]. Lastly, a novel encapsulator was designed to produce GMP grade, large batches of immune-isolated islets for potential clinical transplantation in the future.

First, the potential of skeletal muscle tissue was investigated as an alternative transplantation site of immune-isolated islets. The peritoneal cavity is the most commonly investigated transplantation site for microencapsulated islets due to the large volume of the space available for the graft. However, this site is associated with low oxygen tensions that may not be ideal for islet function. Skeletal muscle tissue was investigated due to the high oxygen tensions of the site that may better support viable and functional islets. In the study, rat muscles were transplanted with empty alginate microcapsules and microcapsules containing isogeneic or allogeneic islets. The grafts were retrieved after 8 weeks and evaluated for material biocompatibility and long-term islet functionality within the skeletal muscle. Results indicate that muscle tissue can tolerate the alginate material as well as support viable isogeneic islets for 8 weeks. Allogeneic islets were found to be fibrosed and rejected after 8 weeks. This suggests that skeletal muscle may represent a transplantation site for immune-isolated islets if a material can prevent allo-rejection.

The next set of experiments conducted at UIC expanded on discoveries made by our collaborators working in Dr. Anderson and Dr. Langer's lab at MIT. Here it was determined that fibrosis of materials is largely dependent on their size and shape, and that large sized alginate capsules 1.5 mm in diameter are more resistive to fibrosis compared to conventional medium sized alginate capsules 0.5 mm in diameter (Veisheh, et al; Nature Materials. 2015). Furthermore, MIT developed a series of chemically modified alginates that are resistive to fibrosis, especially when manufactured at the large 1.5 mm size. These discoveries fit within our research investigations and our team hypothesis that long-term,

SUMMARY (continued)

immune-isolated islet function can only be achieved by a material surface that is permanently free of fibrosis to ensure free oxygen, nutrition and insulin diffusion.

In the established collaboration with MIT, we further investigated how the size/volume of the immune-isolation material affects islet functionality using both *in vitro* and *in vivo* methods. We also investigated the capacity of the chemically modified alginates to protect islet function after transplantation into a NHP allogeneic transplant model.

Initial experiments investigated insulin secretion kinetics of large sized (1.5 mm) encapsulated rat islets in comparison to naked and medium sized (0.5 mm) encapsulated islets. It was determined that islet stimulation kinetics by small molecular weight secretagogues is unaffected by encapsulation or capsule size. For insulin release kinetics, both groups of encapsulated islets experience a loss of phase I insulin secretion and an initial delay in glucose-stimulated insulin secretory kinetics. This delay was not found to be dependent on the capsule size, and overall bulk insulin kinetics for both capsule sizes are well conserved and similar to naked rat islets.

Next, large encapsulated islet function was evaluated using *in vivo* diabetic mice models and a pre-clinical cynomolgus NHP islet source. Cyno islets were encapsulated within 1.5 mm Ba²⁺ alginate and transplanted as a marginal islet mass into STZ induced diabetic nude mice. Encapsulated cyno islets were able to cure STZ nude mice similarly to the same number of naked islets transplanted into the kidney capsule (77% vs. 75%, respectively). Oral glucose tolerance tests performed 30 days post transplantation showed that the large encapsulated islets cleared glucose at similar rates compared to the naked islets transplanted in the kidney capsule. Furthermore, immune-competent STZ diabetic C57b/6 mice were transplanted with same marginal islet mass of large encapsulated cyno islets. Cohorts of mice

SUMMARY (continued)

demonstrated consistent blood glucose levels and increasing weights for up to 180 days (50% cured at day 180).

Encapsulated islets at the large size were also characterized using *in vitro* assays such as dithizone (DTZ) staining, viability, and glucose stimulated insulin secretion (GSIS). The GSIS was performed on day 1, 14 and 28 during culture. Predictably the naked cyno islets tended to decrease insulin secretion in response to high glucose challenges when cultured over time. On the other hand, large encapsulated islets tended to increase insulin secretion in response to high glucose challenges when cultured over time. This decline for naked islets is expected as long-term culture of primary islets typically has an overall negative affect on naked islets. However, an increase in insulin secretion for encapsulated islets was unexpected.

Since encapsulated cyno islets demonstrated increased glucose stimulated insulin secretion after short-term culture in the GSIS assay, we wanted to see if this improvement in functionality would also translate *in vivo*. Encapsulated cyno islets were transplanted into STZ diabetic nude mice on Day 1 and Day 14 post-encapsulation. Short-term culture had no significant effect in the functional ability of encapsulated islets to cure STZ induced diabetic nude mice (88% vs. 86%) or clear glucose in glucose tolerance tests. This suggests that encapsulated islets can be cultured for some days prior to transplantation without negatively affecting functionality. It may also be possible to modulate encapsulated islets' function by chemically altering gene expression prior to transplantation. Also, the additional time will permit proper quality control measures to be conducted as well as a complete analysis of the multiple islet potency assessments performed pre-transplantation. These results can then be used to determine if a particular batch of encapsulated islets is suitable for transplantation.

SUMMARY (continued)

After 30 days post-transplantation into STZ diabetic nude mice, the encapsulated islets were retrieved and evaluated for intracellular calcium influx $[\Delta\text{Ca}^{2+}]_i$, mitochondrial potential changes ($\Delta\Psi_m$), and insulin secretion in response to insulin secretagogues using a microfluidic based perfusion assay. It was found that retrieved encapsulated islets lose Fura-2 signaling (indicator of Ca^{2+} influx) but still maintained positive insulin secretion. Mechanistically, insulin secretion should not occur without an increase in cytosolic Ca^{2+} levels, which causes the fusion of insulin granules with the cell membrane [14]. Combining past results and the literature, there seems to be an effect of barium on cyno islets which affects our ability to measure Fura-2 and $[\text{Ca}^{2+}]_i$ changes. It is still unclear how this change occurs. The importance of these results is also difficult to judge since the due to positive function seen in the various mouse models. A more prudent investigation may determine if there is any barium leakage from the capsules after *in vivo* transplantation. This should be investigated to determine if there is any potential for toxicity associated with the transplantation of barium encapsulated islets prior to human transplantation.

Next, a series of chemically modified alginates developed at MIT were tested for their protective capacity using a NHP allogeneic transplant model. NHP islets were isolated from cynomolgus monkeys and encapsulated in each of the modified materials. They were then transplanted into the lesser sac of non-diabetic allogeneic recipients. The encapsulated islets were then retrieved after 4 weeks and analyzed for viability and functionality. It was determined RZA15 chemically modified alginate at the large 1.5 mm size can protect functioning allogeneic islets ($n = 2$). The large majority of capsules remain free of fibrosis and cellular attachment in this NHP model. The encapsulated islets were found to be viable, DTZ positive, and glucose responsive after one month post-transplantation in a non-immunosuppressed allogeneic NHP transplant model.

SUMMARY (continued)

Experimentation with the number of islets per capsule was then explored as many islets may be required in order to completely reverse diabetes. The limited volume of capsules that can be transplanted into the primates may require more islets to be encapsulated per capsule. Initial experiments have shown that RZA15 did not protect functioning islets at a high density. However, this may be related to transplantations of islets with poor viability and GSIS performed pre-transplantation. Also, the capsules showed the presence of a larger degree of cellular debris throughout the capsules that may have activated the immune system post-transplantation.

In the future, strategies need to be employed to reduce the presence of this cellular debris before the RZA15 chemically modified material can be adequately tested for its protective properties at the higher islet seeding densities. Also, future steps should be taken to assure that batches of encapsulated islets are of high quality prior to transplantation into primates. This may be accomplished by culturing the encapsulated islets for a few days while all the data for the functional assessments can be analyzed.

Lastly, a novel encapsulator was designed with a particular focus on islets. This encapsulator can continuously manufacture uniform, spherical polymer hydrogels with controlled size and gelation time. Three key technologies from previous encapsulation systems were integrated into a single device. This includes an electrostatic system for droplet formation with a loop reactor gelation system for continuous production with controlled gelation time. A ring shaped electrode governs formation of droplets, which then pass through the opening and into the loop reactor. This allows both technologies to be combined.

Also, the device was designed to be user friendly, and once the ideal parameters for encapsulation are established, there is little operator dependency on the final product. This is especially important when submitting to regulatory agencies like the FDA, where a defined cellular/material product must be

SUMMARY (continued)

thoroughly validated for safety, potency, and reproducibility prior to coming onto the market. The unit also satisfies strict sterility standards as well as quality control measures during islet encapsulation. In the future, this encapsulator may be suited to produce GMP grade, large batches of encapsulated cells for clinical transplantation.

1 PROBLEM STATEMENT

1.1 Immuno-isolation strategies for islet transplantation

Pancreatic islet transplantation (PIT) is a promising therapy to restore glycemic control in patients with Type 1 Diabetes Mellitus (T1DM) [15]. Nonetheless, PIT has limitations that need to be rectified before this therapy can be universally applied to treat all patients with T1DM. To inhibit immune rejection of the transplanted islet graft, patients must be continually treated with immunosuppressive drugs. These drugs have associated negative side-effects such as islet toxicity and increased patient susceptibility to infections and oncogenesis [16]. For this reason, PIT together with long-term immune suppression is only reserved for patients with brittle T1DM and severe hypoglycemic unawareness [17]. Another potential limitation of this therapy is a limited supply of suitable pancreata available for transplantation. This is significantly less than the number of patients with T1DM [18]. As islet cells exhibit miniscule *in vitro* proliferation, alternative cell sources such as embryonic stem cell derived β - cells or xenogeneic islet sources are currently being investigated to treat the growing number of patients with T1DM [19-21].

The overarching goal of this thesis was to investigate immune-isolation strategies for islet transplantation in order to mitigate the need for immunosuppressive drugs in the future.

One potential solution to the requirement for immunosuppressive therapy during PIT is to immune-isolate the islets within semi-permeable hydrogels. The hydrogel can impede direct contact of the islets with host immune system which can inhibit graft rejection. The hydrogel still allows the diffusion of essential nutrients for proper islet function and diabetes/glucose control [2, 22, 23]. In practice, this strategy has exhibited certain deficiencies. We have observed that the immune system can react to the

isolation biomaterial. This results in the formation of pericapsular fibrotic tissue overgrowth (PFO), which restricts nutrient diffusion and leads to islet death [12, 13]. Improvements in biocompatibility of isolation materials needs to be investigated before immune-isolation strategies can be reproducibly implemented in the clinic. Various strategies for immune-isolated islets have been employed such as immune modulation strategies via design of novel materials [1, 2], co-encapsulation of islets with immune-modulatory cell types such as MSCs or Sertoli cells [3, 4], and co-encapsulation with immune modulatory molecules [5]. Despite improvements in immune-isolated islet functionality, these strategies have not led to efficacious results in large animal models such as humans or NHP.

In addition, other obstacles regarding microencapsulation still persist. Islets are highly metabolically active and consume vast amounts of oxygen [24, 25]. When separated from other tissues in the body, islets must rely on diffusion of oxygen and nutrients without re-vascularization. This reduced diffusion of oxygen provisions for immune-isolated islets has been associated with inhibited insulin secretion and higher production of pro-inflammatory cytokines [26]. In the future, nutrition of immune-isolated islets needs to be improved in order to achieve long-term functionality of transplanted encapsulated islets. To combat islet hypoxia post-transplantation, researchers have investigated methods including spontaneous oxygen generation or external oxygen provisions to name a few [6-8]. Others have also investigated alternative sites of transplantation that may exhibit preferable qualities for improved function of immune-isolated islets [27-31].

Despite the noted short-comings of immune-isolated islet technologies, transplantation of immune-isolated islets into rodents has demonstrated long-term reversal of diabetes [32-34]. These technologies have shown great promise in mouse models, but these results have not translated well in large animal studies and small scale human clinical trials [35-38]. It has been observed that NHP and humans produce more potent foreign body reactions to transplanted biomaterials. Material properties that may

lead to a foreign body reaction have been suggested for immune-isolation materials, yet the exact mechanism of material identification is still poorly understood [39].

The focus of this thesis was to explore strategies to achieve better oxygenation and functionality of immune-isolated islets by investigating skeletal muscle tissue as an alternative transplantation site for immune-isolated islets. Also, material and size based strategies were investigated in order to provide immune modulation of immune-isolated islets via fibrosis resistive strategies. Lastly, a novel encapsulator was designed to produce GMP grade, large batches of immune-isolated islets for potential clinical transplantation in the future.

2 MATERIALS AND METHODS

2.1 Animals (Rodents)

2.1.1 *Animal care*

All transplant procedures were performed under the guidelines of the National Institutes of Health and approved by the Animal Care Committee at UIC.

2.1.2 *Rodent strains for diabetic studies*

There are many strains of rodents that can be used for diabetes investigations. These can be separated into strains of mice appropriate for biocompatibility testing of materials and strains of mice appropriate to analyze islet graft function in induced diabetic models.

The C57b/6 mouse is an inbred, immune-competent mouse that is commonly used for biocompatibility testing of implantable sterile devices due to its rather potent foreign body reaction to sterile implantable materials [40]. For this reason, this strain of mouse represents a good model to test the biocompatibility of encapsulation materials. Biocompatibility is defined by the propensity of the host immune system to react to the material, and in the case of encapsulation, form a constricting network around the capsule.

The nude mouse is an inbred, immune-incompetent mouse that is genetically altered so it does not have a mature thymus gland. The thymus gland is an important location for the maturation of functional T-lymphocytes, and without this gland, the nude mouse has a compromised immune system [41]. This makes this mouse an important strain for testing the functional capacity of islets to control diabetes through the secretion of insulin. This mouse model can be thought of as a surrogate syngeneic transplant

model when testing islets across various species of animals such as humans or NHP since the mouse's immune system do not reject islets in our experience.

2.1.3 *Rat islet isolation and culture*

Rat islet isolations were conducted using a method previously described [42]. After a laparotomy incision, the pancreas was identified and the sphincter of oddi was clamped. At this step, the animal was euthanized by exsanguination, and immediately, the enzymatic solution type XI collagenase (Sigma) (2.2 mg/mL HBSS, 15 mL) was injected via the common bile duct into the main pancreatic duct for distention of the pancreas. The pancreas was carefully excised and placed in a 50 mL conical tube with 5 mL of its respective perfusion solution. The pancreatic tissue was digested statically in a 37°C water bath for 15 min. After this step, 10 mL of cold HBSS was added, and each pancreas was mechanically shaken until sampling verified the presence of free islets with dithizone (DTZ) staining. Islets were then purified from the exocrine tissue by discontinuous gradient centrifugation (Ficoll density gradients (1.108 g/mL, 1.096 g/mL, 1.069 g/mL, 1.037 g/mL) for 15 min at 640g. Since the islets are less dense than exocrine tissue which forms a pellet in the tube, the islets could be handpicked from the middle layer of the density gradient. The islets were then washed and cultured in RPMI 1640 with glutamine containing 10% FBS, 1% PS, for 24 hours culture at 37°C.

2.1.4 *Diabetes induction via streptozotocin (STZ)*

This method utilized for T1DM studies is to take a wild type mouse of a specific strain and chemically induce diabetes within the mouse. This is accomplished via the intraperitoneal injection of streptozotocin (STZ). STZ is a glucose analog that is taken in by the GLUT-2 transporter of β -cells. It is not recognized by other glucose transporters, which makes it highly sensitive to β -cells. Once inside the β -cell, the STZ alkylates DNA to cause DNA damage and also releases superoxide radicals that cause oxidative stress and necrosis of the β -cells [43]. After a couple of days, the mouse will have a limited

amount of functional β -cells and will become hyperglycemic. Although STZ is significantly β -cell specific, there are associated drawbacks such as nephrotoxicity and liver damage [41].

To perform STZ induction of diabetes in mice, STZ is measured to the appropriate dry weight to perform injections for 5 mice or rats and placed in a 15 mL conical tube (175-220 mg/kg in mice and 80 mg/kg in rats). Different doses are used for different mice strains. The tube is wrapped in foil since STZ is light sensitive and also placed on ice to minimize deactivation of the compound. A separate 15 mL conical tube is filled with 5 mL of sterile citrate buffer (20% wt/vol sodium citrate dissolved in saline) and also placed on ice. Mice or rats are labeled with tail markings using a permanent marker, weighed, and the amount of solution to be injected into each animal is determined. The citrate buffer is then added to dissolve the STZ (3-4 min) and immediately a single IP injection is infused into the animal using an insulin syringe. Diabetes usually occurs 48-72 hours after STZ injection. Blood glucose and weight are evaluated daily with observation of the animals. Two successive daily blood glucose measurements of > 350 mg/dL are considered as diabetic, and then can be used for transplant studies. If the animal is not rendered diabetic after 4 days, the animal should be euthanized since the failure rate is ~10%. Furthermore, if the animal is not used for diabetic transplant studies within 3-4 days, the animal should be euthanized to minimize pain and distress to the animal that occurs from diabetic and STZ complications. STZ treated mice used as controls for transplant experiments are injected with 0.8 U long-acting Glargine insulin BID, to control diabetes in the animals.

2.1.5 Animal monitoring

Post transplantation, animals are monitored according to approved procedures by the veterinary staff. For diabetic studies, the animals are measured for their blood glucose levels (BGL) via tail prick and weight for the first 5 consecutive days post transplantation. The animals are then monitored every 2 or 3 days.

2.2 Microencapsulation of islets

2.2.1 *NTNU, Trondheim, Norway method: Ca^{2+}/Ba^{2+} -alginate encapsulation (0.5 mm)*

The islets were washed three times with HBSS without magnesium or calcium by centrifugation (200g for 1 min at room temperature). This removes any divalent cations that could solidify the gel and clog the nozzle. After the final wash, the islet pellet is resuspended in a small volume of the HBSS and loaded into a 5 mL syringe filled with 2.0% (w/v) sterile-filtered ultra-pure low viscosity high guluronic (UPLVG) alginate (NovaMatrix, Sandvika, Norway) (63 – 67% G, MW 200 – 240 kDa, endotoxin < 100 EU/g) with 0.3 M mannitol (pH 7.2 - 7.4). The alginate-islet suspension (1,000 islets per 0.1 mL 1.8% w/v alginate) is mixed thoroughly in the syringe and dripped into the divalent cation gelling solution using an in-house electrostatic microbead generator (7 kV, flow: 10 mL/hr per 0.35 mm needle) to form microbeads. The gelling solution consists of 1 mM $BaCl_2$ and 50 mM $CaCl_2$ (in 10 mM MOPS, 0.14 M mannitol; pH 7.2-7.4). The microbeads are dripped over a maximum period of 15 minutes and always left in the gelling bath for an additional 5 minutes to ensure that the gelling reached saturation. Microbeads are then washed three times with HBSS (25 mL) containing calcium and magnesium over a period of 5 min and cultured overnight. Encapsulated rat islets were cultured in RPMI 1640 with glutamine containing 10% FBS, 1% PS, for 24 hours culture at 37°C. This type of alginate capsule was used for intramuscular transplantation studies (Chapter 3).

2.2.2 *UIC, Chicago, USA method: Ba^{2+} -alginate encapsulation (1.5 mm)*

The islets were collected into a 50 mL conical tube and pelleted by centrifugation (200g for 1 min at room temperature). The islet pellet was then transferred to a low-retention epindorf tube. The islets were then washed three times with 1.5 mL of HBSS without calcium or magnesium and allowed to settle via gravity sedimentation over 10 minutes per wash. This procedure was used to minimize potential islet stress caused by multiple centrifugations of the islets. After the final wash, the islet pellet was

resuspended in a small volume of the HBSS and loaded into a 5 mL syringe filled with 1.6% (w/v) sterile-filtered ultra-pure low viscosity high guluronic (UPLVG) alginate (NovaMatrix, Sandvika, Norway) (63 – 67% G, MW 200 – 240 kDa, endotoxin < 100 EU/g) with 0.3 M mannitol (pH 7.2 - 7.4). The alginate-islet suspension (1,500 islets per 1 mL 1.4% w/v alginate) was mixed thoroughly in the syringe and dripped into the divalent cation gelling solution using an in-house electrostatic microbead generator (1.5 mm = 3.25 kV, flow: 20 mL/hr per 0.35 mm needle)(0.5 mm = 6.65 kV, flow: 10 mL/hr per 0.35 mm needle) to form hydrogels. The gelling solution consists of 20 mM BaCl₂, 25 mM HEPES, 0.14 M mannitol; pH 7.2-7.4. The hydrogels were dripped over a period of 15 minutes and left in the gelling bath for an additional 5 minutes. Hydrogels were then washed three times (25 mL) with HBSS containing calcium and magnesium over a period of 5 min. Encapsulated rat islets were cultured in RPMI 1640 with glutamine containing 10% FBS, 0.2% PS, for 24 hours culture at 37°C. Encapsulated cynomolgus islets were cultured in CIT supplemented CMRL1066 (Mediatech) containing 10% FBS, 2% Cipro, and 0.1% ITS for 24 hours culture at 37°C. Encapsulated human islets were cultured in CIT supplemented CMRL1066 (Mediatech) containing 2% human albumin and 0.2% Cipro for 24 hours culture at 37°C. This type of alginate capsule was used for *in vitro* and *in vivo* encapsulated islet studies for large encapsulated islets (Chapter 4.1 and 4.2).

2.2.3 MIT, Boston, USA method: Ba²⁺-chemically modified alginate encapsulation (1.5 mm)

The islets were collected into a 50 mL conical tube and washed twice with HBSS without magnesium or calcium by centrifugation (200g for 1 min at room temperature). After the final wash, all the supernatant was removed from the islet pellet. Sterile cotton swabs were then used to remove any residual washing solution that may dilute the alginate solution. Five mL of sterile-filtered 1.4 % chemically modified alginate (70-80 % (w/v) modified PRONOVA SLG20 alginate; 20-30 % (w/v) unmodified PRONOVA SLG100 alginate) (NovaMatrix, Sandvika, Norway) (M/G ≥ 1.5; SLG20 MW 75 – 150; SLG100 MW

150-250; endotoxin < 100 EU/g) in 0.8 % saline (pH 7.2 - 7.4) was added to the dry islet pellet. The islets were mixed in the 50 mL tube and then loaded into a 5 mL syringe using an 18 G needle. The alginate-islet suspension (1,000 islets, 2,000 islets, or 4,000 islets per 1 mL 1.4% w/v alginate) was dripped into the divalent cation gelling solution using an in-house electrostatic encapsulator developed at MIT (1.5 mm = 5.00 kV, flow: 0.18 mL/min per 18 G blunt tip needle) to form hydrogels. The gelling solution consisted of 20 mM BaCl₂, 25 mM HEPES, 0.25 M mannitol; pH 7.2-7.4. The hydrogels were dripped over a period of 15 minutes and left in the gelling bath for an additional 5 minutes. Hydrogels were then washed three times (25 mL) with HBSS containing calcium and magnesium over a period of 5 min. Encapsulated rat islets were cultured in RPMI 1640 with glutamine containing 10% FBS, 0.2% PS, for 24 hours culture at 37°C. Encapsulated cynomolgus islets were cultured in CIT supplemented CMRL1066 (Mediatech) containing 10% FBS, 2% Cipro, and 0.1% ITS for 24 hours culture at 37°C. Encapsulated human islets were cultured in CIT supplemented CMRL1066 (Mediatech) containing 2% human albumin and 0.2% Cipro for 24 hours culture at 37°C. This type of alginate capsule was used for *in vitro* and *in vivo* encapsulated islet studies for large encapsulated islets (Chapter 4.3).

2.3 In vitro islet assessments

2.3.1 *Islet counting*

The Islets are examined using a 10x eyepiece and the 4x objective to give a total magnification of 40x. Using grid lines on the counting petri dish base as a guide, the dish is methodically scrolled through from one side to the other and from top to bottom examining each islet. The islets are counted within the perimeter of the grid's squares, including only islets touching the top and right lines (not the bottom and left lines), to avoid counting the same islet twice. A reticle certified to the 4x objective determines the size of each islet. The distance across the two spaces on the calibrated reticle in the eyepiece equals 50

μm . The total number of islets in each diameter group is counted using a manual cell counter. The dilution factor (if used) is then factored into the calculation to retrieve the total number of islets present.

This procedure is used to determine the appropriate number of islets to be encapsulated at the appropriate volume of alginate material or transplanted into the kidney capsule. In the case of encapsulated islets, using dilution factors resulted in inaccurate and unreproducible counts due to the inhomogenous distribution of the large particles in the solution. To determine encapsulated islet counts to be transplanted into mice, the islets were counted pre-encapsulation and encapsulated at the desired seeding density. Then it was assumed that there no loss of islets during encapsulation. Typically this is less than 10% and that is not out of range than what naked islet counts can be off by. The total volume of capsules made was then measured and used to determine how many islets were in a given volume of capsules. The appropriate volume of capsules/number of islets is then transplanted per mouse.

2.3.2 *Viability*

The viability of islets was evaluated using the inclusion/exclusion dyes FDA/PI. FDA is non-polar and can passively diffuse across intact cell membranes. Live cells contain active esterases that remove the acetyl group to convert FDA to its polar counterpart fluorescein. The polar fluorescein molecules become trapped inside the cell and stain live cells green. PI can only traverse compromised cell membranes of dead cells and intercalates with the DNA to stain dead cell nuclei red [44]. Either naked or encapsulated islets were rinsed twice with HBSS and mixed with 0.46 μM FDA and 14.34 μM PI in 2 mL HBSS. A fluorescent microscope with filters for FDA (excitation wavelength 488 nm, emission wavelength 520 nm) and PI (excitation wavelength 534 nm, emission wavelength 617 nm) was used to assess the viability of the islets. Percentages of total viable cells within 25-50 whole islets were assessed post-isolation, post-encapsulation, pre-transplant, and post retrieval.

2.3.3 *Dithizone (DTZ) staining*

One hundred mg of DTZ is weighed out on an electric balance and added to a 50 mL conical tube. Ten mL of DMSO is then added to the DTZ followed by 40 mL of HBSS. The conical tube is then closed and inverted five times. The DTZ solution is then filtered into a fresh 50 mL conical tube using a 0.22 μ m filter. Approximately 1 mL of DTZ is added to naked islets or encapsulated islets that have been aliquoted in 100 mm petri dishes. Islets are then visualized using brightfield microscopy.

In the case of large 1.5 mm encapsulated islets, the gels maintain the DTZ solution which makes imaging difficult. For these samples, a small sample of the large encapsulated islets is placed in a 50 mL conical tube. DTZ (5 mL) is added to the encapsulated islets and incubated for 3 minutes. The encapsulated islets are then washed 3 times with 10 mL of HBSS quickly. Then the encapsulated islets are washed one more time with 10 mL of HBSS and allowed to incubate for 10 minutes on side. The encapsulated islets can then be imaged using brightfield microscopy.

2.3.4 *Insulin ELISA*

For the determination of insulin concentrations, samples were run on an chromogenic insulin ELISA plate following the manufacturers recommendation (Mercodia, Uppsala, Sweden or ALPCO NH, USA). Insulin samples from the GSIS and perfusion assays were run without dilution. Twenty-five microliters of sample was pipette into each respective well of the 96 well ELISA plate. Samples were measured in duplicate for the GSIS assay and singlet for the perfusion assay due to the large number of samples to be measured per plate. Wells were then incubated for 1 hr with the enzyme conjugate on a shaker. The plates were washed 6 times with wash buffer, and special care was taken to remove excess bubbles in the wells with empty pipette tips. The substrate TMB was loaded into the wells and incubated for 15 minutes. Stop solution was added and the plates were measured immediately for absorbance at 460 nm. Insulin concentrations were then calculated by fitting to a linear regression standard curve.

2.4 **In vivo transplantation procedures and assessments**

2.4.1 *Naked islet kidney capsule transplantation (Mice)*

STZ mice with 2 blood glucose levels above $> 350\text{mg/dl}$ are considered diabetic and used for transplantation experiments. The mice are anaesthetized via isoflurane gas administration. The skin of the mice is sterilized via alcohol paint and a left flank incision ($\sim 2\text{ cm}$) is performed through the skin, subcutaneous tissue, and muscle tissue until the kidney is visualized. The kidney is retracting out of the incision using sterile cotton swabs to minimize any damage to the kidney. The posterior end of the kidney capsule (thin membrane covering the kidney) is carefully opened with the tip of a sterile 21 G needle. A glass capillary with melted end is inserted into the kidney capsule to dissect the membrane from the kidney surface. Naked islets are previously pelleted into an 18 G polyethylene micro tubing and attached to a Hamilton syringe. The tip of the tubing is then carefully inserted through the opening in the posterior end of the kidney capsule, and the tubing is directed toward the anterior end of the kidney. It is important during the procedure to keep the kidney capsule moist and delicately maneuver the tubing inside the kidney capsule as the membrane can tear easily. The islets are then carefully delivered into the anterior end of the kidney. The opening of the membrane is cauterized following removal of the tubing. The kidney is then reinserted into the peritoneal cavity via sterile cotton swabs. Sutures (5-0 monofilament) close the skin and peritoneum simultaneously to close the surgical wound (4-5 interrupted sutures). The surgical wound is then wiped clean with betadine and alcohol paint. Pain management is accomplished by a single injection of slow release buprenorphine (SC 1 mg/kg) administered before the start of surgery. This covers analgesics for three days post surgery. Criteria for monitoring animals post-surgery for signs of pain or distress include: animal cornered in a hunched position, inactive, loss of shine in fur. Animals displaying these traits or large losses in weight associated with diabetic complications are euthanized.

2.4.2 *Encapsulated islet intraperitoneal transplantation (Rodent)*

During the transplantation of the encapsulated islets, the mice are anaesthetized via isoflurane. The mouse is then injected with slow-release (SR) buprenorphine preoperatively (SC 1 mg/kg), which provides analgesics for 3 days post surgery. Fur on the abdomen is shaved (4 x 4 cm) and scrubbed with alcohol paint, the skin is then cut vertically (2 cm). Another small incision (1 cm) of the peritoneum wall exposes the peritoneal cavity. Care is taken to avoid any large capillaries in the peritoneal wall to avoid excessive bleeding. A sterile transfer pipette containing capsules and HBSS (0.3 mL capsules in 1.0-1.5 mL HBSS) will be inserted IP and the capsules will be evenly distributed. The peritoneal wall and skin are simultaneously sutured using a 6.0 monofilament nylon surgical suture. The surgical wound is then scrubbed with Betadine and alcohol paint. The mouse recovers under a heat lamp or on top of a warmed water glove. Once recovered and active, the mouse is placed in a clean cage. The animals are then monitored post-surgery for signs of pain or distress which include: animals cornered in a hunched position, inactive, loss of shine in fur, or more than 20% loss of weight compared to pre-transplantation levels in the case of diabetic animals. These animals are then treated or euthanized accordingly.

The transplantation of microcapsules for rats is identical to mice except for the following changes. After preparation of the incision site, the skin is cut vertically (2 cm). The abdomen is lifted and an 18 G catheter is inserted into the IP cavity. The metal needle portion is removed while leaving the catheter sleeve intact in the peritoneal cavity. The capsules loaded in a 3 mL syringe (1 mL capsules in 2 mL HBSS) are connected to catheter sleeve and injected into the peritoneal cavity. The capsules are then uniformly distributed. The catheter puncture is closed with one suture followed by suturing of the skin using a 4.0 monofilament nylon surgical suture. The incision site is scrubbed with Betadine and alcohol paint. The rat recovers and is post-op monitored using the same procedures followed for mice.

2.4.3 *Oral glucose tolerance test (OGTT)*

Mice are fasted for 6-7 hours prior to starting the OGTT. A 20% sterile glucose solution is prepared. The mice weights and BGL levels are measured from a tail prick of the tail vein. These are recorded as T0 values. PE50 tubing is then attached to a 23 G needle. A 3 mL syringe is loaded with the appropriate volume of glucose to be administered to the mouse at a glucose dose of 3 mg/g mouse. The mouse is anaesthetized via isoflurane and forceps are used to move the tongue to the side of the mouth to facilitate easier gavage of the animal. The 50PE tubing (attached to the glucose loaded syringe) is inserted through the esophagus and into the stomach. It is important that the tubing is not inserted into the trachea since infusion of the glucose solution into the lungs will asphyxiate the animal and cause death. To determine if the tubing is truly in the esophagus, it is possible to measure the length of tubing that can be inserted into the animal until pressure is felt. If the tubing is inserted into the trachea, then very little tubing can be inserted compared to a greater depth into the stomach. The glucose solution is then infused into the animal (extra air is in the syringe to ensure all glucose is infused into the animal). The timer is started and glucose levels are measured from the tail vein using an AlphaTRAK glucometer at T15, T30, T45, T60, T90, and T120 minutes. Statistical significance between groups of animals is then determined by calculating the area under the curves (AUC) of the OGTT blood glucose levels and comparing using an unpaired student T-test ($p < 0.05$ is taken as significant).

2.4.4 *Retrieval of encapsulated islets (Rodent)*

During retrieval of the capsules, the animals must be euthanized in order to harvest all the capsules and observe the affect in the peritoneal cavity. For the retrieval of empty capsules, rodents are first euthanized via CO₂ asphyxiation and cervical dislocation. For the retrieval of encapsulated islets, the encapsulated islets are retrieved while the animals are under anesthesia to minimize warm ischemia and damage to the encapsulated islets. The general procedure is similar to the procedure used for

transplantation, the abdomen is shaved, sprayed with alcohol, and a small incision (2 cm) is made to expose the peritoneal cavity. The peritoneal cavity is flushed using a sterile transfer pipette and warmed HBSS (25-30 mL) to collect the capsules. Then the abdomen is fully exposed to retrieve any capsules or clumps that could not be removed through IP flushing. In the case of encapsulated islets, the animal is then euthanized at this step by exsanguination and cervical dislocation.

2.4.5 Encapsulated islet intramuscular transplantation (Rat)

Microbeads (0.2 mL) are washed three times with 1 mL HBSS and loaded into a 1 mL syringe. Rats are anaesthetized via isoflurane inhalation, the fur on the legs shaved, and skin sterilized with alcohol. A small skin incision (2 mm) is made near the descending gracilis major muscle to expose the skeletal muscle tissue. The syringe bearing an 18 gauge needle is directed into the gracilis major muscle 2 cm deep. Pressure is applied to the plunger to inject the microbeads while simultaneously retracting the syringe in order to evenly distribute the microbeads along the needle tract. A sterile swab is used to prevent any leakage of microbeads, and the small incision in the skin was sutured using 4.0 nylon monofilament reverse cutting sutures (Ethicon, Somerville, NJ, USA).

2.4.6 Laparoscopic encapsulated islet transplantation and retrieval of IP space (NHP)

The NHP is first sedated with ketamine (10 mg/kg/IM), induced with propofol (3-5 mg/kg/IV) and anesthetized using continuous isoflurane gas infusion. Animals are monitored throughout anesthesia for the animal's depth of anesthesia, respiratory rate, heart rate, blood pressure and pulseox. Animals are given the following analgesics: hydromorphone (0.1 mg/kg IV), sufentanil (initial bolus 0.5-1.0 µg/kg/IV and then 0.005-0.02 µg/kg/min/IV continuous infusion), bupivacaine (1 mg/kg/SC) at the incision sites. The animals are also given the antibiotic cefazolin (25 mg/kg/SC), pre-operatively.

The anterior abdomen is shaved and prepped from xyphoid to pubis. Bupivacaine is infused along the incision line. A small (2 cm) supraumbilical incision is performed and a 5 mm trocar is inserted into the peritoneal cavity. CO₂ gas at a pressure of 12 mmHg insufflates the peritoneal cavity, and an endoscopic camera is inserted into the peritoneal cavity through the trocar. Under the view of laparoscopy, another small incision (1 cm) is made and an 8 mm trocar is inserted into the peritoneal cavity posterior to the right medial lobe of the liver. The capsules are transferred into a catheter syringe that is attached to a small length of silicon tubing and a 2 mL pipette. The pipette is inserted into the peritoneal cavity through the 8 mm trocar, and the capsules are evenly distributed in the following spaces: perihepatic, retrogastric, perisplenic, left and colonflexium, omentum, and behind the small bowels. For some encapsulated islet transplantations, laparoscopic graspers and shears are used to make a small incision in the omental tissue posterior to the stomach. This opening allows access to the lesser sac of the peritoneal cavity. The pipette is then inserted through the omental tissue and into the lesser sac. The capsules are then flushed into the lesser sac to distribute evenly between two layers of omental tissue. The trochars are removed, and the peritoneal cavity is deflated. After the operation, the small incisions are sutured by layers using Vicryl 3-0 cutting for muscle and fat tissue and Vicryl 4-0 taper for skin (subcuticular). The recovery of the animal is followed by a trained veterinary staff.

The same general procedure is repeated during the retrieval of capsules. Instead of infusing the empty capsules as described in the previous section, warmed saline or HBSS is flushed into the peritoneal cavity to wash out the capsules using a 60 mL syringe. The capsules can then be analyzed for biocompatibility and islet functionality at various times post transplantation. If the capsules are transplanted into the lesser sac, then the supraumbilical incision is extended and a section of omental tissue is withdrawn through the incision. The tissue is clamped, excised and placed in a bowl with warmed saline. The tissue is agitated to dislodge any capsules from the omental tissue. These are then

collected, washed in a seive, and are analyzed using various *in vitro* assays. If the capsules are found to be clumped and adhered to the tissue, then biopsies are taken and fixed in formalin for histology processing. The post-operative care and post-operative analgesia for the animals is the same as in the implantation surgery.

3 SKELETAL MUSCLE TISSUE AS A POTENTIAL TRANSPLANTATION SITE FOR PANCREATIC ISLETS ENCAPSULATED IN $\text{Ca}^{2+}/\text{Ba}^{2+}$ -ALGINATE MICROBEADS

3.1 Introduction

Microencapsulation is a promising approach to enable long-term survival of pancreatic islet graft function without immunosuppressive medications. Although this approach has been tested successfully in small animal models [32-34], results have not translated well in larger animal species and within small-scale clinical trials [35-38]. Some studies suggest that pericapsular fibrotic overgrowth (PFO) and limited islet nutrition are the major causes for the failure of microencapsulated islet graft function [45]. The PFO is a tight network of cells and extra cellular matrix surrounding microcapsules that may restrict nutrient diffusion, deplete oxygen supplies for the encapsulated islets, and secrete pro-inflammatory signals such as nitric oxide, IL-1b, $\text{IFN}\gamma$, and $\text{TNF-}\alpha$, ultimately leading to islet apoptosis [13, 46]. It is largely believed that the PFO results from a foreign body response to the encapsulation biomaterial [30]; however, encapsulated islets in a nutrient deprived environment can also secrete pro-inflammatory factors such as high mobility group box 1 (HMGB1), MCP-1 or other antigenic epitopes that can then trigger the PFO [47].

The intraperitoneal (IP) space is the most widely chosen transplantation site, mainly due to the ease of access and large volume of space available to accommodate a large quantity of encapsulated islets [45]. However, whether or not the IP cavity is the optimal transplantation site for microencapsulated islets is debatable. Firstly, diffusional transport of molecules both to and from mesenteric blood vessels and systemic circulation has been shown to be rather slow, which may delay insulin action and post-prandial blood glucose levels [48, 49]. Secondly, it has been shown that the IP space has low oxygen tensions

[50-53], which may predictably interfere with the optimal nutrition of the transplanted islets. Thirdly, the IP space has been reported to have a significant population of peritoneal macrophages noted to be important mediators of the foreign body reaction [54, 55].

Ideally, the optimal site of transplantation for encapsulated islets should exhibit rich nutritional availability and sufficient oxygen tensions to sustain the metabolic demand of islets for proper survival and insulin secretion [56]. Skeletal muscle tissue is highly vascularized with oxygen tensions of approximately 32.7 mmHg [57], which is near to 40 mmHg reported for islets in the *in situ* pancreas [58]. Furthermore, skeletal muscle has been reported to exhibit low antigen presenting cell (APC) infiltration [59], and therefore, may represent a less immunogenic site. In fact, transplantation of naked islets into striated muscle has demonstrated significant metabolic control in patients with Type I diabetes as well as other large animal models [58, 60, 61].

We have shown previously that 3,000 human islets encapsulated in $\text{Ca}^{2+}/\text{Ba}^{2+}$ -alginate microbeads can reverse streptozotocin (STZ) induced diabetes in immune incompetent nude mice for approximately 300 days [62] and in immune competent Balb/c mice for approximately 150 days when transplanted into the IP space [63]. These studies have shown this type of microbead to be promising; however, the procedure requires a rather large amount of encapsulated islets in order to reverse diabetes. This requirement for an excess amount of islets may be site-dependent as a result of diminished nutrition and attenuated encapsulated islet function over time. The purpose of this study was to implant $\text{Ca}^{2+}/\text{Ba}^{2+}$ -alginate microbeads both with and without islets into the skeletal muscle tissue of rats to investigate the host immune response to the presence of microbeads and determine if encapsulated islets could be supported for an extended period of time.

3.2 Methods

3.2.1 *Study design*

Lewis male rats (Harlan Industries, Indianapolis, IN, USA) were transplanted with $\text{Ca}^{2+}/\text{Ba}^{2+}$ -alginate microbeads into the skeletal leg muscle (gracilis major). Three groups were used: 1) Empty alginate microbeads (Lewis recipients, $n = 6$); 2) Encapsulated isogeneic islets (Lewis rat islets into Lewis rats, $n = 6$); 3) Encapsulated allogeneic islets (Sprague Dawley rat islets into Lewis rats, $n = 6$). The microbeads were retrieved from all of the recipients at 8 weeks post transplantation and analyzed for host responses to microbeads and long-term survival of encapsulated islets. The transplant procedures were performed under the guidelines of the National Institutes of Health and approved by the Animal Care Committee at UIC.

3.2.2 *Intramuscular retrieval of alginate microbeads*

Microbeads were retrieved 8 weeks post transplantation. Lewis rats were anaesthetized via isoflurane inhalation and euthanized by heart exsanguination. The entire upper leg (gracilis major muscle) was then fixed in 10% formalin for histology. For the retrievals of microbeads from 3 rats in each group, the muscle tissue was further dissected to expose the site of microbead transplantation. Unattached, freely floating microbeads were collected with a spatula and washed three times in HBSS. These were then evaluated for fibrotic tissue overgrowth using a scoring method described below, analyzed for viability, and the remaining microbeads were fixed in 10% formalin for histological analysis. If no freely floating microbeads were obtained, microbead clumps were fixed in 10% formalin for histology.

3.2.3 *Fibrotic overgrowth of retrieved microbeads*

The degree of fibrotic overgrowth of retrieved microbeads was determined by categorizing the microbead surface area that was covered by overgrowth under brightfield microscopy. Two hundred

microbeads per animal were categorized: 0%, <25%, 25-50%, 50-75%, >75% surface area coverage of the microbeads [64].

3.2.4 Histological analysis of retrieved freely floating microbeads

Upon retrieval, freely floating microbeads were rinsed three times with HBSS and fixed in 10% formalin overnight. After fixation, the microbeads were rinsed twice with PBS, and dehydrated in gradually ascending ethanol solutions for 20 min each. The microbeads were cleared in xylene for 10 min, and incubated in a 50/50 solution of xylene and paraffin overnight at 57°C. On day 3, the microbeads were transferred to paraffin twice for 1 hr each, and then embedded in a paraffin mold. Subsequently, embedded microbeads were sectioned at 5 µm thickness onto positively charged lysine microscope slides. Tissue sections were then stained for hematoxylin and eosin (H&E) to assess pericapsular cellular overgrowth and islet morphology. Consecutive slides containing encapsulated islets were also immunohistochemically (IHC) stained for insulin. In short, the deparaffinized and rehydrated tissue sections were immersed in citrate buffer at pH 6 (BD Pharmingen, San Diego, CA, USA) and the heat-induced epitope retrieval (HIER) was performed. Tissue sections were then rinsed in PBS three times and the primary antibody guinea pig anti-insulin (1:200 polyclonal; DAKO, Carpinteria, CA, USA) was then applied. After overnight incubation, the tissue sections were rinsed with PBS three times and incubated for 1 hr with high affinity fluorescently labeled Alexa Fluor secondary antibody for anti-guinea pig 594. Nuclei were counterstained with diamidino-2-phenylindole (DAPI) and coverslips applied with aqueous mounting medium (Fluoromount-G, Southern Biotech, Birmingham, AL, USA).

3.2.5 Histology of microbead grafts embedded in whole leg muscle

Whole leg muscles containing the femur bone were fixed in 10% formalin for 72 hours. The femur bone was then carefully removed, and the whole muscles were rinsed twice with PBS and stored overnight in 70% EtOH. Muscle specimens were further dehydrated the next day in ascending EtOH solutions,

cleared in xylene and embedded in a paraffin block. Subsequently, embedded muscle tissue was sectioned at 5 μm thickness and stained for H&E to evaluate muscle/microbead morphology and to assess tissue overgrowth of the microbeads. If morphological observation of H&E stained tissue sections showed multi-layer cellular overgrowth of the microbeads, immuno-histochemistry (IHC) was performed on the adjacent tissue sections to investigate the cellular population involved in the PFO. Sections were immunofluorescently labeled for mouse CD68^+ tissue derived macrophages, CD3^+ T-lymphocytes and alpha-smooth muscle actin positive ($\alpha\text{-SMA}$) myofibroblasts. Tissue sections were deparaffinized and HIER performed as described above. Tissue sections were then rinsed with Tris-buffered saline (TBS) plus 0.025% triton X-100 and blocked with goat normal serum for 1 hr at room temperature. Primary antibodies mouse IgG against CD3 (1:50 clone SP7; Abcam, Cambridge, MA, USA), mouse IgG1 against CD68 (1:100 clone ED1; Abcam, Cambridge, MA, USA) and rabbit $\alpha\text{-SMA}$ (1:100 polyclonal; Abcam, Cambridge, MA, USA) were applied on serial sections and incubated overnight at 4°C. After rinsing with TBS plus 0.025% triton X-100, fluorescently labeled secondary antibodies Alexa Fluor 594 anti-mouse and 594 anti-rabbit (1:200 Invitrogen, Grand Island, NY, USA) were applied and incubated for 1 hr at room temperature. DAPI nuclear counterstain was then applied and the coverslips mounted. All stained tissue sections were viewed under a Leica DM 200 microscope and images captured with QICAM Fast1394 digital camera and processed with Qcapture Pro5.1 program.

3.2.6 Statistical analysis

Data are depicted as mean \pm SD and analyzed by a two-tailed unpaired student t-test and one-way ANOVA using PRISM software. $p < 0.05$ was considered to be statistically significant.

3.3 **Results:**

3.3.1 *Encapsulation and intramuscular transplantation*

Encapsulated rat islets within $\text{Ca}^{2+}/\text{Ba}^{2+}$ -alginate microbeads maintained their morphology as determined by dithizone staining. Also, no significant differences in terms of viability were detected pre-encapsulation vs. post-encapsulation, respectively ($95.1 \pm 2.2\%$ vs. $94.4 \pm 4.5\%$, $p = 0.18$) (Figure 3-1). Prior to beginning intramuscular transplantations, a sample of microbeads was extruded through an 18 gauge needle to verify that the morphology and size of the microbeads were unchanged during the infusion process (data not shown). Furthermore, no visible leakage of microbeads from the injection site after transplantation was observed, and none of the transplanted animals presented with any health issue or infection.

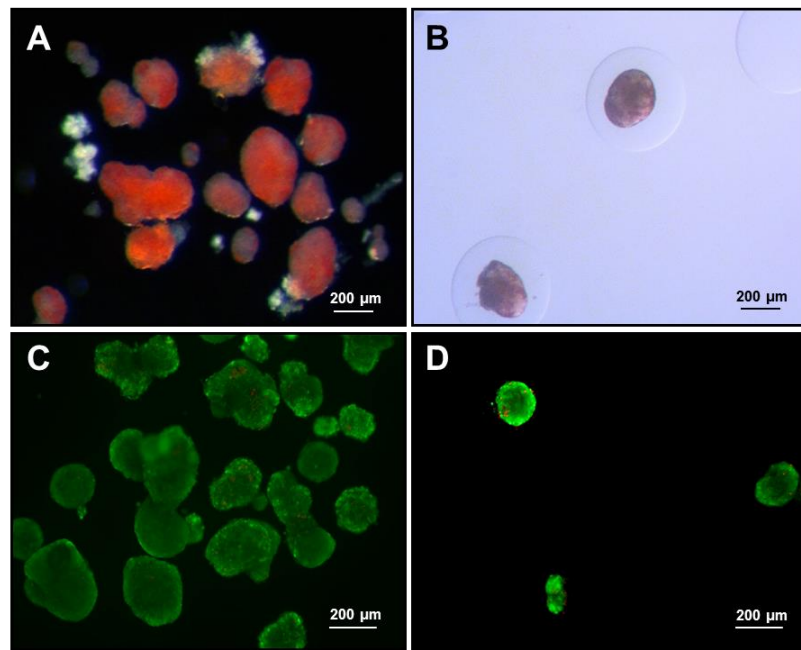


Figure 3-1: DTZ and viability staining of rat islets pre- and post-encapsulation

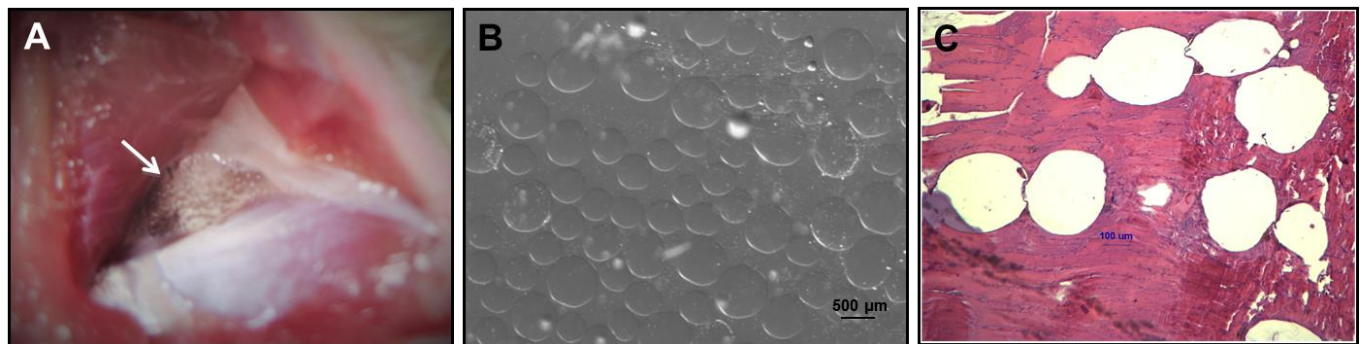
A/C) DTZ and viability staining of rat islets pre-encapsulation. **B/D)** post-encapsulation in $\text{Ca}^{2+}/\text{Ba}^{2+}$ alginate microbeads. (representative images from $n = 3$ encapsulations)

3.3.2 Empty microbeads in the intramuscular space after 8 weeks

Upon dissection of the muscle tissues at 8 weeks post-transplantation, the empty microbeads were found to be transparent with no signs of inflammatory tissue around the microbeads (Figure 3-2:A). The microbeads were easily harvested from the transplant site at a retrieval rate of $71.7 \pm 5.8\%$ (Table I). The bead size post retrieval was comparable to the size before transplantation, respectively ($468 \pm 85 \mu\text{m}$ vs. $444 \pm 79 \mu\text{m}$, $p = 0.31$). No broken microbeads were observed and all maintained proper spherical morphology under brightfield microscopy (Figure 3-2:B). The majority of retrieved empty microbeads was free of cellular attachment and categorized as having 0% tissue overgrowth (Table II). H&E staining of whole leg muscle specimens verified that the empty microbeads remained intact morphologically and free of fibrotic tissue overgrowth at the interface between muscle tissue and microbeads (Figure 3-2:B).

Table I: Microbead characteristics pre-transplant and post 8 week retrieval

	Pre-encap Viability (%)	Post-encap Viability (%)	Retrieval Viability (%)	Pre-tx Microbead Size (μm)	Retrieved Microbead Size (μm)	Percent Breakage (%)	Percent Retrieval Rate (%)
Empty (n=3)	NA	NA	NA	444 ± 79	468 ± 85	0	71.7 ± 5.8
Iso (n=3)	95.2 ± 2.1	94.3 ± 3.8	95.0 ± 1.7	560 ± 96	552 ± 90	0	66.7 ± 2.9
Allo (n=3)	94.9 ± 2.4	94.6 ± 5.1	NA	526 ± 76	NA	NA	~ 0

**Figure 3-2: 8 week retrieval of empty microbeads transplanted intramuscularly.**

A) Overview of dissected muscle tissue with transparent empty microbeads. **B)** Brightfield image of freely floating microbeads flushed from muscle tissue. **C)** H&E of empty microbeads within muscle tissue. (representative images from n = 6 empty retrievals)

3.3.3 Encapsulated isogeneic islets in the intramuscular space after 8 weeks

The results of dissected muscle tissues transplanted with encapsulated isogeneic islets were very similar to those of the retrieved empty microbeads at 8 weeks post-transplantation. The microbeads containing isogeneic islets were transparent with no obvious signs of inflammation (Figure 3-3:A). They were

easily removed from the implantation site at a retrieval rate of $66.7 \pm 2.9\%$, and the size of the microbead did not change significantly over time ($560 \pm 96 \mu\text{m}$ vs. $552 \pm 90 \mu\text{m}$; $p = 0.76$) (Table I). No broken microbeads were observed and the majority was categorized as having 0% tissue overgrowth (Table II). The viability of the retrieved isogeneic islets was $95 \pm 1.7\%$, which was comparable with the islets viability before transplantation ($94.3 \pm 3.8\%$; $p = 0.24$) (Figure 3-3:B). The retrieved isogeneic islets also stained positive for dithizone (Figure 3-3:C). H&E staining of whole muscle specimens showed that microbeads containing isogeneic islets were free of fibrosis at the microbead/muscle interface (Figure 3-3:D). H&E stains of harvested freely floating microbeads demonstrated encapsulated islets with plump round morphology (Figure 3-3:E) and IHC positive insulin staining (Figure 3-3:F).

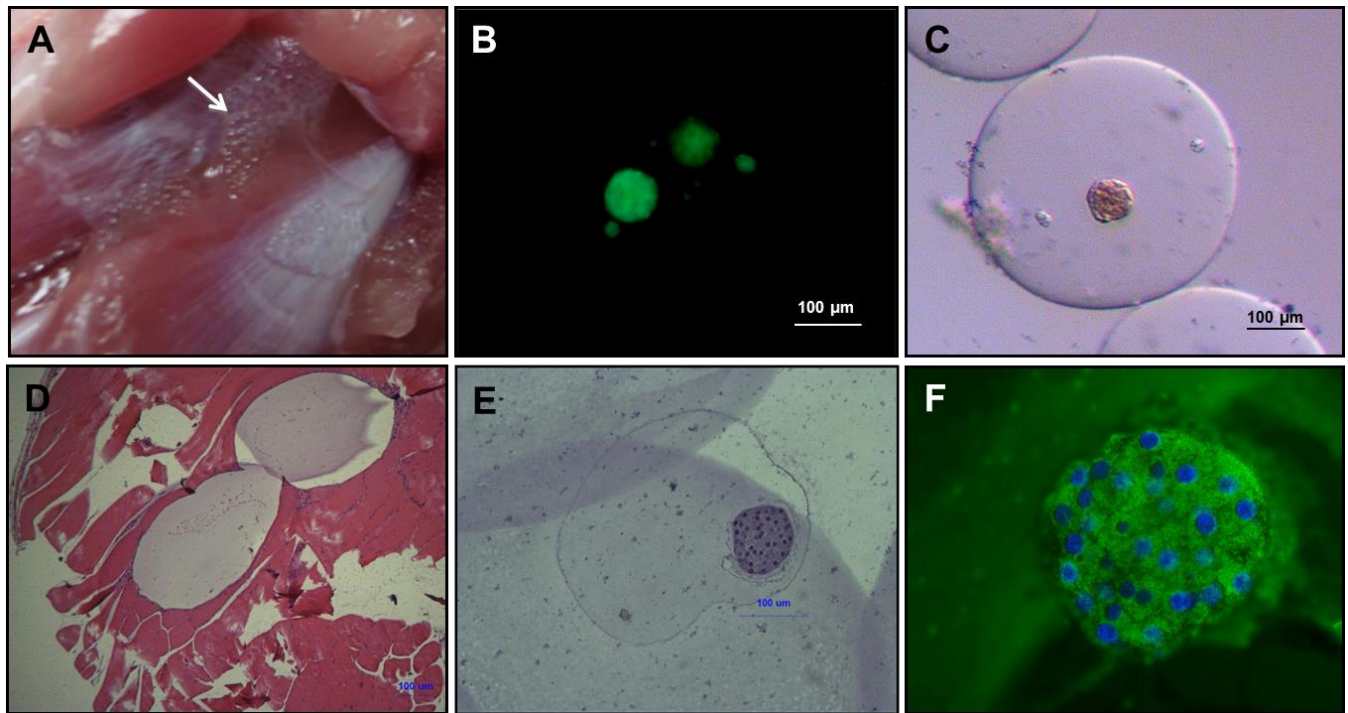


Figure 3-3: 8 week retrieval of encapsulated isogeneic islets transplanted intramuscularly.

A) Overview of dissected muscle tissue with transparent microbeads containing isogeneic islets. **B)** Viability of retrieved encapsulated isogeneic islets. **C)** DTZ staining of freely floating encapsulated isogeneic islet harvested from muscle tissue. **D)** H&E of encapsulated isogeneic islets within muscle. **E)** H&E staining of retrieved encapsulated isogeneic islet. **F)** IHC insulin staining of retrieved encapsulated isogeneic islet. (representative images from n = 6 encapsulated isogeneic islet retrievals)

3.3.4 Encapsulated allogeneic islets in the intramuscular space after 8 weeks

Upon dissection of muscle tissues transplanted with encapsulated allogeneic islets, the microbeads were clumped together, opaque, and adhered to the surrounding muscle tissue that appeared visually inflamed (Figure 3-4:A). The clumps of microbeads were separated from the muscle tissue and found to be entrapped within fibrotic tissue that had become neovascularized (Figure 3-4:B). The majority of the microbeads containing allogeneic islets were characterized as having 100% tissue overgrowth (Table II). H&E staining showed that the microbeads were surrounded with cellular overgrowth of 10-20 cell layers

thick (Figure 3-4:C). Possible fragments of islets were detected inside the microbeads; however, these fragments exhibited poor islet morphology and stained negative for insulin in IHC stains (data not shown).

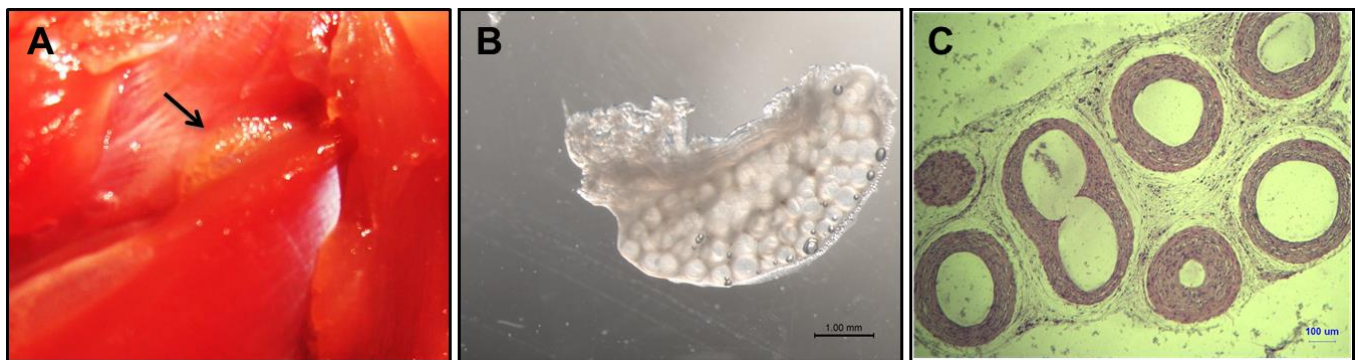


Figure 3-4: 8 week retrieval of encapsulated allogeneic islets transplanted intramuscularly (n = 6)

A) Overview of dissected muscle tissue with opaque microbeads containing allogeneic islets. **B)** Neovascularized fibrotic clump of encapsulated allogeneic islets. **C)** H&E staining of clumped encapsulated allogeneic islets and islet fragments. (representative images from n = 6 encapsulated allogeneic islet retrievals)

3.3.5 Fibrotic tissue overgrowth of retrieved microbeads

The retrieved microbeads (n = 200 per rat) from each group were assessed under brightfield microscopy for the degree of overgrowth. Results are presented in Table II.

Table II: Percentage of microbeads with surface area covered by tissue overgrowth

	0%	0-25%	25-50%	50-75%	75-100%
Empty (n=3)	91.3 ± 1.6	8.8 ± 1.7	0	0	0
Iso (n=3)	87.1 ± 3.1	13.0 ± 3.2	0	0	0
Allo (n=3)	9.3 ± 16.2	2.7 ± 4.6	0	0	88.0 ± 20.8

3.3.6 Immune cells involved in rejection of allogeneic encapsulated islets

H&E slides showed dense cellular regions 10-20 cell layers thick proximal to the microbeads containing allogeneic islets (Figure 3-5:A). These cell layers were largely composed of alpha smooth-muscle actin positive (α -SMA⁺) myofibroblasts (Figure 3-5:B) as suggested by IHC staining. These were then surrounded by interstitial tissue with a much lower cellular density. The interstitial regions were populated with CD68⁺ tissue derived macrophages (Figure 3-5:C) and CD3⁺ T-lymphocytes (Figure 3-5:D), typically in groups of 5-10 individual cells.

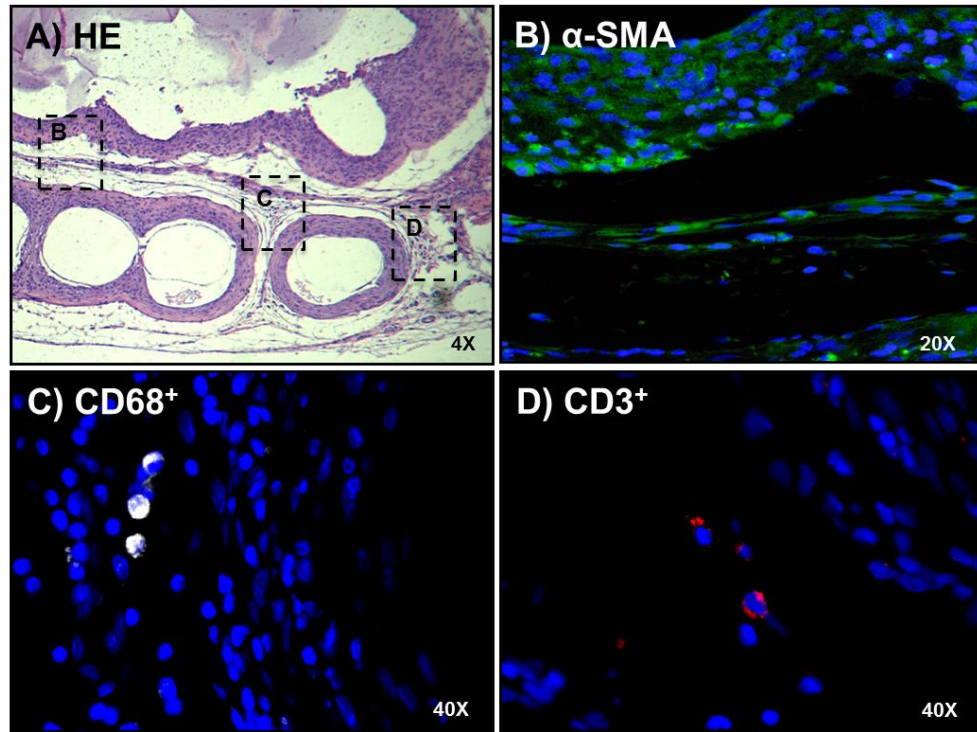


Figure 3-5: H&E/IHC staining for specific immune cell type and localization within allo-clump.

A) H&E overview of clumped encapsulated allogeneic islets and indicated areas of α -SMA (myofibroblast), CD 68⁺ (macrophage) and CD 3⁺ (T-lymphocyte) on consecutive slide sections. **B)** α -SMA⁺ myofibroblasts directly on the surface of microbeads containing allogeneic islets. **C)** CD 68⁺ tissue macrophage in the interstitial tissue. **D)** CD 3⁺ T-lymphocyte in the interstitial tissue.

(representative images from $n = 3$ consecutive slide staining of clumps from each allogeneic rat).

3.4 Discussion:

The present study investigated the feasibility of transplanting islets encapsulated in $\text{Ca}^{2+}/\text{Ba}^{2+}$ -alginate microbeads into skeletal muscle tissue via a minimally invasive syringe injection. This procedure is highly applicable in a clinical setting as a relatively large volume of encapsulated islets can be distributed into multiple muscle sites available in a recipient. Importantly, these preliminary results indicate there is only a minimal host reaction to the presence of empty alginate microbeads and

microbeads containing isogeneic islets within the skeletal muscle tissue. Furthermore, skeletal muscle can support viable encapsulated islets for an extended period of time of at least 8 weeks. Although encapsulated allogeneic islets suffered from allorejection within the intramuscular site, the alginate (UPLVG) and gelling ion combination ($\text{Ca}^{2+}/\text{Ba}^{2+}$) used in this study may not provide allo-protection in rats, and in this respect, these results do not diminish the potential of skeletal muscle as an alternative transplant site in the future.

Alternative transplantation sites for microencapsulated islets have been investigated in rodents including the liver [27], kidney capsule [28], subcutaneous [29], intra-epididymis [30], and bone marrow cavity [31] with limited improvement in islet survival and functionality. The lack of success in these sites may be due to similar issues as the IP space such as inadequate islet nutrition or heavy immune infiltration and PFO.

An ideal transplantation site for encapsulated islets should be endowed with robust nutritional provisions to satiate islets' high metabolic demands for insulin production and secretion, and also allow for repeat transplants over time [6]. This becomes increasingly difficult as encapsulated islets rely solely on diffusion of nutrients and oxygen from blood vessels to achieve nutrition without becoming revascularized. Improving encapsulated islet nutrition may be accomplished by choosing alternative transplantation sites with dense capillary beds and oxygen tensions that more closely mimic the microenvironment of the *in situ* pancreas. The increased vasculature should not only provide better nutritional exchange but also decrease the response time of encapsulated islet function to detect hyperglycemia and secrete adequate insulin back to the vasculature for blood glucose homeostasis. A caveat to increased density of capillary beds is a higher potential for bleeding during the transplantation process which has been shown to enhance fibrotic tissue overgrowth and failure of the graft [40]. In our model, we only observed minimal to no bleeding in the transplant site.

Our first concern was how microbeads, and specifically encapsulated islets, would react to the continual application of external mechanical forces within skeletal muscle since its primary function is to contract and relax for locomotion. When retrieved at 8 weeks, no broken microbeads were observed, and all maintained spherical morphology within the muscle tissue. This indicates that the mechanical forces and spherical feature of the microbeads can be well tolerated in the muscle tissue. Furthermore, muscle tissue was able to support viable encapsulated islets with insulin production for at least 8 weeks. This suggests that islets can also tolerate any mechanical forces in the muscle as well as receive adequate nutrition to maintain long-term insulin production. Lastly, no PFO was evident at the interface of muscle tissue and empty microbeads or microbeads with iso-grafts. This indicates that alginate microbeads are biocompatible in the muscle transplant site in rats and are not major activators of innate immune cells such as macrophages, neutrophils, mesothelial cells or myofibroblasts typically associated with foreign body responses (FBR) to implanted biomaterials [40].

As the alginate microbeads (empty and with encapsulated isogeneic islets) were shown to be biocompatible within the muscle tissue, this suggests that the PFO in the intramuscular site was only initiated due to the immunogenicity of allogeneic tissue. Allogeneic results indicate that cells involved in adaptive immunity such as T-cells or B-cells may be responsible for the recruitment of macrophages and myofibroblasts that are classically associated with FBR and chronic inflammation to implanted biomaterials. Prior to transplantation, allogeneic and isogeneic encapsulated islets showed similar islet quality measures such as viability and morphology, which suggests that the fibrosis seen with allogeneic islets may not be related to a poor batch of encapsulated islets with a higher leakage of debris from dead cells. It is still unclear which soluble factors may leak from the microbeads to initiate the cellular cascade involved in allorejection; however, it is most likely due to indirect antigen presentation to T-cells as others have hypothesized [65]. Once T-cells are alerted to the presence of foreign tissue, they

can recruit other immune cells such as macrophages and myofibroblasts through cell-cell communication via the secretion of chemokines such as IFN- γ , MCP-1, and MIP-1 [66, 67].

Staining profiles of the allogeneic clumps demonstrated dense regions of cells on the immediate surface of encapsulated allogeneic islets, and further staining indicates these are α -SMA⁺ myofibroblasts. It seems the tight network of fibrosis was dominated by α -SMA⁺ myofibroblasts, and this cell-type may be primarily responsible for restricting nutrient diffusion and consuming the oxygen supply to the encapsulated islets. Leakage of soluble factors from capsules that contain allogeneic or xenogeneic tissue may be an inevitable process that is very difficult to ameliorate without negatively affecting the nutrition of encapsulated cells. However, as the death of the allogeneic islets in this study may be a direct consequence of nutrient restriction by the myofibroblast network, investigations to impede cell-cell signaling or myofibroblast activation and migration seem to be good targets to improve islet encapsulation in the future. This may be accomplished by localized immune modulation to impede the proliferation of myofibroblasts [5, 68]. Also, the development of encapsulation biomaterials or strategies that can resist cellular attachment may provide a synergistic effect [69]. These materials should be very biocompatible by eliciting a minimal foreign body reaction but may also provide allo or xeno protection. Even if there is leakage of soluble antigenic factors and some activation of the adaptive immune system, activated cells may not be able to attach to the microbead surface to form the suffocating network.

A limitation that was discovered during the study was that the rat model may not be optimal for intramuscular transplantation studies, largely related to the small size of the animal. Rats were chosen instead of mice since the muscles of mice are very small and would make the transplantation procedure very difficult to target specific muscle groups. Nonetheless, using even larger animal models with larger muscles may be beneficial to better target muscle groups with optimal properties for encapsulated islet function. Skeletal muscle is composed of various fiber types with different metabolic and contractile

properties [70]. Type I or “slow twitch” muscles contain rich capillary beds, low contractile forces, and high resistance to fatigue. Type IIB or “fast twitch” muscles contain less capillary beds, high contractile forces, and fatigue easily [71]. Muscle groups are typically a combination of fiber types with a higher or lower percentage of Type I fibers. The larger muscle groups in larger animal models should allow for better targeting of transplants into muscle groups with a higher percentage of Type I fibers such as the soleus muscle [72], which may improve encapsulated islet function. As the soleus muscle diameter is only 2-3 mm in rats [73], the gracilis major muscle was chosen due to the larger size.

3.5 Conclusion:

Alginate microbeads remain intact without fibrosis when implanted into a highly active muscle group. Also, encapsulated isogeneic islets can survive in this site for at least 8 weeks, which was the end point of this study. However, in this animal model, this type of alginate microbead did not prevent allogeneic islet rejection.

4 ANTI-FIBROTIC STRATEGIES FOR IMMUNE-ISOLATION DEVICES: LARGE SIZED 1.5 mm ENCAPSULATED ISLETS FOR THE TREATMENT OF DIABETES

4.1 Introduction:

Microencapsulated islet transplantation as potential cure of T1DM has been researched for decades [22]. This strategy earned heightened attention after (Soon-Shiong et al., 1994) was the first to report a successful human encapsulated islet transplant (9 months normoglycemia) in an immunosuppressed diabetic patient. The recipient also received immunosuppressive medications to maintain a functioning kidney allograft [74]. Positive function of microencapsulated xenogeneic islets transplanted into diabetic NHP was also described by (Sun et al., 1996) [75]. Nonetheless, these results have not been replicated by others in the field of microencapsulation [76].

Many researchers have attempted to reduce the size for microencapsulation since the small distance between islets and the capsule interface should provide the best diffusion kinetics and nutrition of the encapsulated islets [77]. On the contrary, researchers in Dr. Anderson and Dr. Langer's lab at MIT observed that as they increased the size of the alginate capsules, the less fibrosis that was observed after retrieval. This conflicts with conventional thought that small encapsulated islets should function better than large encapsulated islets [78]. They then encapsulated rat islets at the conventional medium size (0.5 mm) and large size (1.5 mm) and transplanted 500 IEs into STZ induced diabetic C57b/6 mice. They found that the large 1.5 mm encapsulated islets could reverse diabetes for over 120 days; whereas, the medium sized 0.5 mm encapsulated islets failed after 30 days. This was largely attributed to reduction in fibrosis of the large encapsulated islets. Furthermore, transplanted spheres made of various materials were also found to be significantly less fibrosed at the large size. (Veisheh et al., Nature

Materials, 2015) thus discovered that the size and shape of implanted materials significantly correlates with the development of fibrosis [69]. They thus determined that larger capsules may be better suited for encapsulated islet function after transplantation into the peritoneal cavity. Interestingly, many of the encapsulated islets systems that were shown to work well in rodent models by other researchers in the field were composed of relatively larger capsule versions (0.8-1.0 mm) [32, 79, 80]. The relatively larger size of these capsules may have augmented the successful functionality of islets within the larger capsules through fibrosis reduction.

In the established collaboration with MIT, we wanted to build on the positive results seen with large sized 1.5 mm capsules. We began to focus on the encapsulated islets in order to investigate how the size/volume of the immune-isolation material affects islet functionality. This investigation used a combination of both *in vitro* and *in vivo* methods. Furthermore, MIT developed a series of chemically modified alginates that are resistive to fibrosis, especially when manufactured at the large 1.5 mm size. We also investigated the capacity of the chemically modified alginates to protect islet function after transplantation into a non-immunosuppressed NHP allogeneic transplant model.

4.2 Methods:

4.2.1 *Real-time fluorescence imaging of islet intracellular calcium*

Real-time fluorescence imaging of islet intracellular calcium $[Ca^{2+}]_i$ was performed in a microfluidic device modified for encapsulated islets [11]. In brief, fifty Sprague Dawley rat islets naked or encapsulated in alginate capsules (0.5 mm and 1.5 mm diameter) were incubated with 5 μ M Fura-2/AM (Molecular Probes, CA, USA) at 37 °C in Krebs-Ringer buffer (KR) supplemented with 2 mM glucose (KR2) and 0.5% BSA for 35 min. The islets were then loaded into the microfluidic device mounted on an inverted epifluorescence microscope (Leica DMI 400B, IL, USA). Excess dye was washed out with

KR2 for 35 min at 500 $\mu\text{L}/\text{min}$. Dual-wavelength Fura-2/AM dye were excited ratiometrically at 340 and 380 nm, and changes in the $[\text{Ca}^{2+}]_i$ levels are expressed as F340/F380 (% increase from basal 2 mM glucose). Excitation wavelengths were controlled by excitation filters (Chroma Technology, VT, USA) mounted in a Lambda DG-4 wavelength switcher. Emission of Fura-2/AM was filtered using a Fura2/FITC polychroic beamsplitter and a double band emission filter (Chroma Technology. Part number: 73.100bs). SimplePCI software (Hamamatsu Corp, IL, USA) was used for imaging acquisition and analysis. These images were collected with a high-speed, high-resolution charge coupled camera (CCD, Retiga-SRV, Fast 1394, QImaging).

4.2.2 Intracellular calcium $[\text{Ca}^{2+}]_i$ stimulation kinetics

Individual rat islet intracellular calcium responses were assessed for the three conditions using the same microfluidic device and the same perfusion protocol: 1) KR2 (0-5 min); 2) 20 mM glucose (5-25 min); 3) KR2 (25-45 min); 4) 30 mM KCL (45-60 min); 5) KR2 (60-70 min). The area under the curve for each time period was calculated for each individual islet in order to statistically compare groups using one-way ANOVA ($p < 0.05$ as significant). Three separate batches of rodent isolations were used for assessments where each condition was tested from the same batch of islets.

4.2.3 Insulin secretion kinetics

Islet insulin responses were assessed by loading 50 rat islets naked or encapsulated at 0.5 mm and 1.5 mm alginate capsules into the same microfluidic device used for calcium measurements. Perifusate samples were collected every minute (500 $\mu\text{L}/\text{min}$) by an automated fraction collector (Gilson, model 203B, WI, USA). Insulin concentrations were quantified every other minute using a rodent chemiluminescent insulin ELISA (Alpco, NH, USA). The following perfusion protocol was used: 1) KR2 (0-20 min); 2) 20 mM glucose or 30 mM KCL (20-55 min); 3) KR2 (55-100 min). The area under

the curve for each insulin curve was calculated in order to statistically compare groups using one-way ANOVA ($p < 0.05$ as significant).

4.2.4 *Glucose static insulin secretion (GSIS) assay*

Initial GSIS experiments for large 1.5 mm Ba^{2+} alginate encapsulated islets were performed using the same protocol applied during UIC Clinical Islet Transplantation. This protocol resulted in high basal insulin secretion profiles of the large encapsulated islets due to insufficient washing and removal of insulin within the capsules. Cynomolgus islets are cultured with additional insulin, which caused issues with high basal insulin levels. A new protocol was developed with more extensive washing procedures prior to loading in the simulation solutions.

Batches of encapsulated islets (2 mL) were collected in separate 50 mL conical tubes and washed with 25 mL of sterile saline. This was repeated 3 times very quickly to remove bulk insulin from the culture media. The conical tubes were then filled with 25 mL of Kreb's ringer buffer containing 2 mM glucose (KR2). The conical tubes were laid on their side for 10 min. This was repeated 3 times in order to drive the diffusion of insulin out of the capsules by re-establishing the concentration gradient 3 times. The encapsulated islets were then poured into a medium petri dish and filled with 20 mL of fresh KR2. Encapsulated islets (10) were then hand-picked under a microscope and placed into sieves with a 12 μ m porous PET membrane. The first three rows of a 24 well culture plate were filled with 1 mL of KR2 and the bottom row was filled with 1 mL of KR(High Glucose). High Glucose for each species of islets: rat islets (20 mM), NHP cynomolgus monkey islets (18 mM), and human islets (25 mM). Sieves containing 10 picked islets were dried on sterile gauze and placed into the top row KR2 solution for 30 min (Pre-wash). The sieves were dabbed on gauze and moved to the next row (KR2) for 1 hour (Wash). The sieves were scraped along the edge of the wells to collect the supernatant, then dabbed on gauze, and

moved to the next row (KR2) for 1 hour (Low). The sieves were scraped along the edge of the wells to collect the supernatant, then dabbed on gauze, and moved to the next row (KR-high glucose) for 1 hour (High). After high glucose stimulation, the sieves were scraped along the edge of the wells and placed in small petri dishes filled with 7 mL of culture media. Supernatants were collected from wash (KR2), low (KR2), and high (KR-high glucose) into 1.5 mL Eppendorf tubes and insulin concentrations were quantified via ELISA.

The encapsulated islets and naked islets were cultured in the sieves and media was exchanged every 2-3 days. The GSIS protocol was repeated on day 14 and 28. The same series of wash steps and incubations in KR2 (Pre-Wash, Wash, Low) and KR-high glucose were repeated. These wash steps were conducted in the petri dishes where KR2 was poured into the petri dish taking care not to pour into the wells which would remove the islets from the sieve. Then the wash KR2 was aspirated using a sterile pipette attached to vacuum for suction.

4.3 Results and discussion:

4.3.1 Insulin secretion kinetics of naked and encapsulated rat islets within medium 0.5 mm and large 1.5 mm Ba²⁺ alginate capsules

In beta-cells, glucose-induced insulin secretion is a complex process involving glucose metabolism, mitochondrial energy production, potassium-dependent ATP channels (K_{ATP} channels), voltage-dependent calcium channels (VDCCs), calcium influx, and insulin secretion, which has a biphasic and oscillatory kinetic pattern [14]. In this study, we applied a microfluidic perfusion device to dynamically measure intracellular calcium influx and insulin concentrations in the perfusate samples of naked rat islets, 0.5 mm and 1.5 mm Ba²⁺ alginate encapsulated rat islets after stimulation with insulin secretagogues. Intracellular calcium influx is a downstream and immediately proximal trigger for the

fusion of insulin granules to the plasma membrane for insulin exocytosis. By measuring both insulin secretion coupling factors and insulin secretion, the kinetics of stimulation and actual insulin release could be characterized in order to determine the impact of encapsulation and capsule size on insulin secretory kinetics of rat islets.

As shown in Figure 4-1, glucose-induced intracellular calcium signals were similar among the three groups with typical phase responses in all three groups. No significant differences were observed from the start time of calcium influx up to the maximal calcium peak in response to both 20 mM glucose and 30 mM KCl challenges ($p = 0.27$ and 0.41 (respectively, glucose); $p = 0.15$ and 0.43 (respectively, KCl)). Additionally, the areas under curves (AUC) of calcium concentrations during glucose and KCl stimulation were not significantly different ($p = 0.35$ and $p = 0.24$; respectively) (Fig.1B). However, the time to reach maximal calcium level for the 1.5 mm capsules was statistically delayed in response to glucose compared to the naked islets and 0.5 mm capsules ($p = 0.03$), but not statistically delayed in response to KCl stimulation ($p = 0.17$).

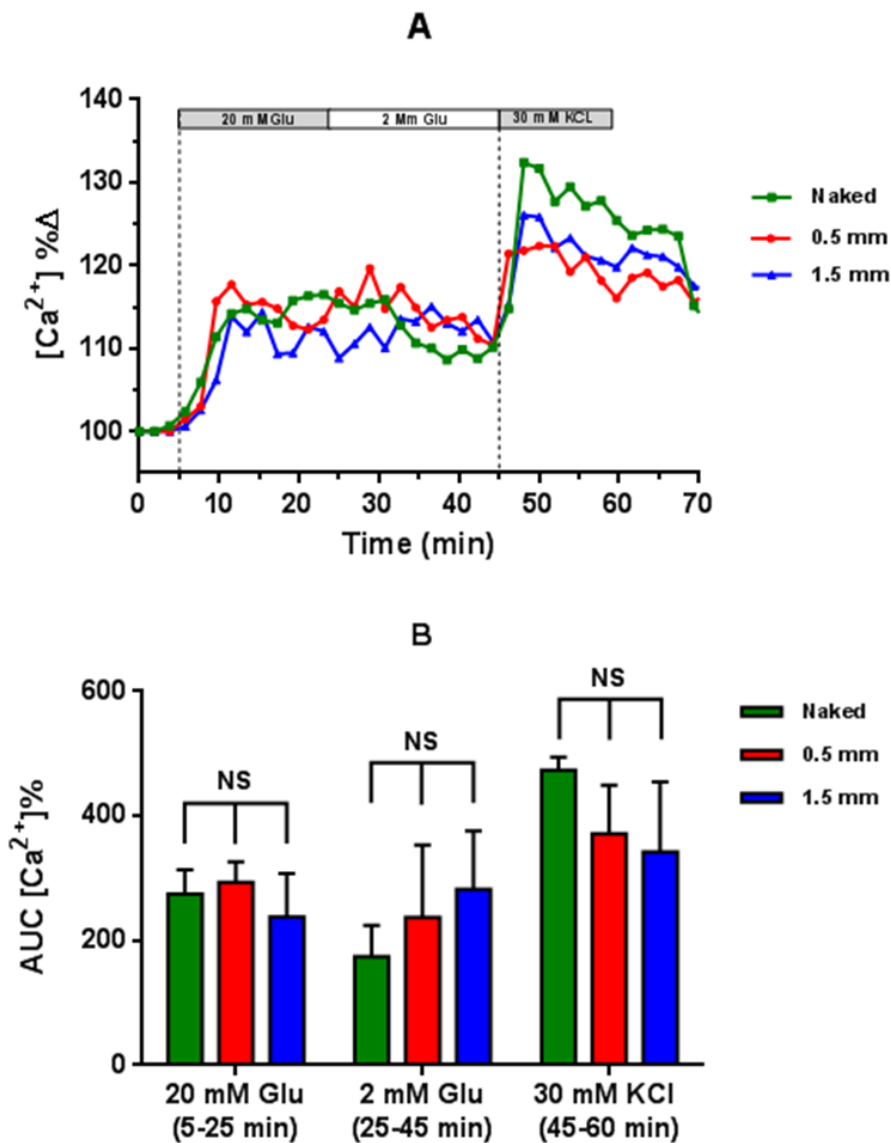


Figure 4-1: Intracellular calcium responses of naked and encapsulated rat islets in response to insulin secretagogues.

A) Representative traces of intracellular calcium of single rat islets in response to 20 mM glucose and 30 mM KCl (potassium chloride) stimulus.

B) Average AUC $[Ca^{2+}]_i$ % of calcium influx in response to 20 mM, 2 mM glucose and 30 mM KCl. (Mean \pm SEM; Naked $n = 59$; 0.5 mm $n = 49$; 1.5 mm $n = 43$ islets analyzed).

*Veisheh et al., Nature Materials. 2015

Our results suggest that small molecules, such as glucose (180.2 daltons) and KCl (74.6 daltons), diffuse very rapidly into the alginate capsules and efficiently induce calcium influx at a similar rate as naked islets. This suggests that the encapsulation process and alginate material do not acutely impede glucose metabolism or insulin stimulator-secretion coupling factors such as mitochondrial energy production and ion channels that are important for *in vitro* and *in vivo* function. Furthermore, diffusion efficiency in the capsule may depend on molecular weight of the analyte since there was a delayed time to reach maximal calcium level in the 1.5 mm capsules in response to glucose (180.2 daltons), but not to KCL (74.6 daltons).

Next, we investigated the insulin secretion kinetics of the naked and encapsulated islets. Naked islets show typical biphasic insulin secretion patterns in response to glucose, while both encapsulated islet groups show loss of the biphasic pattern and no sharp increase in phase I insulin secretion (Figure 4-2).

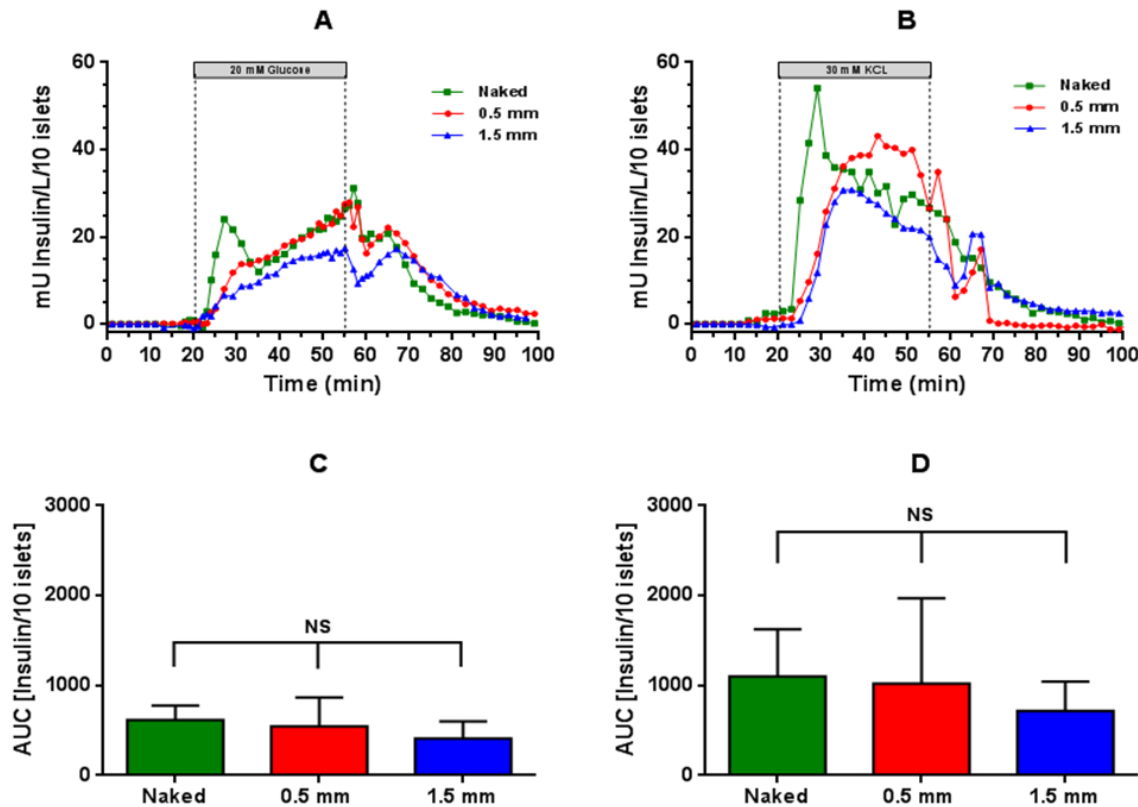


Figure 4-2: Insulin secretion of naked and encapsulated rat islets in response to insulin secretagogues.

A) Average insulin secretion kinetics in response to 20 mM glucose. **B)** Average insulin secretion kinetics in response to 30 mM KCl (potassium chloride). **C)** AUC [Insulin/10 islets] secreted during time of 20 mM glucose stimulation (Mean \pm SD). **D)** AUC [Insulin/10 islets] secreted during time of 30 mM KCl stimulation; (n = 3 runs, each run 50 islets from 3 separate isolations and encapsulations).

*Veisheh et al., Nature Materials. 2015

When compared to naked islets, the encapsulated islets demonstrated a delayed time to reach maximal insulin secretion from both high glucose and KCl ($p < 0.0001$ and 0.04 ; respectively). Also, less total insulin was secreted during the first ten minutes of stimulation for both secretagogues ($p = 0.02$ and 0.04 ; respectively). This data further suggests that the larger molecular weight of the insulin (5,808 Da)

might be the determining factor resulting in longer diffusion time through the alginate gel into the perfusate chamber for both encapsulated groups compared to naked islets.

The total insulin secreted by all groups during stimulations (20-55 min) and during the wash out period after stimulations (55-100 min) were found not to be significantly different in response to both secretagogues ($p = 0.59$ and $p = 0.76$; (20-55 min) respectively; $p = 0.88$ and $p = 0.73$; (55-100 min) respectively) (Figure 4-2 C/D). This suggests that overall bulk insulin secretion is unaffected by encapsulation or size of capsule. More importantly, encapsulated islets returned to basal insulin secretory levels similarly to naked islets. This is a critical factor when considering future clinical application as prolonged insulin secretion after stimulation could cause dangerous hypoglycemia.

Islets can exhibit heterogeneous responses from isolation to isolation [81, 82], and the main aim of this study was to investigate how the kinetics of insulin secretion is affected by encapsulation at larger sizes. Although the standard deviations are relatively high (islet variability), the total amount of insulin secreted during the first ten minutes of stimulation were found to be significantly higher for naked islets compared to encapsulated islets as previously mentioned (Figure 4-3:A/B). The insulin secretion data was then further analyzed where each response was normalized to the batch of islets as an internal islet control. This was accomplished by calculating the percentages of insulin that was secreted during ten minute intervals in comparison to the total insulin that was secreted during perfusion of a batch of islets (Figure 4-3C/D). This allows for a better understanding of the kinetics of insulin secretion, and how insulin diffuses through the gels. Furthermore, this reduces an effect of islet potency that can contribute to high standard deviations and confound results if purely trying to study insulin secretion kinetics. Percentages of glucose-stimulated insulin secretion suggest that encapsulated islets secrete half as much insulin in the first 10 minutes of stimulation compared to naked islets (Figure 4-3C). This correlates to

roughly a 5 minute delay in glucose-stimulated insulin secretion for both groups of encapsulated islets regardless of size in comparison to naked islets.

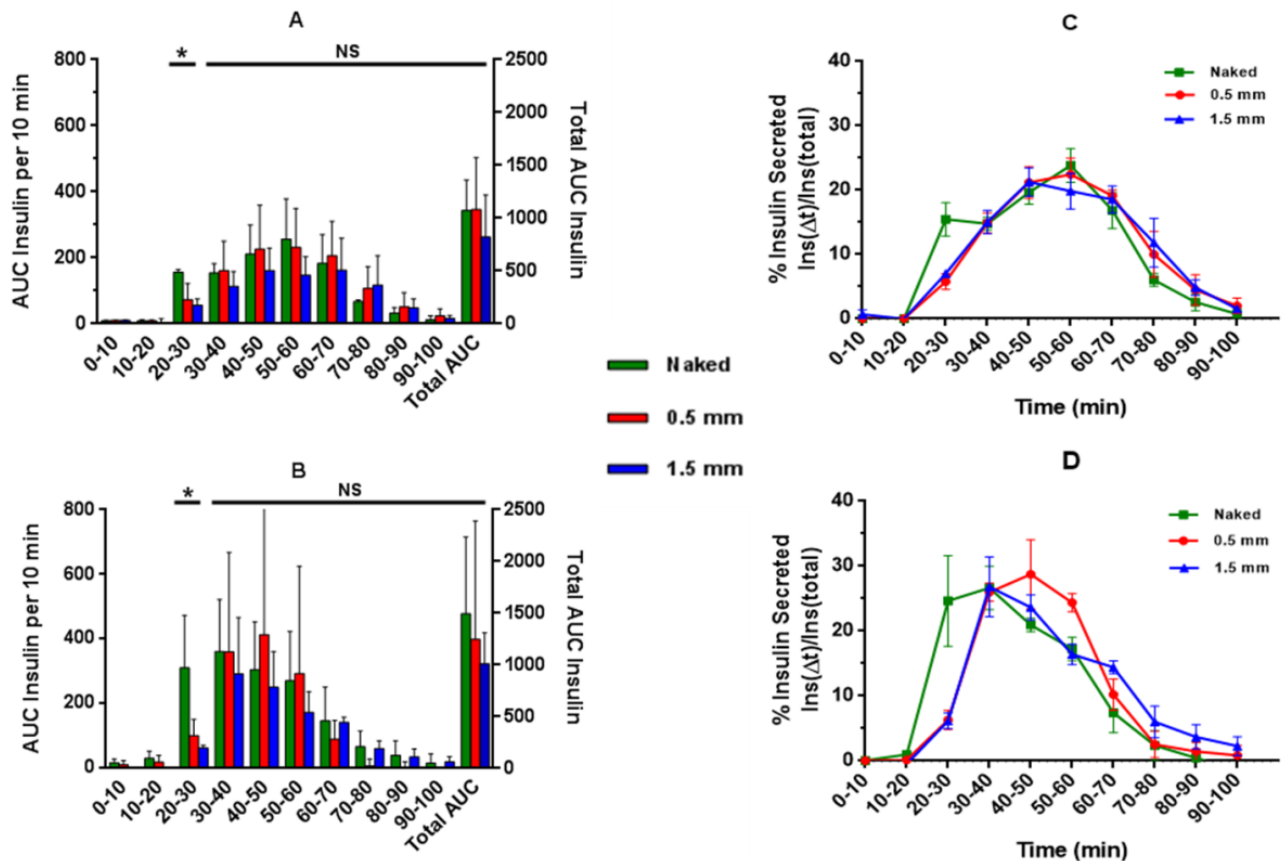


Figure 4-3: Size-dependent insulin secretion kinetics per 10 minutes

A) Bulk insulin secretion kinetics of glucose-induced insulin secretion (AUC per 10 min). **B)** Bulk insulin secretion kinetics of KCl-induced insulin secretion kinetics (AUC per 10 min). **C)** Normalized glucose-induced insulin secretion kinetics per 10 minutes (normalized to each batch of islets). **D)** Normalized KCl-induced insulin secretion kinetics per 10 minutes (normalized to each batch of islets). (n = 3 separate isolations, each run ~50 islets, Mean \pm SD).

The delay between encapsulation groups was only discernible when looking at KCl stimulated insulin secretion. KCl insulin secretion is non-physiological but exhibits qualities that are beneficial if investigating diffusion kinetics through gels. KCl stimulated insulin secretion bypasses upstream events of glucose mediated insulin secretion and causes immediate depolarization of the cell membrane, VDCC opening and calcium influx, and results in a large spike of insulin exocytosis [83]. This is similar to a pulse insulin waveform and potentially better at discerning how a large bolus of insulin diffuses through gels of different sizes. Looking at normalized percentages of KCl insulin release, both encapsulated groups experience a consistent initial delayed insulin release profile for the first 20 minutes in comparison to naked (Figure 4-3D). Subsequently, 1.5 mm encapsulated show a more drawn out insulin profile compared to 0.5 mm encapsulated possibly due to the larger volume of material the insulin must diffuse through. Although KCl induced insulin release shows a difference in kinetic responses between the encapsulated groups at the two sizes, this is insignificant as glucose-stimulated insulin secretion was found to be extremely similar and is more of an indicator of physiological responses.

In summary, islet stimulation kinetics by small molecular weight secretagogues is unaffected by encapsulation or capsule size. However, both groups of encapsulated islets experience a loss of phase I insulin secretion and an initial delay in glucose-stimulated insulin secretory kinetics. This delay was not found to be dependent on the capsule size, and overall bulk insulin kinetics for both capsule sizes are well conserved and similar to naked islets.

4.3.2 *In vitro and in vivo characterization of cynomolgus monkey islet functionality within large 1.5 mm Ba²⁺ alginate capsules using diabetic rodent models*

Since large encapsulated islets showed adequate insulin secretion kinetics, we wanted to evaluate *in vivo* function of large encapsulated islets using diabetic mice models. NHP islets (cynomolgus monkey) were chosen for these encapsulation studies in order to prepare for future preclinical studies using an

allogeneic NHP model. In general, NHP islets are similar to pig islets and tend to be more fragile when compared to islets from other species [84]. We have found cynomolgus islets to be less fragile compared to other NHP models such as baboons but are still more difficult to isolate and encapsulate when compared to rodent and human islets. Nonetheless, the FDA requires efficacy of encapsulation technologies to be first established in NHP prior to the submission of any innovative new drug (IND) applications for study in humans [77].

First, cyno islets were isolated using a method previously described [85]. The isolated islets were cultured overnight and encapsulated within 1.5 mm Ba^{2+} alginate as previously described in the methods section. DTZ staining of cyno islets was performed post-isolation, post culture/pre-encapsulation, and post- encapsulation (Figure 4-4). Cyno islets from separate isolations show varying degrees of fragmentation (fluffy, uncompact edge) that occurs from the isolation process and highlights their fragile nature (A-D). Cyno islets were still successfully encapsulated and maintained dense DTZ staining (E).

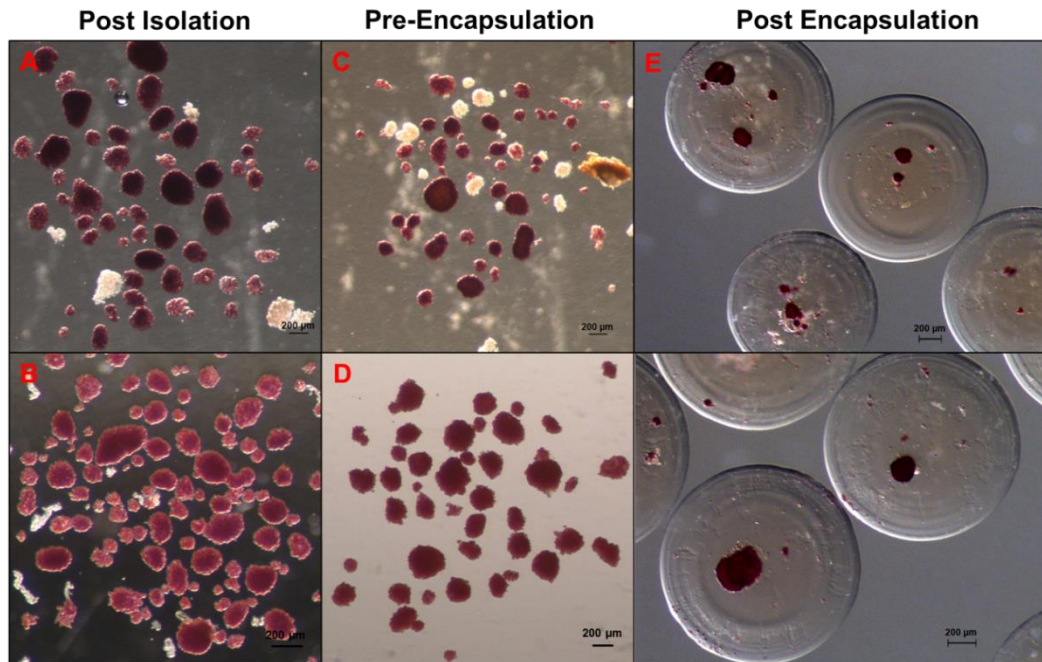


Figure 4-4: Dithizone (DTZ) staining of cynomolgus islets post-isolation, post 1 day culture/pre-encapsulation, and post-encapsulation within 1.5 mm Ba²⁺ alginate beads.

A/B) DTZ staining of cynomolgus islets immediately post-isolation (n = 2 batches of isolations). **C/D)** DTZ staining post 1 day culture/pre-encapsulation (n = 2 isolations from A/B). **E)** DTZ staining 1 day culture post encapsulation within 1.5 mm Ba²⁺ alginate beads and prior to transplantation into STZ induced diabetic nude mice (isolated islets depicted in A/C).

For transplantation studies, STZ diabetic nude mice were selected as an immune-incompetent model in order to evaluate how large encapsulated cyno islets functioned without the potential for immune rejection. Large encapsulated islets were also compared to the same number of naked cyno islets transplanted into the kidney capsule as a control. Prior to transplantation, *in vitro* functional assays such as viability (Figure 4-5), DTZ staining (Figure 4-4), and a glucose stimulated insulin secretion assay (GSIS) were performed. Results of the GSIS performed pre-transplantation will be discussed in future sections (Figure 4-8). The viability of encapsulated cyno islets was found to be consistently over 90%. Also, viability staining of the encapsulated islets tended to show cellular debris or small groups of cells

dispersed throughout the alginate material. The encapsulated islets also tended to appear more compact in comparison to naked cyno islets, which appeared to have a fluffy edge and more fragmented in viability staining (Figure 4-5:A/C). The cellular debris in the alginate material may have been cells that were stripped from the islet surface when mixing with the rather viscous alginate.

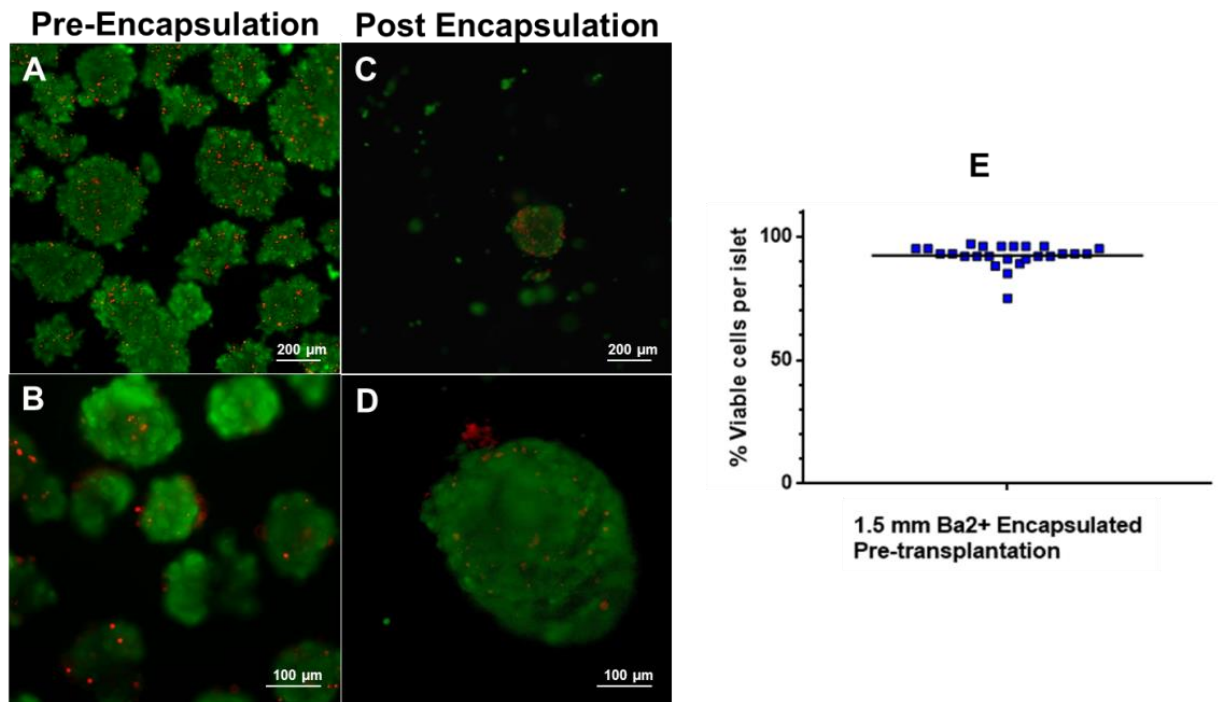


Figure 4-5: Viability of cynomolgus islets 1 day post isolation/pre-encapsulation and 1 day culture post-encapsulation/pre-transplantation into STZ induced diabetic nude mice.

Islets were stained with viability dyes fluorescein diacetate (FDA) to stain live cells green and propidium iodide (PI) to stain dead cells red and imaged with fluorescent microscopy. **A/B)** Naked Pre-encapsulation **C/D)** Post-encapsulation. **E)** Scatter plot of estimated percentages of total viable cells in whole islets (n = 25 islets).

Cyno islet clusters (1,500 naked or encapsulated in large sized Ba^{2+} alginate capsules) were then transplanted into STZ diabetic nude mice into the kidney capsule (naked) or intraperitoneal cavity (encapsulated). A marginal islet mass was transplanted where only ~75% of mice are intended to reverse diabetes. This is a good model to discern slight differences in islet functionality between groups. Blood glucose levels were monitored in the mice for 30 days post-transplantation followed by an oral glucose tolerance test (OGTT).

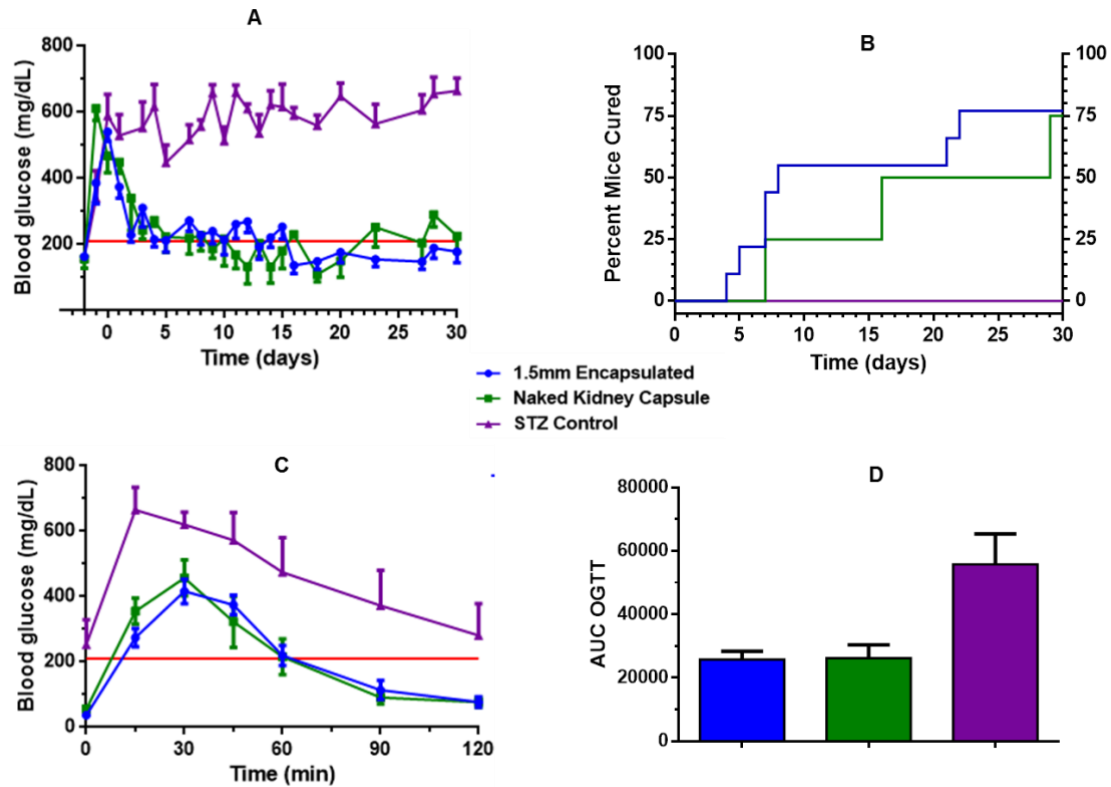


Figure 4-6: *In vivo* functionality of 1.5 mm alginate encapsulated cyno islets transplanted IP compared to naked cyno islets transplanted into the kidney capsule of immune-compromised STZ diabetic nude mice.

A) Average daily blood glucose levels of STZ diabetic nude mice transplanted with 1,500 cynomolgus islets. **B)** Cure rates of STZ nude mice. **C)** Oral Glucose Tolerance Test (OGTT) profiles performed on Day 30 post-transplantation. **D)** Area under the curve (AUC) of blood glucose levels during OGTT assessment ($p = 0.93$). ($n = 9$ (1.5 mm encapsulated cyno islets); $n = 4$ (naked kidney capsule); $n = 4$ (STZ control) (Mean \pm SEM).

In a marginal islet mass transplant model, 1,500 Ba^{2+} alginate encapsulated islets were able to cure STZ nude mice (3 consecutive readings below 210 mg/dL) similarly to naked islets transplanted in the kidney capsule (30 day cure rate: 77% vs. 75%) (Figure 4-6:A/B). During the OGTT test, a bolus of glucose solution was administered into the stomach of the transplanted mice, and blood glucose levels were measured from the tail vein at various times after administration. Mice transplanted with large

encapsulated islets were able to clear the glucose at similar rates compared to mice transplanted with naked islets in the kidney capsule (Figure 4-6:C/D). The areas under the curves of glucose levels during the OGTT test were not found to be significantly different between groups. This suggests that the small delay in glucose-stimulated insulin secretion seen with encapsulated rat islets in the previous insulin secretion kinetics study does not have a significant impact in acute blood glucose control in transplanted mice.

As large Ba^{2+} alginate encapsulated islets functioned well in an immune-incompetent nude mouse model, we wanted to see if similar efficacy could be achieved using a more difficult immune competent mouse model. Our collaborators had previously shown that larger 1.5 mm capsules are less prone to fibrosis and can protect properly functioning rat islets for up to 120 days in STZ diabetic C57b/6 mice. This was significantly different than 0.5 mm encapsulated rat islets, which lost curative function after 30 days. These results were significantly correlated to increased fibrosis of 0.5 mm encapsulated islets and graft failure [69]. Others have also shown long-term *in vivo* functionality of encapsulated islets using rodent models in allogeneic settings [2, 32] and xenogeneic settings [63, 79, 86]. However, these studies have often used large islet doses that may limit the efficacy for future clinical application. In the next set of experiments, the same marginal islet transplant mass used in STZ nude mice studies (1,500 cyno islets/1.5 mm Ba^{2+} alginate) were transplanted into the peritoneal cavity of STZ diabetic C57b/6 mice as a xenogeneic model. Blood glucose levels and weight were monitored over time (Figure 4-7).

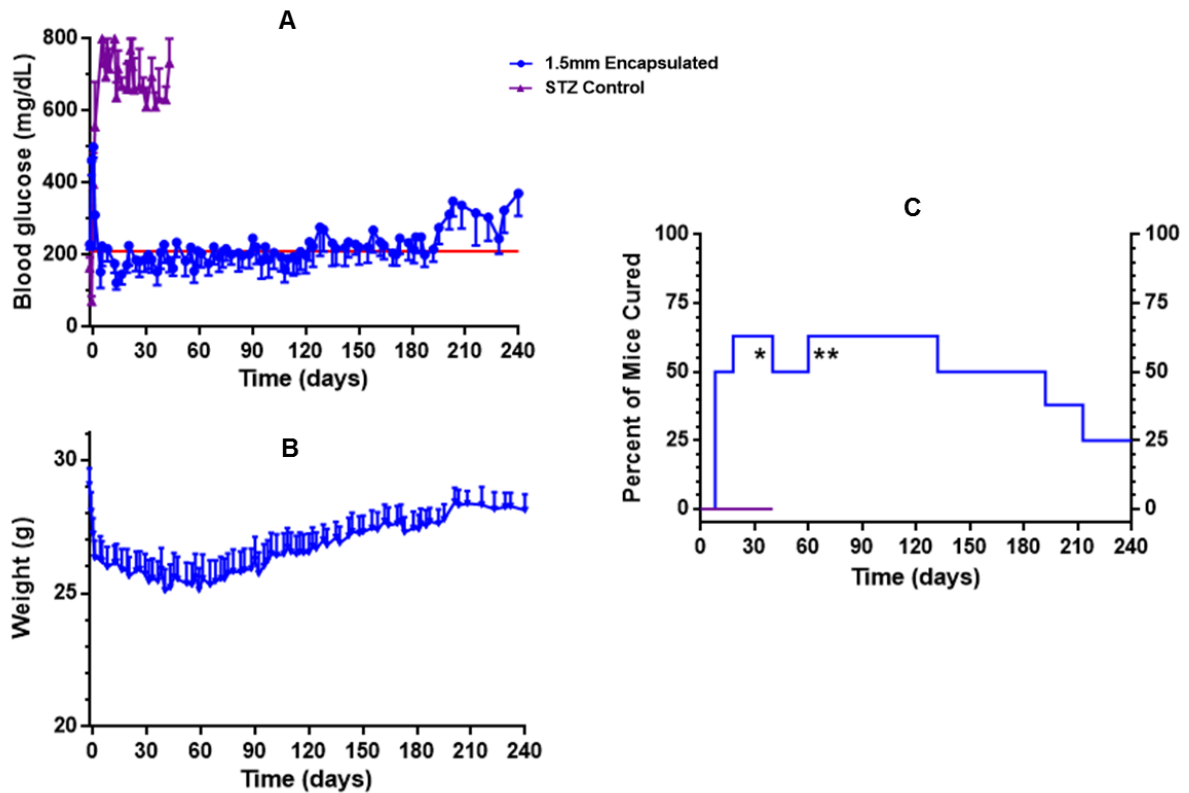


Figure 4-7: *In vivo* functionality of 1.5 mm encapsulated cynomolgus islets in immune-competent STZ induced diabetic C57b/6 mice.

A) Average daily blood glucose levels of STZ induced diabetic C57b/6 mice transplanted with 1.5 mm encapsulated islets (1,500 cyno islets).

B) Average daily weight of STZ C57b/6 mice. **C)** Cure rates of STZ C57b/6 mice. (Mean \pm SEM; 1.5 mm encapsulated $n = 8$; STZ control $n = 3$)

* 1 cured mouse died at Day 40 for unknown causes

** 1 mouse achieved cured status (4 consecutive readings below 210) at Day 60

STZ C57b/6 mice transplanted with Ba^{2+} alginate encapsulated cyno islets demonstrated consistent blood glucose levels for up to 180 days. Many of the transplanted mice hovered near the 210 cutoff line and some days were above or below the 210 threshold. This can be attributed to the use of a marginal mass model. However, the standard error of the blood glucose measurements for the cohorts of mice remained very stable over 180 days. Cure rate plots initially defined cured as 3 measurements below 210 and graft failure as 3 consecutive measurements above 210. Since the mice hovered at the 210

threshold, mice flip flopped between cured and failed graft. To facilitate a more straight forward depiction of function, mouse cure rates were subsequently defined using more stringent definitions and 4 consecutive measurements. Using this method, 63% of transplanted mice were cured by day 18 and largely remained at this level until day 180 (50% cured). One mouse died at day 40 due to unknown reasons and is not contributed to diabetic complications since blood glucose levels were consistently below 210 and weight was stable. Another mouse achieved cured status at day 60 when blood glucose readings became more consistently below 210. The weight of the transplanted mice also continued to rise over time after transplantation. Weight is an indicator of the diabetic state of the animal where weight loss is associated with poor glycemic control [87]. The average weight of all transplanted mice stopped increasing after 180 days when glucose levels were also on the rise. Even so, two transplanted mice have consistent cured blood glucose measurements at day 240 (time of thesis submission). The positive results obtained in this immune-competent fibrosis mouse model demonstrate the potential of 1.5 mm Ba^{2+} alginate encapsulated islets, and it will be interesting to see how these function in a more difficult NHP model.

It has been shown that Ba^{2+} alginate encapsulated cyno islets display potent functionality *in vivo*; however, some interesting results have been obtained during *in vitro* characterizations of the encapsulated cyno islets. The glucose stimulated insulin secretion assay (GSIS) is an *in vitro* glucose challenge assay that indicates how well isolated or encapsulated islets are functioning by measuring stimulated insulin secretion in 1 hour increments. In the GSIS assay, 10 encapsulated or naked islets are loaded into sieves with 12 μm pores and incubated in Kreb's buffer solution containing low glucose (2 mM) and high glucose (18 mM) for 1 hr each. The insulin in the supernatant is then quantified via insulin ELISA.

Initial results of GSIS that were performed pre-transplantation on the naked and encapsulated cyno islets prior to transplantation into STZ nude mice yielded significantly diminished secretion levels for encapsulated cyno islets compared to naked cyno islets. This contrasted *in vivo* functional results where encapsulated and naked islets functioned similarly in the mice. Also, the comparatively lower insulin secretion levels for encapsulated cyno islets did not match the insulin kinetics study where bulk insulin secretions of naked and encapsulated rat islets were found to be similar. Some batches of encapsulated cyno islets were cultured for an extended period of time, and it was also observed that many of the islets appeared to become more compact and exhibited better islet morphology. Others have also noted improved or steady *in vitro* function of islets from species such as pig islets, canine, and rodent islets during long-term culture of encapsulated islets [88-90]. Lastly, encapsulated islets are trapped in their environment indefinitely and do not become revascularized. Naked islets are typically transplanted soon after isolation to begin the revascularization process. Since there may be some benefit in culturing encapsulated islets in terms of islet recovery/equilibration to the alginate environment, or even extra time to analyze all results of functionality assessments performed prior to transplantation into the patient, the effect of culture on encapsulated islet function was analyzed using the GSIS method. The GSIS assay was performed on both naked and encapsulated cyno islets on day 1 post-encapsulation and throughout the time of culture on days 14 and 28 (Figure 4-8).

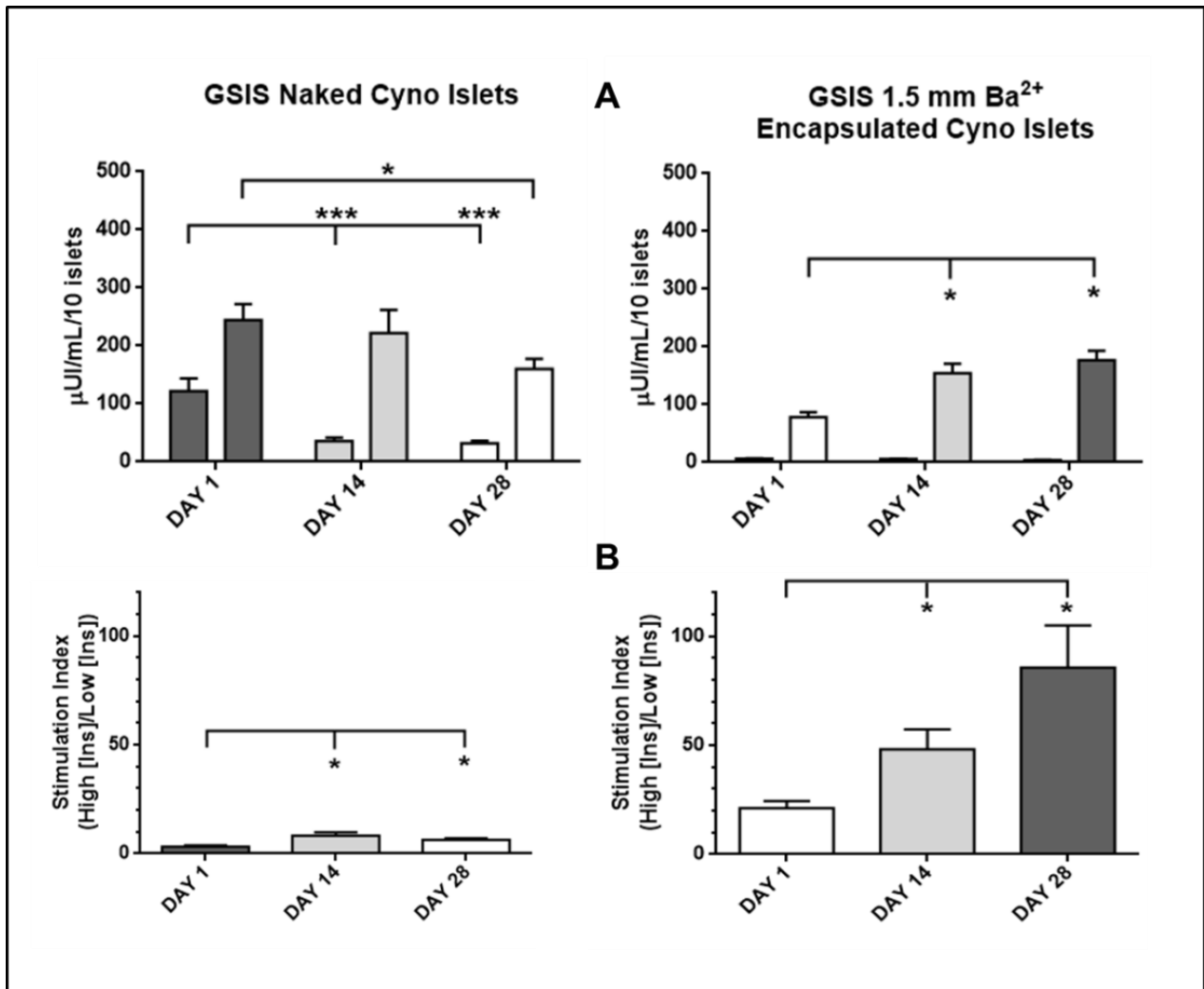


Figure 4-8: Glucose Stimulated Insulin Secretion (GSIS) under low glucose (2 mM) and high glucose (18 mM) of naked and 1.5 mm Ba²⁺ encapsulated cynomolgus islets over time.

A) Graphs depict total insulin secreted by 10 islets in sieves when stimulated for 1 hr with low glucose (2 mM) and high glucose (18 mM). These were repeated at Day 1, 14, and 28 post-encapsulation (Mean \pm SEM) (1.5 mm encapsulated $n = 36, 42, 62$ sieves, respectively; over $n = 8$ separate isolations and encapsulations) (naked $n = 21, 27, 33$ sieves, respectively; over $n = 4$ separate isolations)

B) Stimulation Index (SI = High [Ins]/Low [Ins]) of encapsulated and naked cynomolgus islets over time. (Mean \pm SEM) (1.5 mm encapsulated SI = $21.3 \pm 3.2; 48.2 \pm 59.4; 152.6 \pm 19.4$, respectively) (Naked SI = $3.2 \pm 0.5; 8.3 \pm 1.5; 6.4 \pm 0.7$, respectively). *** $p < 0.0001$; ** $p < 0.001$; * $p < 0.01$

Results of the GSIS assay performed throughout culture show that naked cyno islets tended to decrease insulin secretion in response to high glucose challenges when cultured over time; however, statistically significant values were only found when comparing Day 1 and 28 ($p < 0.01$). This is not unexpected as long-term culture of primary islets typically has an overall negative affect on islet functionality [91]. Cultured naked islets can dissociate into single cells post-isolation, and commonly there is a 20-30% islet loss following overnight culture [92]. Naked islets can also aggregate and merge into larger clusters if they stick to each other during culture [93]. These larger islet clusters then suffer from increased central necrosis due to nutritional limitations in the central core [94]. For these reasons, intraportal transplantation of naked islets occurs within the first 72 hours post-isolation to minimize both islet loss, and the formation of large islet clusters that may clog infusion tubing during transplantation [95]. In fact, the UIC Clinical Islet Transplantation program aims for a minimal culture time of around 12 hours prior to transplantation into a patient.

Interestingly, Ba^{2+} alginate encapsulated islets tended to increase insulin secretion in response to high glucose challenges when cultured for 14 days ($p < 0.01$), with no significant decline thereafter. Encapsulated islets secreted significantly less insulin in response to high glucose on Day 1 when compared to naked islets ($p < 0.0001$). This result is perplexing since previous *in vivo* results indicate that encapsulated and naked cyno islets function similarly in STZ diabetic nude mice. There might be some initial negative effect of the Ba^{2+} alginate encapsulation process on cyno islet functionality that is quickly reversed during the post-transplantation engraftment process in mice. At Day 14 and 28, high glucose insulin secretion levels for encapsulated islets were found to be similar to cultured naked islets. This further suggests that there may be some islet recovery post-encapsulation that occurs similarly during culture as well as during post-transplantation engraftment in mice.

Another interesting phenomenon was observed when analyzing the amount of insulin that was secreted during basal low glucose incubations for naked and encapsulated islets. Initial basal insulin secretion on Day 1 was fairly high for naked islets, and then these levels significantly declined at Day 14 and 28 ($p < 0.0001$). Encapsulated islets exhibited extremely low basal glucose insulin secretion levels 10-50 times less than naked islets and these levels remained very low at day 1, 14, and 28. Researchers have found that high insulin secretion during basal glucose levels correlates with stressed and improperly functioning islets [96, 97]. This suggests that there might be some benefit to encapsulation of islets in a matrix that may provide mechanical transduction signals similar to the *in situ* microenvironment of the native pancreas. This might result in contact induced islet integration into the gel, which results in less stressed islets and lower basal insulin secretion.

On the other hand, insulin must diffuse from the alginate gel in order to be detected in the supernatant. Secreted insulin may have to first diffuse and roughly equilibrate within the gel before diffusing into the supernatant. The amount of residual insulin within the capsules thus may have matched the amounts detected for naked islets. However, similar basal profiles seen for naked islets would have been expected for encapsulated islets. Encapsulated islets should have demonstrated high basal secretion on day 1, which they did not. Furthermore, islets can secrete insulin inadvertently by mechanical perturbations associated with the assay [98]. Sieves containing the islets must be scraped along the edge of a well in order to collect the supernatant during the GSIS assay. The resulting mechanical frequencies from scraping may have induced some insulin release for naked islets sitting on the bottom of the sieve. The alginate gel may dampen these mechanical perturbations for encapsulated islets. Since naked islets basal insulin secretion reduced after day 1, but then stayed consistent at day 14 and 28, this suggests that there are factors other than mechanical perturbations that cause the initial high basal secretion on day 1. This reduction in basal insulin after 14 day culture of naked islets might be attributed to a recovery of islet

ECM structure post-isolation. The alginate gel in the case of encapsulated islets may provide a similar recovery of ECM structure signaling that occurs immediately post-encapsulation.

Often islet researchers describe GSIS results as a stimulation index or the total amount of insulin secreted under high glucose divided by the total amount of insulin secreted under low glucose. This is a simple method to normalize the GSIS data since the number and size of islets may vary from experiment to experiment [99]. Typically, reporting stimulation indexes for glucose stimulation assays is acceptable, but these values can also vary between institutions. This variability may stem from different high glucose concentrations used for stimulations or other inconsistencies in the protocol such as washing time or BSA concentration [100]. The GSIS data can also be normalized to total protein, total insulin, or total DNA of the challenged islets [101]. This is beneficial to normalize insulin secretion to a consistent islet/cell number, yet this is a time consuming process. For these reasons, GSIS stimulation indexes showing improved function are often compared to an internal control such as untreated islets in the case of drug studies, or accompanied by *in vivo* results and other islet characterization assays [102]. These methods are appropriate for naked islets and can allow the researcher to present their story appropriately.

Many times researchers investigating encapsulated islets likewise report stimulation indexes, and this can be misleading. Figure 4-8B shows the stimulation indexes for naked and encapsulated cyno islets. The stimulation index for naked islets on Day 1 was 3.2 ± 0.5 . This value is an acceptable value for naked cyno islets, which have published SI ranges (2-9) [103, 104]. The stimulation index for encapsulated islets on Day 1 is 21.3 ± 3.2 . This is significantly higher than naked islets and correlates to the extremely low basal insulin secretion. If purely looking at SI of naked and encapsulated islets, encapsulated islets would seem to be the best functioning, and the most ideal for transplantation. However, this is very misleading since the total amount of secreted insulin by the encapsulated islets is substantially reduced. In another example, encapsulated islets can be retrieved post transplantation and

tested using the GSIS assay to see how well the islets are surviving *in vivo*. The stimulation indexes obtained can be on the order of 8-10, which for naked islets would seem like perfectly functioning islets. However, due to the extremely low basal insulin secretion of encapsulated islets, the actual amount of insulin being secreted under high glucose could be so miniscule that any effect on glycemic control would be arbitrary.

For these reasons, I believe that raw insulin concentrations obtained during the GSIS assay should always be reported and not stimulation indexes in the case of encapsulated islets. Raw insulin data may also prove beneficial when attempting to determine the amount of encapsulated islets that may be required in order to cure a diabetic NHP. It might be possible to compare the GSIS raw insulin values of encapsulated islets retrieved from cured diabetic mice and encapsulated islets retrieved from NHP. This may provide a reasonable estimation of how many islets will be needed in order to have a high probability of successful reversal of diabetes after transplantation, or at least if the encapsulated islets are functioning within a suitable range.

Since encapsulated cyno islets demonstrated increased glucose stimulated insulin secretion after short-term culture, we wanted to see if this improvement in functionality would also translate *in vivo*. For this experiment, cyno islets were encapsulated in Ba^{2+} alginate capsules and transplanted into STZ diabetic nude mice on Day 1 and Day 14 post-encapsulation. Following encapsulation, the islets were divided into 1,500 islet aliquots and cultured in separate petri dishes. Aliquots of encapsulated islets were then randomly selected and transplanted into STZ diabetic nude mice. The remaining aliquots received culture media exchanges every 2-3 days, and then were transplanted into STZ diabetic nude mice on Day 14 post-encapsulation. Separate batches of STZ treated mice were used for transplantations but cohorts exhibited similar characteristics such as age, weight, and duration of hyperglycemia prior to

transplantation. Blood glucose levels of the mice were followed for 30 days and an OGTT was performed 30 days post transplantation (Figure 4-9).

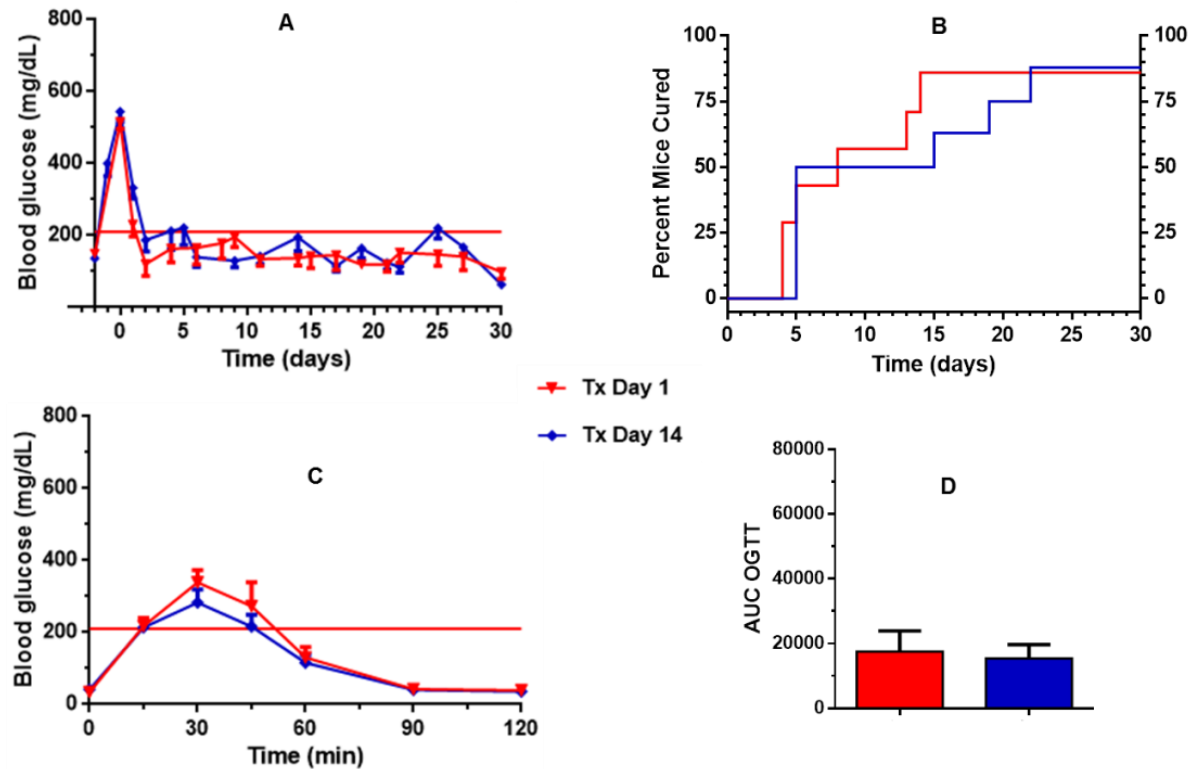


Figure 4-9: *In vivo* functionality of short-term cultured 1.5 mm encapsulated cynomolgus islets in immune-compromised STZ diabetic nude mice.

Batches of cynomolgus islets were encapsulated and transplanted into STZ induced diabetic nude mice on Day 1 or after 14 days of culture. **A)** Average daily blood glucose levels of nude mice transplanted with 1.5 mm encapsulated islets (1,500 cyno islets). **B)** Cure rates of STZ nude mice. **C)** OGTT profiles performed on day 30 post-transplantation. **D)** Area under the curve (AUC) of blood glucose levels during OGTT assessment. (Tx Day 1 n = 7; Tx Day 14 n = 8; n = 2 batches of cyno isolations/encapsulations) (Mean \pm SEM).

Results indicate that short-term culture of 1.5 mm Ba^{2+} alginate encapsulated cyno islets does not significantly affect islet functionality or the ability of encapsulated islets to cure STZ induced diabetic nude mice (30 day cure rate: 88% vs. 86%); (AUC OGTT, $p = 0.43$). Cohorts of mice transplanted on day 1 and day 14 with the same number of encapsulated islets from the same preparation demonstrated similar blood glucose control. This suggests that functional islet masses can be maintained during short-term culture of encapsulated islets, which may not translate to naked islets due to reasons described above. Since encapsulated islets withstand culture for some time prior to transplantation, this may prove important for *in vitro* modulation of encapsulated islets to improve islet function or gene expression through the use chemical compounds during culture.

The previous GSIS results showed that initial glucose stimulated insulin secretion was rather low, and these levels rose after culture for 14 days. This would suggest that culture might actually improve encapsulated islet *in vivo* function. Results showed that short-term cultured islets functioned just as well as encapsulated islets transplanted immediately. This may provide further evidence that there is some islet recovery from the encapsulation process that occurs at similar rates during *in vivo* and *in vitro* culture situations.

Since encapsulated islets function can be maintained in culture for up to 14 days, transplantation into animals or patients does not have to occur immediately. This may prove vital for patients in the future to ensure that each batch of encapsulated islets functions adequately prior to transplantation. A few extra days will give investigators sufficient time to conduct proper quality control measures and analyze multiple islet potency assessments prior to transplantation. Also, this may be important if encapsulated islets from multiple donors are needed to achieve a significant islet mass and a high probability of successful reversal of diabetes in a single patient. It is difficult to perform multiple isolations and encapsulations on the same day. Furthermore, an immune-incompetent nude mouse model was used in

order to investigate the effect of short-term culture on purely islet functionality. It would be interesting to repeat this experiment using an immune-competent C57b/6 model to see if the immunogenicity of encapsulated islets is altered during short-term culture [105].

The 1.5 mm Ba^{2+} alginate encapsulated cyno islets were then retrieved from STZ diabetic nude mice. The *in vitro* assessments that were performed pre-transplantation were then performed on the retrieved encapsulated islets. The retrieved encapsulated cyno islets stained densely for DTZ staining (Figure 4-10). The islets also tended to become more compact in comparison to islets stained pre-transplantation. The capsules maintained their spherical integrity and exhibited very low cellular attachment or fibrosis.

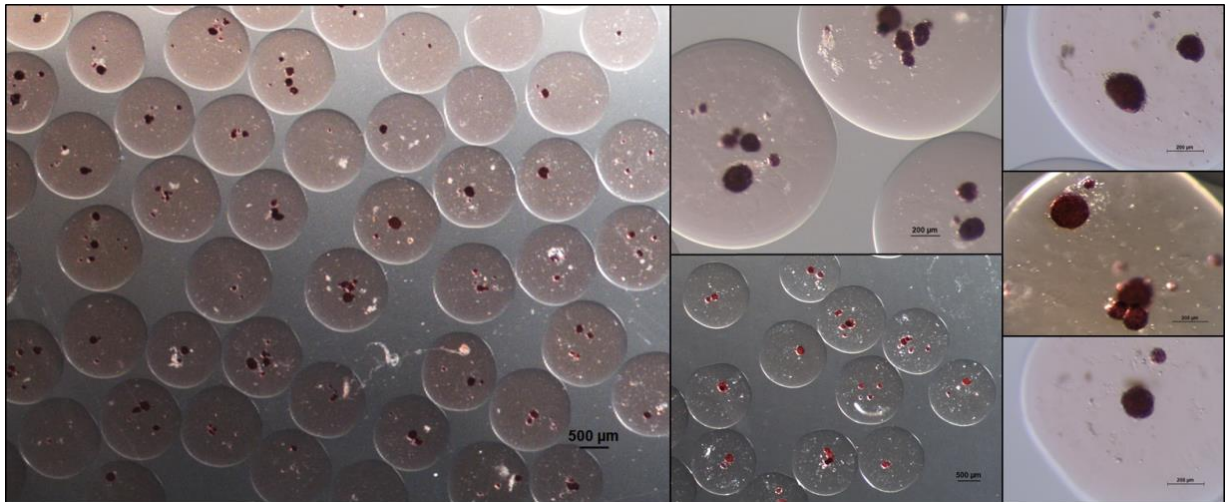


Figure 4-10: Dithizone (DTZ) staining of 1.5 mm Ba^{2+} encapsulated cynomolgus islets retrieved from STZ diabetic nude mice 30 days post-transplantation.

DTZ stained 1.5 mm Ba^{2+} encapsulated cynomolgus islets retrieved from STZ diabetic nude mice 30 days post transplantation (n = 3 separate batches of cyno isolations/encapsulations/retrieved mice).

The retrieved encapsulated cyno islets exhibited high viability scoring. Figure 4-11:B shows the presence of some pericapsular cell attachment on the surface of the encapsulated islets. This minimal fibrosis never escalated to complete coverage of the encapsulated islets in the nude mice.

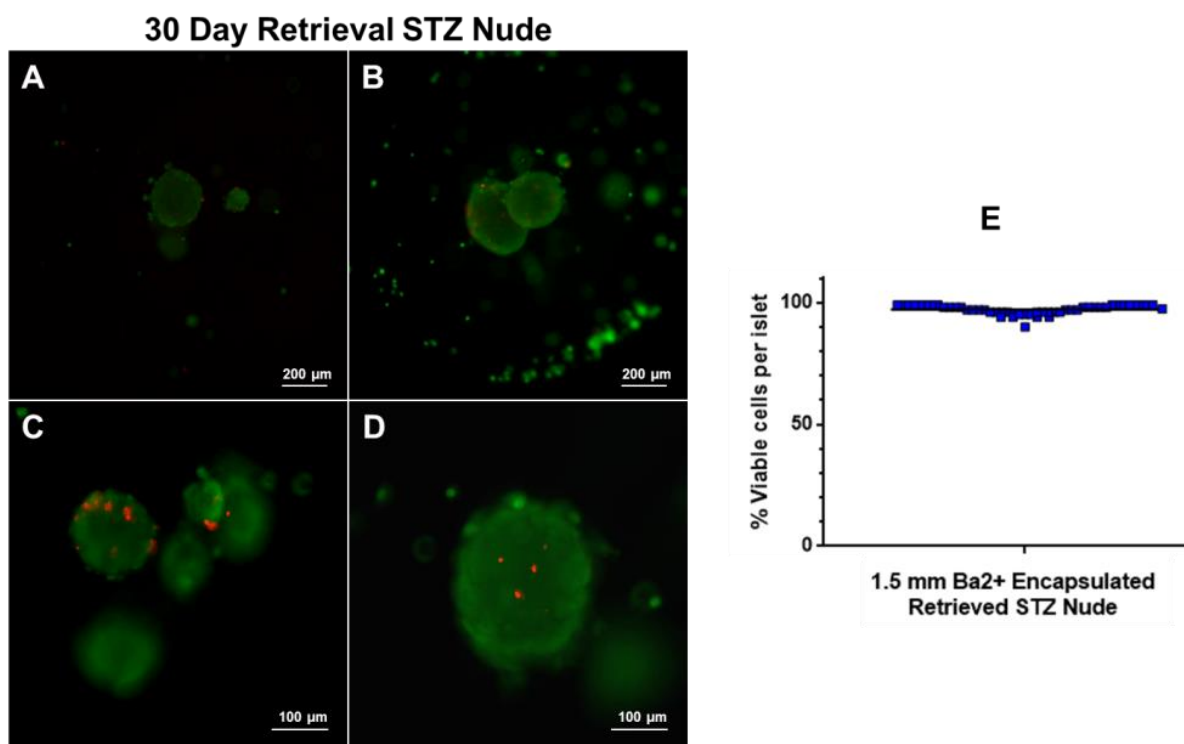


Figure 4-11: Viability of 1.5 mm Ba²⁺ alginate encapsulated cynomolgus islets retrieved from STZ diabetic nude mice 30 days post transplantation.

A/B) Viability staining of retrieved encapsulated islets from STZ diabetic nude mice (whole capsules). **C/D)** Islets. **E)** Scatter plot of estimated percentages of total viable cells in whole islets (n = 50 islets).

The retrieved encapsulated cyno islets were also tested using the GSIS assay and compared to pre-transplantation levels (Figure 4-12). The GSIS shows a decreasing trend in high glucose insulin release from encapsulated cyno islets after retrieval from STZ diabetic nude mice. This contrasts cultured encapsulated islets which demonstrated an increasing trend in high glucose insulin release after culture for 14 days.

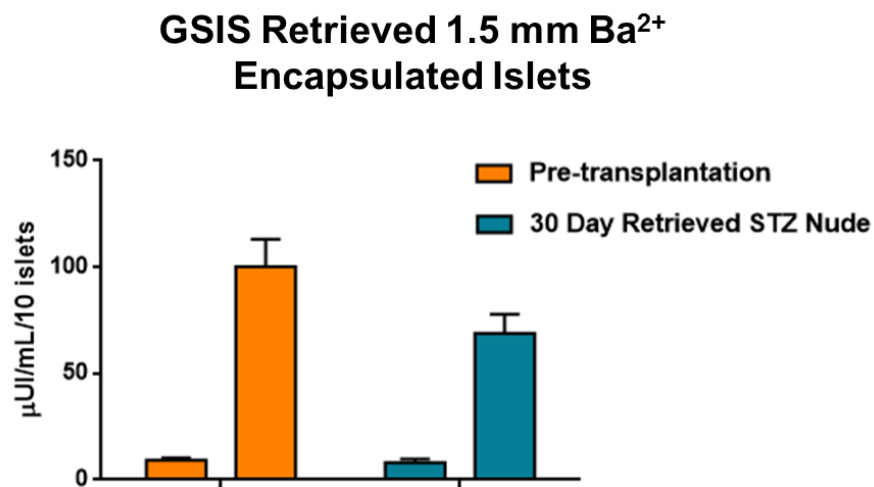


Figure 4-12: GSIS of 1.5 mm Ba²⁺ alginate encapsulated cynomolgus islets that were retrieved from cured STZ diabetic nude mice

Graph depicts total insulin secreted by 10 encapsulated islets in sieves when stimulated for 1 hr with low glucose (2 mM) and high glucose (18 mM). ($p = 0.051$) (Retrieved $n = 23$ sieves; 5 individual cured STZ nude mice; 3 separate isolations/encapsulations/transplants) (Pre-transplantation $n = 21$ sieves; 5 separate isolations/encapsulations) (Mean \pm SEM)

Previous experiments performed on retrieved encapsulated cyno islets, suggested that overnight culture is required to allow time for the islets to recover from the retrieval procedure. GSIS and intracellular calcium responses for retrieved encapsulated cyno islets were assessed immediately following retrieval and after 5 hours or overnight culture (Figure 4-13, Figure 4-14). Cultured retrieved cyno islets exhibited better functional responses in both assays so for all future assessments retrieved islets were

cultured overnight. Since there seems to be some recovery from the retrieval procedure, it is difficult to accurately assess how the islets were truly functioning in the *in vivo* situation. Upon retrieval, the encapsulated islets are stripped from their accustomed environment, and may experience different oxygen tensions and environmental cues. These may cause a lessened response compared to what the islets may have been secreting after engraftment in the mice. Nonetheless, if applying the same retrieval procedure for encapsulated islets that were transplanted into another animal model, GSIS levels can be reasonably compared to postulate if islet potency is sufficient to yield a high probability of reversing diabetes if enough islets are transplanted.

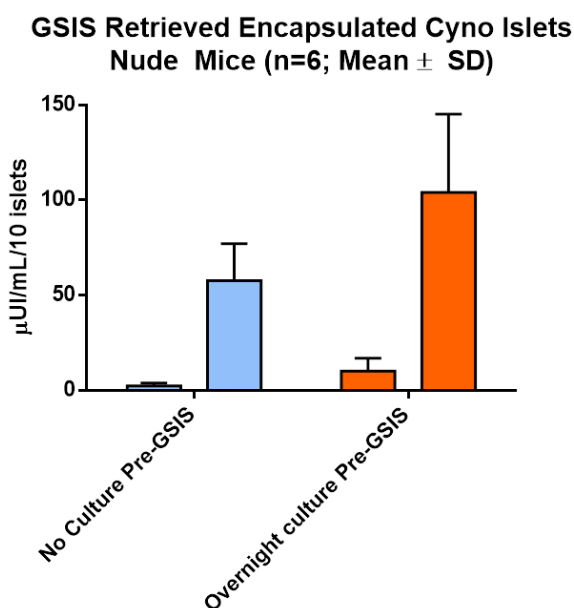


Figure 4-13: GSIS of encapsulated cyno islets performed immediately post retrieval from STZ nude mice and after over-night culture (1.5 mm Ba²⁺ alginate encapsulated cyno islets).

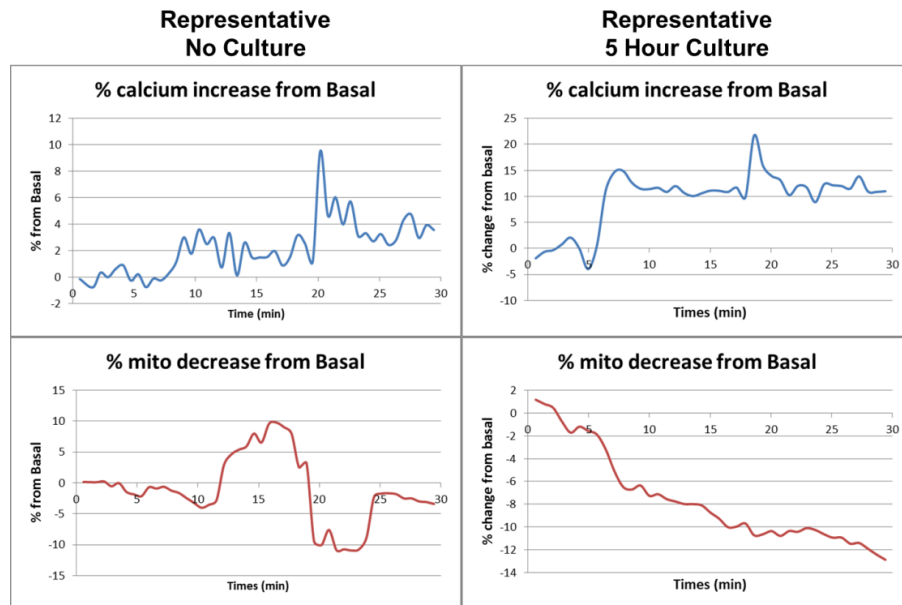


Figure 4-14: Representative intracellular calcium influx [ΔCa^{2+}]_i, and mitochondrial potential changes ($\Delta\Psi_m$) in response to insulin secretagogues of single encapsulated cyto islets performed immediately post-retrieval from mice and after 5 hour culture. (0.5 mM Ca^{2+} / Ba^{2+} alginate encapsulated cyto islets)

The retrieved encapsulated cyto islets were also evaluated for intracellular calcium influx [ΔCa^{2+}]_i, mitochondrial potential changes ($\Delta\Psi_m$), and insulin secretion in response to insulin secretagogues using a microfluidic based perfusion assay (Figure 4-15). Results indicate that there is a loss in the Fura-2 signaling for encapsulated cyto islets post retrieval from STZ diabetic mice. Fura-2 signaling is used to measure the intracellular calcium influx [Ca^{2+}]_i in response to insulin secretagogues. The changes in mitochondrial potential (Ψ_m) were found to be conserved for retrieved encapsulated islets and similar to profiles obtained for naked cyto islets that were performed pre-transplantation. Interestingly, insulin secretion for retrieved encapsulated islets was found to be similar to naked islets in response to insulin secretagogues. This insulin secretion contrasts predicted levels according to Fura-2 signaling. The starting baselines of the fluorescent intensities used to measure [Ca^{2+}]_i and (Ψ_m) were not significantly different between naked and retrieved encapsulated cyto islets.

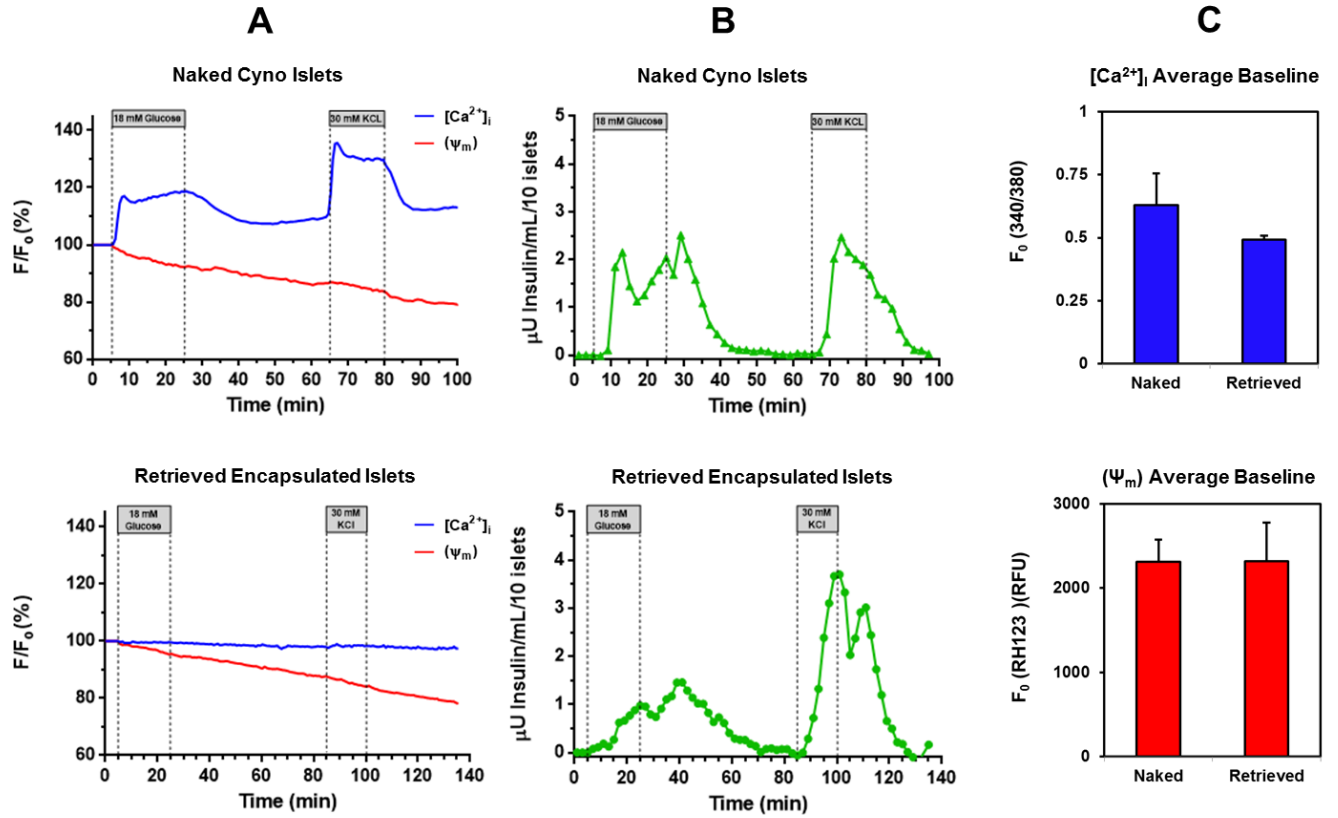


Figure 4-15: Intracellular calcium $[Ca^{2+}]_i$, mitochondrial potential (Ψ_m), and insulin secretion profiles of naked (pre-transplantation) and retrieved encapsulated cyno islets (STZ nude mice) in response to insulin secretagogues using a microfluidic-based perfusion assay.

A) Average intracellular calcium $[Ca^{2+}]_i$ responses and mitochondrial potential (Ψ_m) changes in response to insulin secretagogues of naked cyno islets and retrieved encapsulated cyno islets. **B)** Average insulin secretion in response to insulin secretagogues of naked cyno islets and retrieved encapsulated cyno islets. **C)** Average initial baseline fluorescent intensities of Fura-2 $[Ca^{2+}]_i$ ($F_0(340/380)$) and Rh123 (Ψ_m) ($F_0(RFU)$); (Mean \pm SD). (n = 3 runs per condition; 50 islets per run; 3 separate isolations/encapsulations/retrieved mice)

Intracellular calcium influx is a proximal trigger for the fusion of insulin granules to the plasma membrane and insulin exocytosis. This is why these results are so interesting. Retrieved encapsulated islets exhibited no intracellular calcium influx ($[\Delta Fura-2]_i$) but positive insulin secretion. At times,

poorly functioning islets will display no calcium influx in response to high glucose. These types of islets rarely cure STZ diabetic nude mice when transplanted into the kidney capsule. Nonetheless, there is almost always an intracellular calcium response after KCl stimulation, albeit sometimes very small percentages. The retrieved encapsulated islets demonstrated no change in Fura-2 signaling even under KCl stimulation.

Fura-2 is a fluorescent molecule that indirectly measures $[Ca^{2+}]$ concentrations by exhibiting a different excitation wavelength (340 nm) when bound with one Ca^{2+} ion. In a Ca^{2+} bound or unbound state, the Fura-2 molecule can be excited by 380 nm to give a measure of the total Fura-2 concentration in the cell [106]. The emission wavelength for Fura-2 is consistent at 510 nm even if excited at either wavelength. Thus Fura-2 is ratiometric and can measure the amount of bound Ca^{2+} ions in relation to the total amount of Fura-2 in the cells [107]. This is beneficial in measuring intracellular calcium levels since it eliminates confounding variables such as the amount of dye loaded per cell or factors that may diffract emitted light such as cell thickness [108]. As a change in Fura-2 signaling was non-existent for the retrieved encapsulated islets, we began to postulate possible explanations for this observed phenomenon.

Alginate is translucent so this should not have a substantial effect on excitation or emission spectra of the dye. Fura-2 measurements of the 1.5 mm Ba^{2+} encapsulated islets that were performed pre-transplantation also exhibited positive $[\Delta Fura-2]_i$ changes in response to insulin secretagogues (Figure 4-16). In a previous section, it was mentioned that we had determined that retrieved encapsulated cyno islets required a rest period prior to obtaining relevant intracellular calcium responses and GSIS insulin secretion. These particular experiments were performed on retrieved cyno islets that were encapsulated in 0.5 mm Ca^{2+}/Ba^{2+} alginate capsules (Figure 4-14). The same alginate was used for both sets of experiments so we determined that the only variables that had changed between the two experiments were the size of the capsules (0.5 mm vs 1.5 mm) and the amount of Ba^{2+} used during gelation (1 mM

vs. 20 mM). Since Fura-2 signaling could be measured in the large capsules pre-transplantation, we hypothesized that there seems to be an influence of Ba^{2+} on the Fura-2 measurements, and this only occurs after *in vivo* incubation.

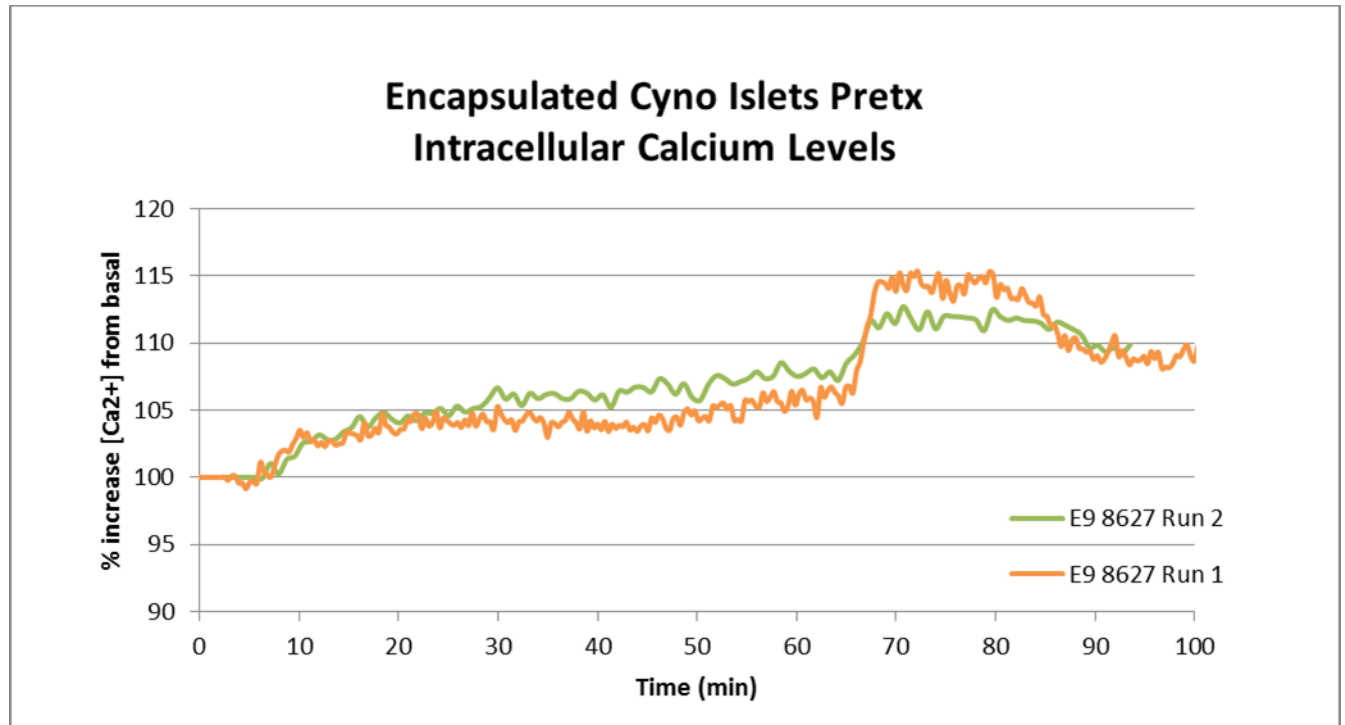


Figure 4-16: Intracellular calcium levels of 1.5 mm Ba^{2+} alginate encapsulated islets performed pre-transplantation (n = 2 runs; 50 encapsulated islets per run)

The main question to be determined was if the flat Fura-2 signaling was related to a change in the high barium alginate capsule material or something changed with the islets after *in vivo* incubation. We performed a series of experiments to begin probing the mechanism behind the loss of Fura-2 signaling. First, retrieved encapsulated islets were tested using a different calcium indicator Fluo-4. This indicator

exhibits different excitation/emission wavelengths (488/494 nm) to see if somehow the wavelengths of Fura-2 were distorted by the retrieved alginate [109]. Fluo-4 signaling was similar to the Fura-2 signaling so the wavelength of light used does not seem to be a contributing factor.

After incubating the retrieved islets with the fluorescent probes, it was observed under fluorescent microscopy that the islet cells exhibited decreased fluorescent intensity compared to pre-transplantation islet cells. The concentrations of the fluorescent probes were then doubled to investigate if intracellular concentrations of the dyes were too low for detectable changes. Increasing the concentration of Fura-2 similarly had no effect on Fura-2 signaling and remained flat despite an increased cellular brightness. This led us to believe that binding to alginate or free Ba^{2+} in the capsule material was not an issue. Experiments were also conducted using naked islets and Ba^{2+} in the perfusion solution instead of Ca^{2+} . Here we determined that in fact Ba^{2+} can enter the islets cells and can cause increases in $[\Delta\text{Fura-2}]_i$ signaling.

A literature search of Ba^{2+} and islets verified that Ba^{2+} can enter islet cells and result in insulin release by β -cells [110]. These references also noted that once Ba^{2+} enters the β -cells, it can become sequestered in intracellular organelles and has difficulty coming out of the cells [111]. If indeed barium is sequestered inside the islets, then one might expect higher initial ratiometric Fura-2 baselines due to an increase in the bound state of the dye. However, β -cells maintain strict balances of ion concentrations and potentials [112]. The sequestered barium may be compensated for by the β -cells through the maintenance of ion channels and intracellular ion concentrations at similar levels as if there were no sequestered barium. Fura-2 baselines may then not be higher due to the consistent ion concentrations in the cell. The islets may also compensate for the excess intracellular barium by not taking in as much calcium during stimulation. This small influx in calcium may not be detectable by the methods employed during these measurements. Although maybe unlikely, it might be plausible that β -cell physiology changes so

extracellular calcium does not enter cells but intracellular barium is released to cytoplasm. No changes in Fura-2 signaling may be observed if ion flux is all internally regulated and not influenced by extracellular ion populations. Many of these hypothesis hinge on the assumption that barium is being sequestered in the islets. Through the use of Electron Microscopy (EM), it may be possible to visualize if indeed there is barium accumulation within the retrieved islet cells.

Another plausible explanation for a lack of Fura-2 signaling that has been suggested is that the peripheral islet cells that are fluorescently imaged are non-functional; yet, islet cells in the inner core are functional and responsible for the insulin release. The fluorescent microscope used for imaging in the perfusion assay mostly measures the cells on the periphery of the islets due to resolution limitations restricted to peripheral cells in the focal plane [107]. Furthermore, the Fura-2 dye has been shown to penetrate only the superficial layers of islet cells [113]. Based on these observations, the peripheral cells in the islets may be the primary cells measured in the assay may not be functional. The inner cells of the islets cannot be measured using our current set-up and are the cells responsible for insulin secretion. Perhaps in the future using a combination of confocal fluorescent microscopy along with a Ca^{2+} indicator or conjugated delivery system (Au-nanoparticles) that can penetrate into the core of the islets, may be a method to resolve intracellular signaling at the cellular level of retrieved encapsulated islets. This technique would allow islet cells in the core to be resolved and compared to cells on the periphery of the islets. Also, investigating if insulin secretion can be blocked using various membrane ion channel agonists/inhibitors such as diazoxide and phenytoin may elucidate if ion channels sensitivities are altered for the retrieved encapsulated islets [114, 115].

These experiments and observations from the literature suggest that there is an effect of barium on islets and is likely in some way affecting our ability to measure Fura-2 and $[\text{Ca}^{2+}]$ changes for retrieved encapsulated islets. Since these observations only became apparent in 20 mM barium gelled alginate

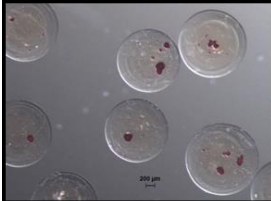

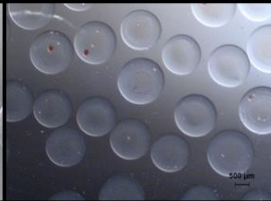

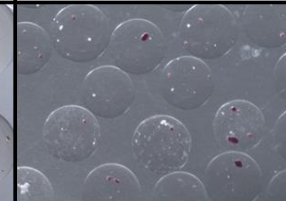
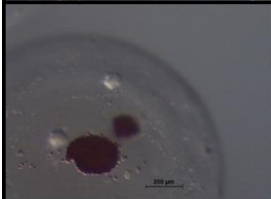
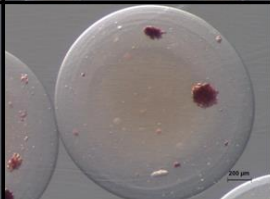

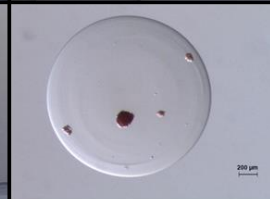
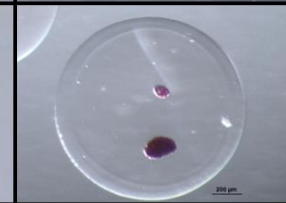
capsules and barium is known to exhibit cytotoxicity, the peripheral cells in the retrieved islets may be exposed to a higher concentration of barium after transplantation that renders these islet cells non-functional. Nonetheless, the importance of these results is difficult to ascertain since 1.5 mm Ba^{2+} alginate encapsulated cyno islets are functioning very well within diabetic mice models. Investigations concerning the effects of barium and islets are might be better suited to see if barium exposure affects the long-term duration of islet function. Also exploring patient safety with barium based capsules is important to discern if or how much barium leaks from the capsules, and if these levels can cause patient toxicity after transplantation.

4.3.3 In vitro and in vivo characterization of cynomolgus monkey islet functionality within large 1.5 mm Ba^{2+} chemically modified alginates using an allogeneic NHP transplantation model

Our collaborators at MIT not only determined that large 1.5 mm alginate capsules are more resistant to fibrosis after transplantation into the peritoneal cavity but also developed a series of chemically modified alginates that are resistive to cellular attachment and fibrosis [116]. Small capsules (0.3 mm) made of these chemically modified alginates are even resistive to fibrosis after transplantation in the peritoneal cavity of C57b/6 mice for two weeks. We then wanted to investigate the anti-fibrotic properties of these chemically modified alginates using a difficult cynomolgus monkey (NHP) transplant model. First, we laparoscopically transplanted empty 1.5 mm capsules that were made of the chemically modified alginate derivatives into the peritoneal cavity of naïve cynomolgus monkey recipients. These were retrieved after 2 weeks, 4 weeks and 6 months. Two modified alginate derivatives E9 and RZA15 were found to be mostly free of fibrosis even after 6 months post-transplantation. We then initiated encapsulation experiments to test the ability of the chemically modified alginate derivatives to protect encapsulated cyno islets using a non-immunosuppressed pre-clinical NHP allogeneic model.

The allo recipients were chosen to be non-diabetic in order to reduce the stress that hyperglycemia can have on islets. First, cyno islets were encapsulated in E9 and RZA15 chemically modified alginate derivatives at a low islet seeding density (1,000 islets/mL alginate or 0-2 islets per capsule). This approach was taken to reduce the potential stress to the encapsulated islets as the IP environment may have reduced nutritional provisions that may be compounded if too many islets are within one capsule. Also, the protective capabilities of the modified alginates could be adequately tested without potentially overwhelming the recipient immune system. All encapsulated cyno islets were prepared at the 1.5 mm size and gelled using a 20 mM BaCl₂ solution. A single donor was isolated for encapsulation batches, and each batch was transplanted into a single recipient primate. The large 1.5 mm Ba²⁺ plain alginate capsule (labeled SLG20) that was previously shown to be efficacious in the STZ diabetic mice was also transplanted into a primate. *In vitro* characterizations of encapsulated islet functionality were performed pre-transplantation and after 4 weeks post-transplantation in the NHP allogeneic transplant setting. Pre-transplantation DTZ staining is presented in Table III.

Table III: DTZ staining of encapsulated cyno islets prior to allogeneic transplantation
(Low islet seeding density)

Encapsulated Islet Transplantation using an NHP Allogeneic Transplant Model				
<ul style="list-style-type: none"> • Non-diabetic cynomolgus recipient to limit islet stress from hyperglycemia • 1.5 mm Ba²⁺ encapsulated cynomolgus islets using chemically modified and unmodified alginates • Low islet seeding density (1,000 islets/1 mL alginate or 1-2 islets per capsule) 				
PRE-TRANSPLANTATION (DTZ)				
SLG20-Allo-1	E9-Allo-1	E9-Allo-2	RZA15-Allo-1	RZA15-Allo-2
				
				

The capsules sizes for each batch of encapsulated cyno islets were on average 1.5 mm but did vary between 1.35-1.65 mm. At times the modified alginates do not form perfect spheres and have protrusions from the surface of the capsules. These were removed by visual inspection under brightfield microscopy and sterile forceps. Pre-transplantation encapsulated cyno islets demonstrated dense DTZ staining with little presence of cellular debris that was seen during some of the mice transplants. The SLG20 encapsulated islets were also prepared at a slightly higher islet seeding density of 1,500 islets/1 mL alginate in order to stay consistent with previous data obtained in mice.

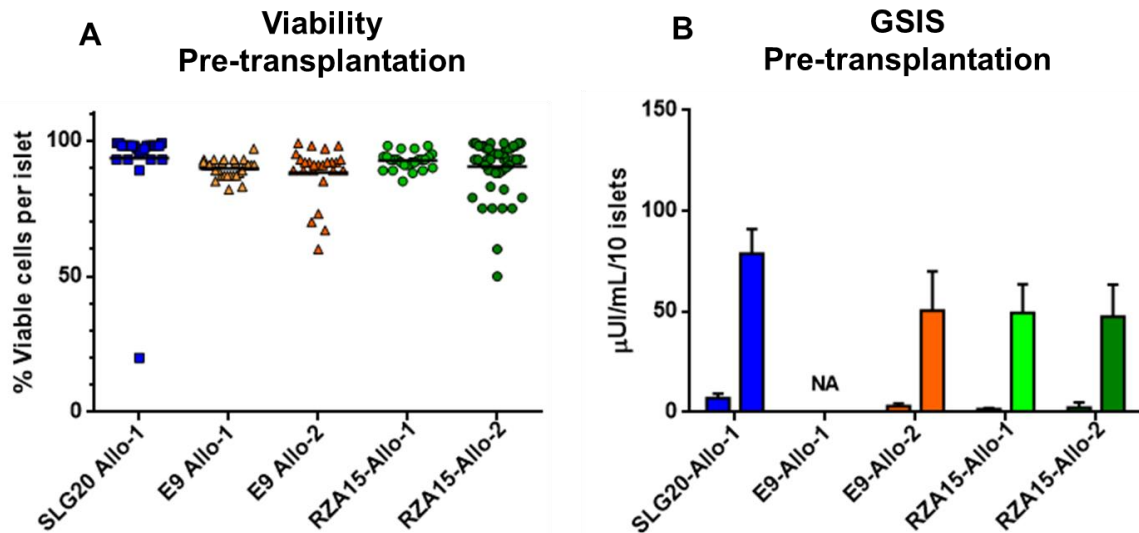


Figure 4-17: Viability and glucose stimulated insulin secretion (GSIS) of encapsulated cyno islets prior to allo-transplantation into non-diabetic recipients (Low islet seeding density).

A) Scatter plot of estimated percentages of total viable cells in whole islets for each batch of encapsulated islets ($n = 25-50$ islets). SLG20 is an unmodified alginate, E9 and RZA15 are chemically modified alginates. Each batch represents isolated/encapsulated islets from a single donor that was transplanted into a single recipient. **B)** Graph depicts total insulin secreted by 10 encapsulated islets in sieves when stimulated for 1 hr with low glucose (2 mM) and high glucose (18 mM). (Mean \pm SD; $n = 3-6$ sieves per batch).


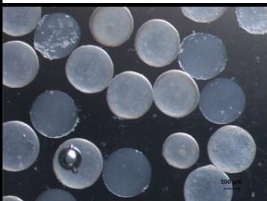
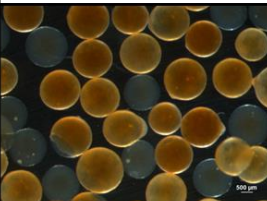
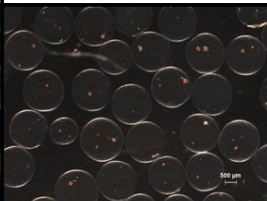
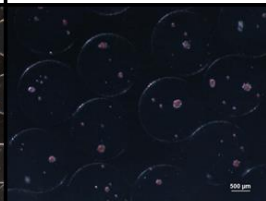

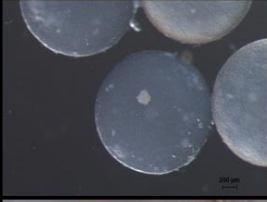
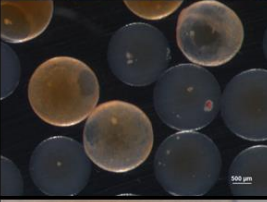
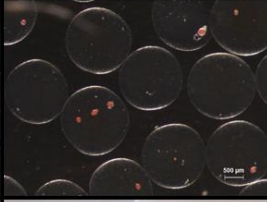
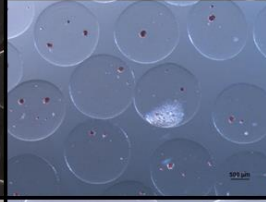




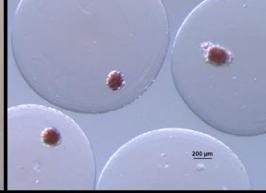
*E9-Allo-1 GSIS was performed with a previous protocol

** No significance between any groups (Viability/GSIS)

Viabilities for each batch of encapsulated cyno islets at the low islet seeding density were not found to be significantly different and on average had 90% viability. GSIS results also indicate that high glucose stimulated insulin secretion for each batch of the chemically modified encapsulated islets were not found to be statistically different. The SLG20 encapsulated islets did exhibit increased insulin secretion in comparison to the chemically modified alginates; yet, this may be attributed to the higher seeding density used during this encapsulation. The SLG20 encapsulated islets contained more islets per capsule and thus required less capsules to be picked to obtain 10 islets per sieve. The basal insulin secretion for

the SLG20 encapsulated islets was also comparatively higher than the chemically modified alginates. This may correlate to improper picking of islets or further suggest that insulin concentrations in the gels must equilibrate prior to being detected in the supernatant. This equilibration levels in the gels may be higher if more islets are encapsulated within one capsule.

Table IV: Brightfield and DTZ staining of retrieved encapsulated cyno islets following 4 weeks of allogeneic transplantation (Low islet seeding density).

Encapsulated Islet Transplantation using an NHP Allogeneic Transplant Model				
<ul style="list-style-type: none"> Low islet seeding density (1,000 islets/1 mL alginate or 1-2 islets per capsule) 				
4 WEEK RETRIEVAL FROM CYNO (DTZ)				
SLG20-Allo-1	E9-Allo-1	E9-Allo-2	RZA15-Allo-1	RZA15-Allo-2
				
				
				

Following 4 weeks post-transplantation into the peritoneal cavity of non-diabetic allogeneic recipients, the encapsulated islets were retrieved under laparoscopically by repeated lavage flushing with saline. Retrieved encapsulated islets were then processed for biocompatibility assessments (completed at MIT) and placed in culture for islet functionality assessments completed at UIC.

Results presented in Table IV suggest that plain alginate (SLG20) at the large 1.5 mm size cannot protect encapsulated islets in an allogeneic NHP setting. These encapsulated islets were not retrievable by lavage flushing and omental biopsies showed fibrosis with neovascularization around the encapsulated islets. Since this capsule type was only tested in one primate, distinct conclusions cannot be made. However these results showing a lack of protection are consistent with previous NHP allotransplants using plain alginate at the 0.5 mm size and small scale clinical trials [21, 35-38, 117, 118]. This is also interesting since this capsule type was shown to provide Xeno protection in a C57b/6 mouse setting (Figure 4-7).

Results of the E9 encapsulated islets show a mixture of capsules that were completely surrounded in fibrosis and relatively clean capsules with little cellular attachment. The first two images of E9-Allo-1 are unstained images, and the bottom image is an islet stained with DTZ. The majority of retrieved encapsulated islets for E9-Allo-1 exhibited few islet cells that stained positive for DTZ, even if there was no complete cellular coverage of the capsules. E9-Allo-2 images were all stained for DTZ, which gives capsules with complete cellular coverage an orange hue. Some retrieved E9 encapsulated islets that were free of fibrosis did stain positive for DTZ. No positive DTZ staining was found for islets within completely covered capsules. These mixed results do not show ideal islet protection by the E9 encapsulation material, but the small number of transplants ($n = 2$) make it difficult to draw definitive conclusions. Further transplant experiments using the E9 material are required and possibly additional

strategies during encapsulation may need to be implemented when combining fragile cyno islets with the E9 material.

Results of the RZA15 encapsulated islets were extremely positive with almost all capsules exhibiting none or little cellular attachment and overgrowth. The retrieved encapsulated islets at the low seeding density demonstrated positive DTZ staining for almost all the retrieved islets from both recipients. The RZA15 encapsulation material can protect functional islets for at least 1 month in an allogeneic NHP model (n = 2). RZA15 encapsulated islets have even demonstrated positive DTZ staining at 4 months post-transplantation (Figure 4-18).

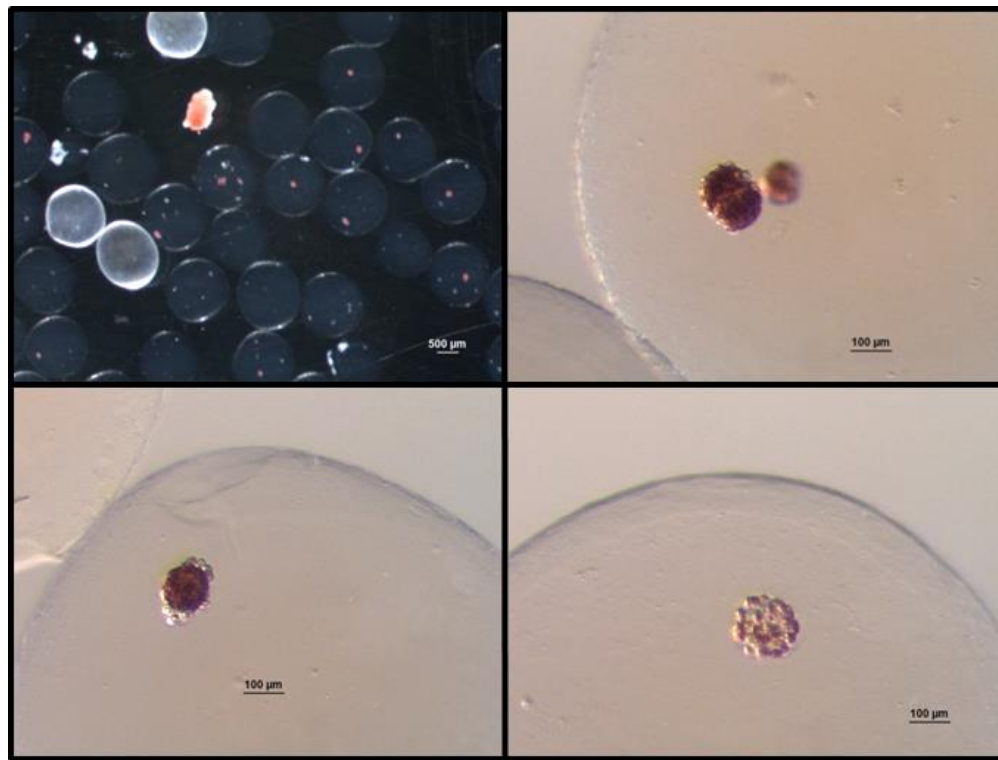


Figure 4-18: DTZ staining of RZA15-chemically modified alginate encapsulated cyno islets retrieved 4 months post-transplantation in non-diabetic cynomolgus recipient (n = 1)

Very few groups have shown encapsulated islet protection in a non-immunosuppressed NHP allogeneic transplant model [21, 119]. This demonstrates the great potential of the RZA15 chemically modified alginate material. Nonetheless, some interesting observations have been made related to the retrieved encapsulated islet morphology that may need to be investigated prior to evaluating encapsulated islet function in a diabetic primate model. The retrieved encapsulated islets tend to be smaller than pre-transplantation sizes. Furthermore, the majority of islets display hypertrophic peripheral cells that do not stain for DTZ. There is debate if these non-staining cells were originally endocrine islet cells or residual exocrine cells from the isolation process. Pre-transplantation DTZ images show islets of high endocrine purity without a skirt of exocrine non-staining cells. This suggests that the peripheral non-staining cells may not be exocrine tissue and are degenerated or hypertrophic islet cells. Cellular marker expression of

these cells would have to be investigated in order to make an accurate conclusion. If these cells in fact were once islet cells, the cause of this degeneration is unclear. The peripheral degeneration may be the result from proximity to the anti-attachment RZA15 material, an effect of islet hypoxia, an effect of damaging inflammatory cytokines such as TNF α or IFN γ , a combination of all, or another unknown contributor. Peripheral non DTZ staining cells have been obtained from plain alginate encapsulated islets retrieved from nude mice as well as long-term cultured islets (Figure 4-19). This makes it difficult to ascertain factors that may lead to the peripheral degeneration.

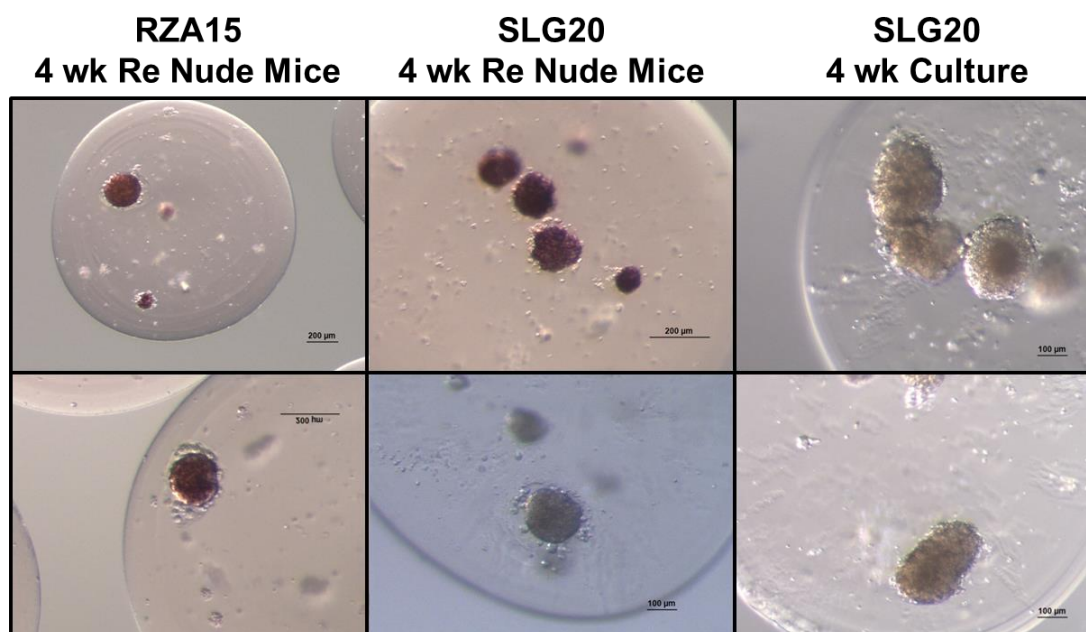


Figure 4-19: Peripheral degeneration of cells for encapsulated cyno islets after 30 day retrieval from nude mice (RZA15 and SLG20) and long-term cultured encapsulated islets (SLG20).

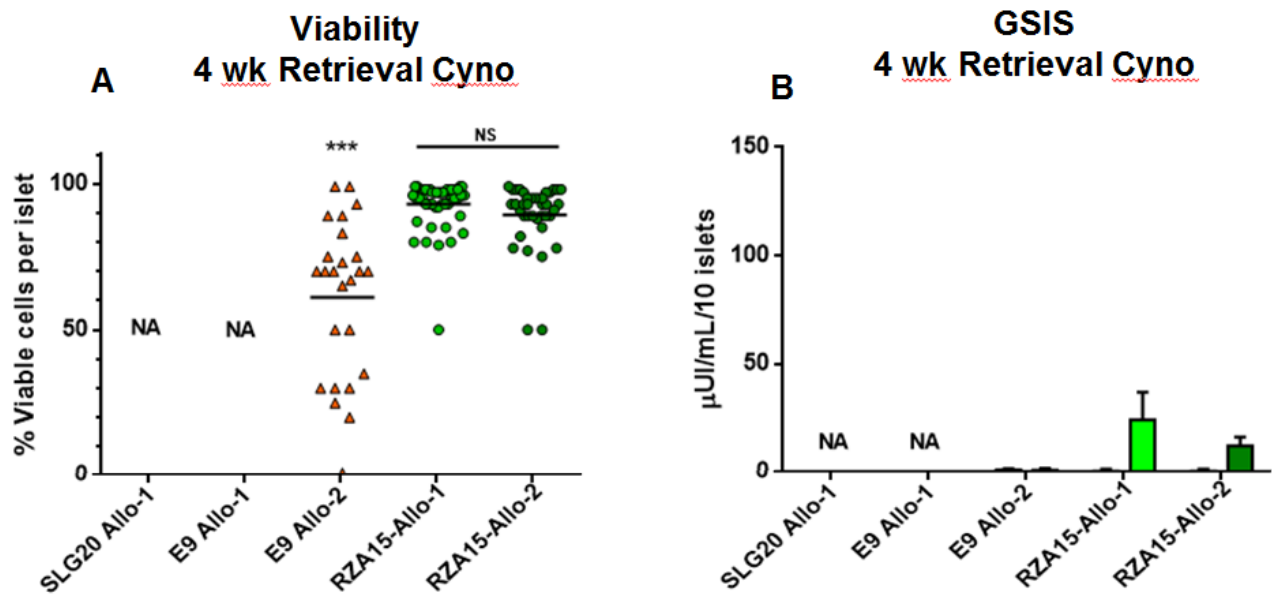


Figure 4-20: Viability and glucose stimulated insulin secretion (GSIS) of encapsulated cyno islets post 4 week retrieval from cynomolgus monkey recipients (Low islet seeding density).

A) Scatter plot of estimated percentages of total viable cells in whole islets for each batch of retrieved encapsulated islets (n = 25-50 islets). *** $p < 0.0001$ compared to pre-tx viability; NS (not significant) compared to pre-tx viability. **B)** Graph depicts total insulin secreted by 10 retrieved encapsulated islets in sieves when stimulated for 1 hr with low glucose (2 mM) and high glucose (18 mM). (Mean \pm SD; n = 6 sieves per retrieved batch).

* NA - SLG20 and E9-Allo-1 Viability and GSIS could not be performed due to fibrosis.

In vitro characterizations of the encapsulated islets that were retrieved from primate recipients 4 weeks post-transplantation show that the RZA15 encapsulated islets were viable and glucose responsive in the GSIS assay (Figure 4-20). Estimated islet viabilities of retrieved RZA15 encapsulated islets were not found to be significantly different when compared to pre-transplantation levels ($p = 0.22$). The amount of insulin secreted by the retrieved RZA15 encapsulated islets in response to high glucose was found to be significantly less than pre-transplantation levels ($p < 0.0001$). This trend was also seen during GSIS assessments of encapsulated islets retrieved from STZ diabetic mice ($p = 0.058$). Comparing stimulated

insulin levels for both pre-transplantation and retrieved RZA15 encapsulated islets from cynos to the pre-transplantation and retrieved SLG20 encapsulated islets from STZ nude mice, a decrease in stimulated insulin secretions was found ($p = 0.02$ and $p = 0.0003$; respectively) (Figure 4-21). However, different seeding densities were used for the encapsulation transplants. More islets per capsule may result in higher insulin concentrations in the supernatant by reaching insulin equilibration in the gels much faster. This may be indicated by the higher basal insulin secretion levels for the SLG20 encapsulated islets compared to the RZA15 encapsulated islets ($p = 0.0005$, pre-transplantation). Also, other factors associated with the procedure may affect the comparison of results. During the laparoscopic retrievals from NHP, the encapsulated islets cannot be placed in culture immediately due to sample processing and lab logistics. This is also comparing retrieval results from only two NHP. Overall, the GSIS results of the small set of retrieved encapsulated cyno islets from NHP display glucose responsiveness and are not out of the range for those obtained in cured STZ nude mice.

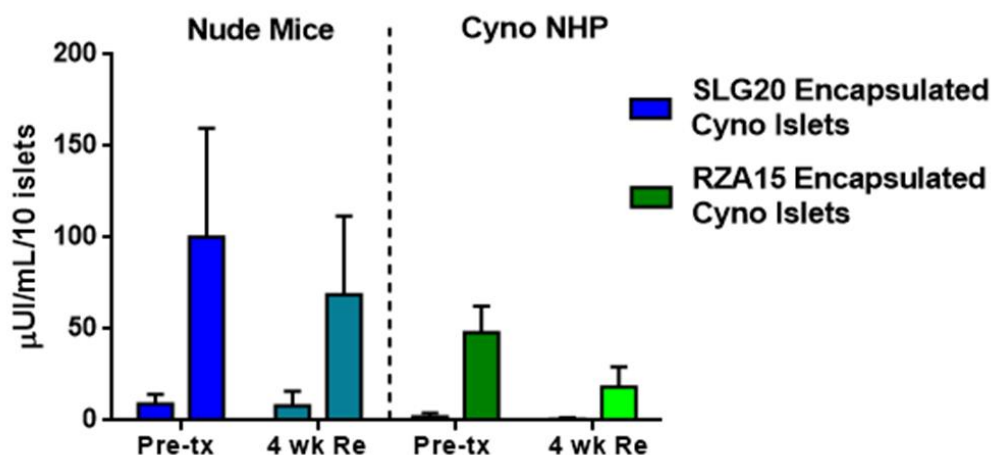


Figure 4-21: Average GSIS of retrieved encapsulated cyno islets from STZ nude mice (SLG20) and Cyno NHP (RZA15)

Average GSIS performed pre-transplantation and post retrieval for SLG20 encapsulated cyno islets retrieved from STZ cured mice and RZA15 encapsulated cyno islets retrieved from non-diabetic NHP. (Mean \pm SD).

*SLG20 (2-4 islets per capsule) (n = 21 sieves over 5 isolations/encapsulations/mice)

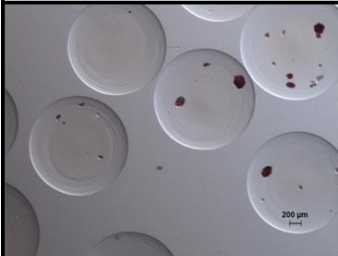
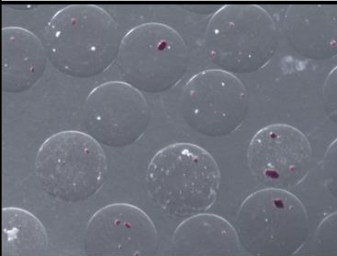
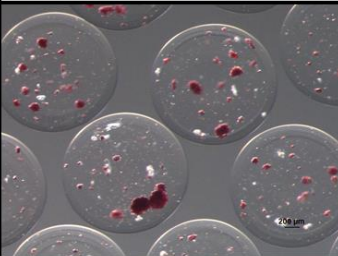
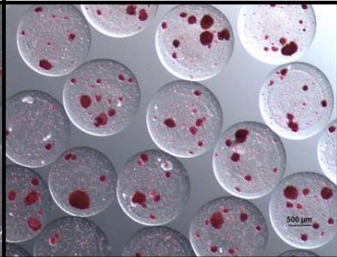
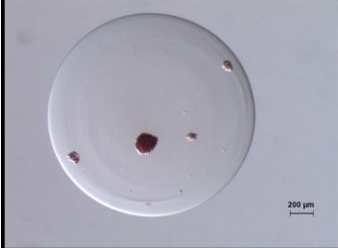
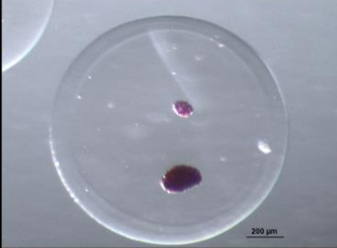


*RZA15 (1-2 islets per capsule) (n = 9 sieves from 2 isolations/encapsulations/NHP)

E9-Allo-2 displayed a mixture of viabilities with some viable islets and some islets completely dead. The overall poor viability was also verified in the GSIS, where the retrieved islets exhibited very minimal glucose-responsiveness. These levels should not be efficacious in curing diabetes in the case of these two transplant experiments. Interestingly, E9 in its empty state demonstrates biocompatibility that is similar to RZA15 in both mice and NHP. Long-term culture of E9 encapsulated cyno islets has also displayed positive functionality. A larger number of E9 transplant experiments are required to make an accurate assessment of the potential of this modified alginate.

The RZA15 modified alginate was shown to protect viable and functional islets in an allogeneic NHP transplant model at a low seeding density. Nevertheless, the number of islets transplanted at this density

may not be adequate to achieve a curative status in a diabetic NHP model considering transplant volume restrictions associated with large sized capsules. As many as 200,000 cyno islets may be required in order to cure a 4 kg weight cynomolgus monkey, and 200 mL of capsules would be too great a volume for the site. We then repeated the non-diabetic allogeneic transplants using a high islet seeding density of 4,000 islets/mL alginate or 4-10 islets per capsule. This approach might provide an islet dose at a reasonable volume of capsules that will have a high probability of achieving curative status in a diabetic NHP model. A caveat to more islets per capsule is that limited nutritional availability after transplantation might be too low. Many islets may consume oxygen at a higher rate than can diffuse into the capsule. Furthermore, more islets per capsule may cause increased leakage of immunogenic epitopes that alerts the immune system to the presence of foreign cells. However, this seeding density was successively applied using isolated rat islets transplanted into STZ diabetic C57b/6 mice at MIT and warranted an investigation. DTZ staining of RZA15 encapsulated islets at the high seeding density is presented in Table V.

Table V: DTZ staining of encapsulated cyno islets prior to allogeneic transplantation (High islet seeding density)

Encapsulated Islet Transplantation using an NHP Allogeneic Transplant Model			
<ul style="list-style-type: none"> • More islets per capsule may be required in order to reverse diabetes with a limited transplant volume available • Experiments were repeated with lead material RZA15 and a High islet seeding density (4,000 islets/1 mL alginate or 4-10 islets per capsule) 			
PRE-TRANSPLANTATION (DTZ)			
RZA15-Allo-1	RZA15-Allo-2	RZA15-Allo-3	RZA15-Allo-4
			
			
Low Seeding Density		High Seeding Density	

Encapsulated islets at the high seeding density show dense DTZ staining of the cyno islets. These encapsulated islets also display variable populations of single and small clusters of cells dispersed throughout the capsules. This was comparatively much higher than encapsulated islets at the low seeding density. *In vitro* islet functional assessments were performed pre-transplantation and after 4 weeks post-retrieval from non-diabetic allogenic NHP. Capsule characteristics in terms of size were found to be consistent to low islet seeding density experiments. Isolated islets from two donors were used for RZA15-Allo-3, and isolated islets from one donor were used for RZA15-Allo-4.

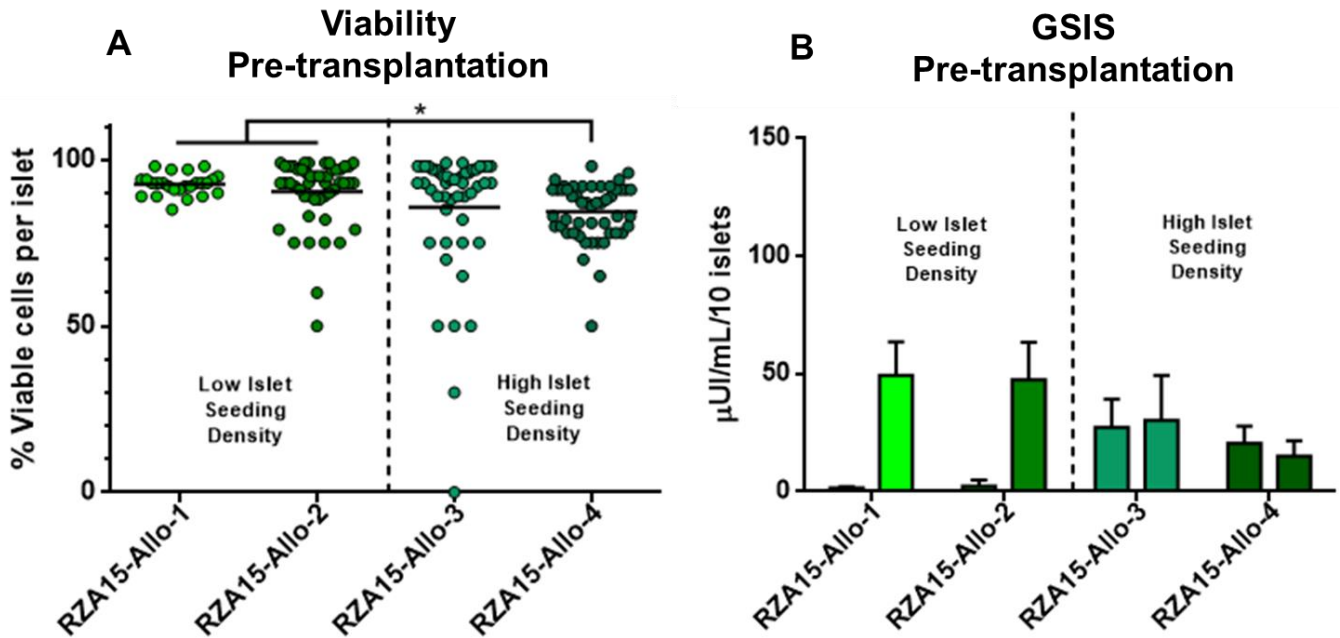


Figure 4-22: Viability and glucose stimulated insulin secretion (GSIS) of encapsulated cyno islets prior to allo-transplantation into non-diabetic recipients (High islet seeding density).

A) Scatter plot of estimated percentages of total viable cells in whole islets for each batch of encapsulated islets ($n = 25-50$ islets) (* $p < 0.01$) **B)** Graph depicts total insulin secreted by 10 encapsulated islets in sieves when stimulated for 1 hr with low glucose (2 mM) and high glucose (18 mM). (Mean \pm SD; $n = 3-6$ sieves per batch).

The viability of transplanted encapsulated islets at the high density (RZA15-Allo-4) was found to be significantly lower when compared to the low density encapsulated islets ($p < 0.01$) (Figure 4-22). RZA15-Allo-3 displayed lower islet viability, but this was not found to be significantly different ($p = 0.11$). GSIS performed pre-transplantation showed that the high density encapsulated islets displayed minimal or no glucose responsiveness. These encapsulated islets also displayed high basal insulin secretion compared to previous low density RZA15 experiments. It was suggested previously that high basal secretion may be related to stressed or improperly functioning islets. However, the basal insulin secretion of high density encapsulated cyno islets manufactured for another experiment displayed

similar high basal insulin secretion. In this experiment, 4 batches of cyno islet encapsulations at the high density were manufactured using various washing protocols in an attempt to remove cellular debris seen at the high densities (Figure 4-23). These encapsulated islets also demonstrated similar high basal insulin secretion. Even so, a comparatively higher glucose stimulated insulin response was achieved for the non-transplanted batch of islets. The comparative poor glucose responsiveness of the transplanted encapsulated islets suggests that the RZA15 islets used for transplantation into the NHP may not have been of ideal quality. Also, the consistent high basal insulin levels seen in the multiple batches of encapsulations at the high density may provide further justification that more islets per capsule results in higher insulin concentrations in the supernatant by reaching insulin equilibration in the gels much faster. Overall, the lower viability and GSIS results suggest that these two batches of high density RZA15 encapsulated islets were not high quality islet preparations.

**GSIS High Density Encapsulated Cyno Islets
(n=6 per purification protocol)**

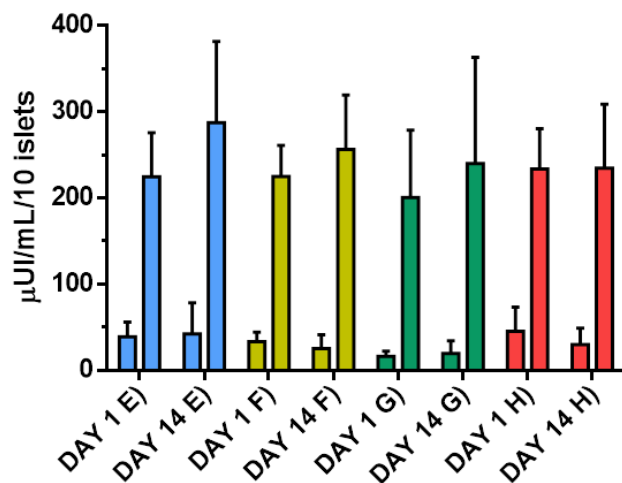
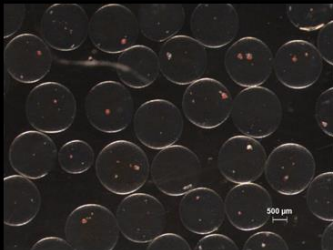
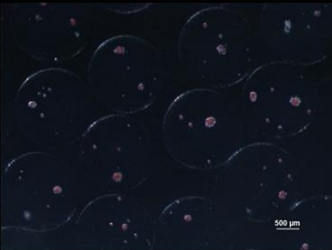

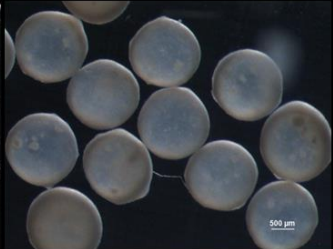
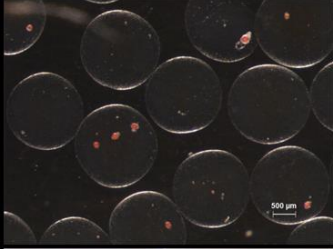
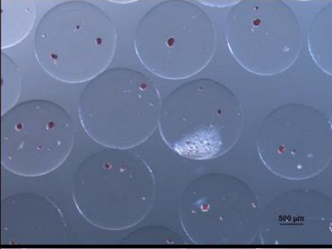


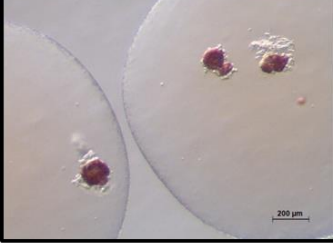
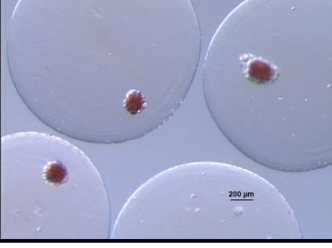




Figure 4-23: GSIS of encapsulated cyno islets at the high seeding density using 4 purification protocols

Purification protocols were applied to cyno islets prior to encapsulation: **E/F** used minimal centrifugation (1x) during the rinsing of islets with HBSS without calcium or magnesium. **G/H** used centrifugation (3x) during the rinsing of islets with HBSS without calcium or magnesium. **E/G** incorporated an additional step of gravity sedimentation of islets in 50 mL culture media for 15 min (2x), prior to beginning the rinsing procedures with HBSS without calcium or magnesium. No reduction in cellular debris within the encapsulated islets were observed under brightfield microscopy. (n =6 sieves per group; Mean \pm SD; same islet batch; one experiment)

Table VI: Brightfield and DTZ staining of retrieved encapsulated cyno islets following 4 weeks of allogeneic transplantation (High islet seeding density).

Encapsulated Islet Transplantation using an NHP Allogeneic Transplant Model			
<ul style="list-style-type: none"> RZA15 High islet seeding density (4,000 islets/1 mL alginate or 4-10 islets per capsule) 			
4 WEEK RETRIEVAL FROM CYNO (DTZ)			
RZA15-Allo-1	RZA15-Allo-2	RZA15-Allo-3	RZA15-Allo-4
			
			
			
Low Seeding Density		High Seeding Density	

RZA15-Allo-3 encapsulated islets at the high density were retrievable but showed a mixture of capsules completely covered with overgrowth and capsules with no cellular attachment upon 4 week retrieval post-transplantation. Some of the clean encapsulated islets did stain positive for DTZ, but many islets also exhibited no staining and appeared degenerated. RZA15-Allo-4 encapsulated islets were found to be opaque and adhered to omental tissue. Very few encapsulated islets could be retrieved. The small

sample of capsules obtained displayed complete coverage by overgrowth, and the inner islets appeared dark and degenerated. The functional assessments of RZA15-Allo-3 were found to be very similar to E9-Allo-2 at the low seeding density. The encapsulated islets were a mixture of very viable and completely dead islets (Figure 4-24). These islets also demonstrated minimal glucose responsiveness in the GSIS assay.

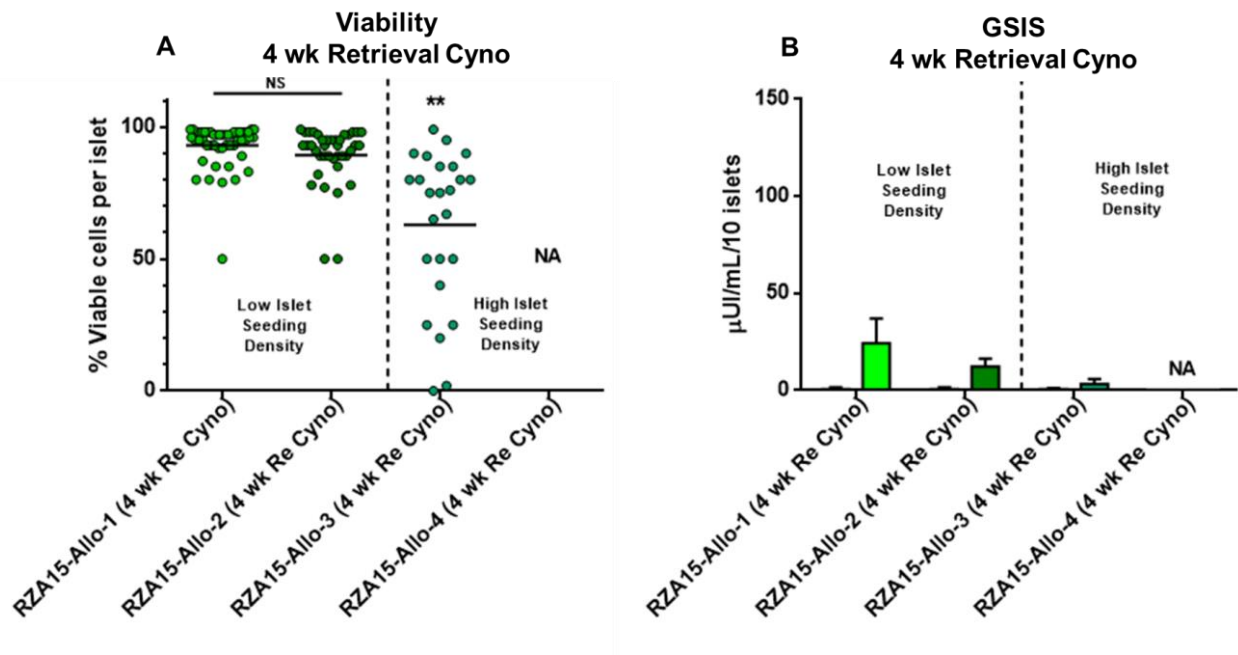


Figure 4-24: Viability and glucose stimulated insulin secretion (GSIS) of encapsulated cyno islets post 4 week retrieval from cynomolgus monkey recipients (High islet seeding density).

A) Scatter plot of estimated percentages of total viable cells in whole islets for each batch of retrieved encapsulated islets (n = 25-50 islets). ** $p < 0.001$ compared to pre-tx viability; **B)** Graph depicts total insulin secreted by 10 retrieved encapsulated islets in sieves when stimulated for 1 hr with low glucose (2 mM) and high glucose (18 mM). (Mean \pm SD; n = 6 sieves per retrieved batch).

* NA – RZA15-Allo-4 Viability and GSIS could not be performed due to fibrosis.

The RZA15 encapsulation material did not provide ideal protection for the encapsulated islets at the high seeding densities in the case of these two allogeneic NHP transplantations. However, encapsulated islets characterizations that were performed pre-transplantation suggest that further testing is required to determine RZA15 protection at the higher islet seeding density. The encapsulated islets used for these transplants did not appear to be of ideal quality by exhibiting lower viability and poor insulin secretion responses pre-transplantation. The lower islet quality may have activated the recipient immune systems and led to the poor transplantation results. In statistical analysis, positive associations were found between pre-transplantation viability and GSIS with post-transplantation retrieval outcomes for the RZA15 high seeding densities. This was determined by comparing pre-transplantation viability and GSIS of the RZA15 low islet seeding density with their positive retrieval outcomes. Interestingly, no associations between pre-transplantation viability and GSIS were found for transplantation outcomes of the different encapsulation materials at the low islet seeding density. For the low density experiments, batches of encapsulated islets in the different encapsulation materials demonstrated similar viability and GSIS pre-transplantation. This suggests that pre-transplantation results of viability and GSIS assays may be predictive of transplantation outcomes; yet, there are other factors involved that lead to the success or failure of transplanted encapsulated islet grafts that may not be predicted using these two assays.

Pre-transplantation DTZ staining showed the presence of cellular debris throughout the high density capsules when compared to the low density capsules. This cellular debris may have increased the leakage of immunogenic epitopes from dead or dying cells that led to an activation of the recipient immune systems. The cellular debris could have also resulted in a higher probability of cells protruding from the capsule surface or incomplete encapsulation. This cellular exposure may also have led to an activation of the recipient immune systems. Furthermore, RZA15-Allo-4 demonstrated a greater degree of cellular debris, and these encapsulated islets were comparatively all engulfed in cellular overgrowth.

RZA15-Allo-3 encapsulated islets demonstrated less cellular debris and were found to be only partially overgrown. These factors associated with the high cellular debris and potentially poor islet quality may have led to the poor transplantation results, yet the exact method of rejection seen in these two transplants is still unknown.

Also, it cannot be disregarded that the RZA15 material cannot protect functional islets at the high seeding density in the peritoneal cavity of NHP. Nutritional availability in the site might be too low to support that many encapsulated islets per capsule. The deprived islets may have secreted factors such as high mobility group box 1 (HGBM-1) or MCP-1, which then resulted in fibrosis of the encapsulated islets [13, 46, 47]. Nonetheless, in order to accurately investigate the ability of RZA15 to protect functional islets at the high density, certain strategies should be employed. Elimination of the cellular debris seen at the high densities is required before accurate assessments can be made.

Preliminary experiments have modified the washing procedures pre-encapsulation in hopes of elimination of the cellular debris seen within the capsules. Various washing protocols were employed using gravity sedimentation to remove fragmented islets that tend to settle at slower rates due to higher drag forces on the fluffy islets. Also, passing the islets through a 40 μ m cell strainer can remove small cellular debris without the loss of many small islets. These techniques were applied for the experiment previously described (Figure 4-23) with no significant improvement in the removal of the cellular debris. It is still unclear where the cellular debris originates from. This may be due to forces associated with encapsulation and passing a highly concentrated number of islet particles from a 5 mL syringe through a small gauge needle. Passing densely concentrated particles through a small diameter opening may cause some of the islets to become dissociated. Also, cyno islets are rather fragile and often slightly fragmented from the isolation procedure. The islets are not as compact as rat or human islets, and

peripheral cells that are not tightly integrated into the islet ECM may become dislodged from the islet surface from shear forces when mixing with the rather viscous alginate solutions.

An experiment was performed where human islets were cultured for 4 days and then encapsulated at low, medium and high islet seeding densities (Figure 4-25). There appeared to be no cellular debris even at the high islet seeding density. These islets were more compact to start and not fragmented compared to cyno islets that were encapsulated at the high densities. This suggests that the debris seen with encapsulated cyno islets may be resultant from the shear forces stripping peripheral cells when mixing with the alginate solution and not as dependent on the encapsulation parameters. However, due to the fragile nature of cyno islets the effect of encapsulation parameters cannot be disregarded. It may prove interesting to encapsulate cyno islets first in alginate using calcium as a gelation solution. These types of capsules can be easily dissolved by a calcium chelator such as EDTA or sodium citrate [7]. After dissolving the encapsulated islets and removing the cellular debris, the encapsulated islets can be re-encapsulated to investigate where the cellular debris originated. If this method can successfully remove the cellular debris, then this strategy could be employed for future RZA15 encapsulations of cyno islets at the higher seeding density. If the cellular debris is not removed, then changes to the encapsulation system will have to be modified or a different seeding density may have to be considered.

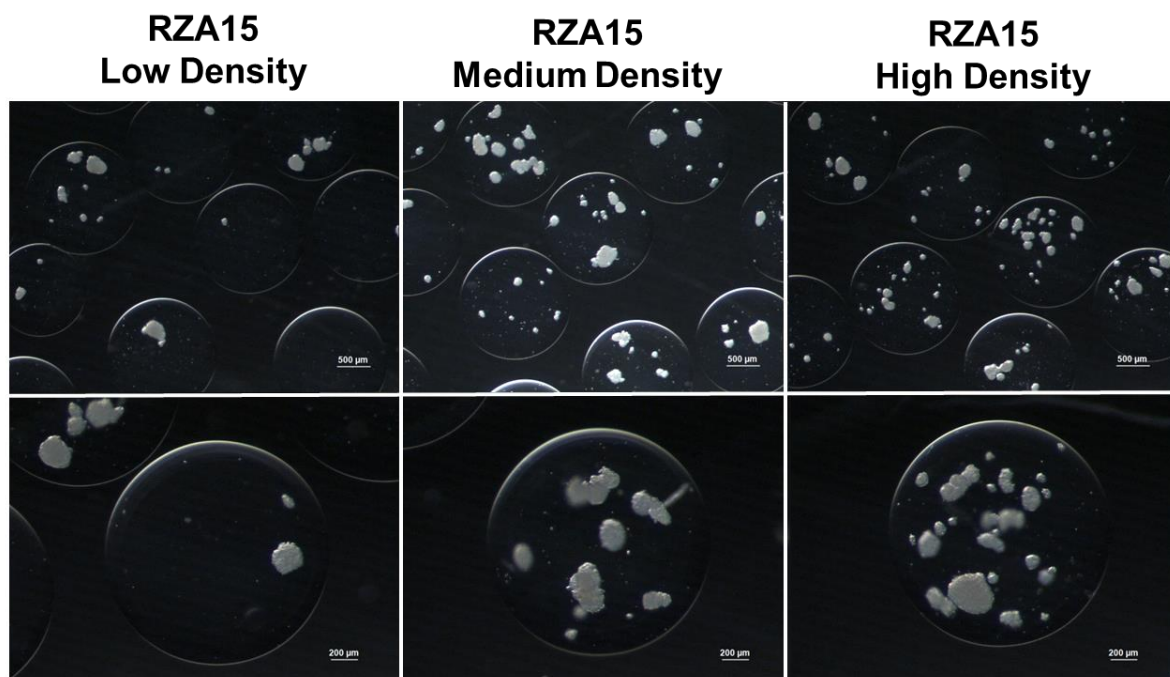


Figure 4-25: Encapsulated human islets within chemically modified RZA15 alginate 1.5 mm Ba²⁺ at low, medium, and high islet seeding densities.

Human islets from the same preparation were cultured for 4 days prior to encapsulation. Three islet seeding densities were investigated low, medium and high, (1,000, 2,000, and 4,000 islets per 1 mL alginate; respectively). Representative brightfield images.

Another important detail learned during the high density RZA15 transplantations into NHP is that it is important to ensure islet quality is satisfactory prior to transplantation. It may not guarantee success but should give a higher probability of success instead of retrospective analysis showing islet quality may not have been ideal. Since short-term culture of encapsulated islets has been shown not to have a detrimental effect on islet functionality *in vitro* and in STZ nude mice, culturing encapsulated islets for a few more days prior to transplantation may not greatly affect transplant outcomes in the allogeneic NHP transplant model. These few extra days should be sufficient in order to obtain all the results of the

functional assessments so a more enlightened decision can be made if the encapsulated islets are suitable for transplantation.

4.4 Conclusion: Large 1.5 mm encapsulated islets

Large 1.5 mm Ba^{2+} alginate encapsulated islets were shown to demonstrate adequate functionality in both *in vitro* and *in vivo* assays. Islet stimulation kinetics by small molecular weight secretagogues was shown to be unaffected by encapsulation or capsule size. For insulin release kinetics, encapsulated islets experience a loss of phase I insulin secretion and an initial delay in glucose-stimulated insulin secretory kinetics. However, bulk insulin kinetics is well conserved between encapsulated rat islets at different sizes and was found to be similar to naked rat islets.

To investigate *in vivo* islet functionality, large 1.5 mm Ba^{2+} alginate encapsulated cyno islets were transplanted as a marginal islet transplant mass into various STZ diabetic mouse models. The large encapsulated islets were found to cure immune-incompetent STZ nude mice similarly to naked islets transplanted into the kidney capsule. The same marginal islet transplant mass cured STZ immune-competent C57b/6 mice for up to 180 days. The effect of short-term culture on encapsulated islet functionality was also tested. It was found that large 1.5 mm Ba^{2+} alginate encapsulated cyno islets cured STZ nude mice similarly no matter if transplanted immediately on day 1 or after 14 days of culture.

Most importantly, cyno islets were encapsulated in large 1.5 mm chemically modified alginates that have been found to be resistive to fibrosis and transplanted into an NHP allogeneic transplant model. Here, preliminary data suggests the RZA15 chemically modified alginate at the large 1.5 mm size can protect functioning allogeneic islets. This was evidenced by capsules almost completely free of cellular attachment. The retrieved encapsulated islets were found to be viable, DTZ positive and glucose

responsive 4 weeks post-transplantation into a non-immunosuppressed allogeneic NHP transplant model. Indeed certain hurdles may have to be overcome such as peripheral islet cell degeneration, determination and execution of the optimal islet seeding density for encapsulated islet transplantation, or even islet potency assurances before immune-isolation technologies can be implemented in the clinic. Yet this is a huge leap forward in the encapsulation field, and the chemically modified materials display characteristics that may prove vital for a plethora of biomedical applications in the future.

5 A NOVEL ENCAPSULATOR FOR THE CONTINUOUS PRODUCTION OF CAPSULES WITH CONTROLLED SIZE AND GELATION TIME

5.1 Introduction

Islet encapsulation represents an interesting challenge that encompasses diverse fields such as islet physiology, polymer science, engineering, and medicine. Expertise from each specialty is required to ultimately design an encapsulation system that is suitable for future clinical application of encapsulated islet technologies. There are many excellent cell encapsulation systems on the market, yet many of these devices are not suitable for islets. Islets are rather fragile cell clusters with complex intracellular machinery that is imperative for the proper function of the cells. Encapsulation systems that impose high shear stresses or harsh chemical environments may damage the delicate cellular machinery and are not ideal for islet encapsulation.

Islet clusters vary in size from 50-400 μm and can exhibit irregular shapes at times. This further complicates the encapsulation process since their diverse size and shape inevitably produces an inhomogeneous solution when mixed with polymers. Also, polymers themselves can behave inhomogeneously through chain-chain interactions, which are not seen with small-molecule solutions. This overall inhomogeneity in the polymer and islet solution leads to variable fluid dynamics and fluctuating magnitudes of force that are applied to the polymer droplets during extrusion. Furthermore, polymer interactions with extrusion components that have surface imperfections from improper manufacturing can compound the variations. Overall, these inconsistencies during islet encapsulation can cause polydispersity in droplet sizes and affect results. The polydispersity of hydrogels seen with encapsulation devices currently in practice can be controlled by adjustments made by very skilled

technicians. However, this showcases another limitation of islet encapsulation systems currently in practice. They are highly artisanal and require much experience to make precise adjustments to the encapsulation system in order to produce monodisperse, uniform batches. This operator dependency hinders the widespread application and dissemination of a defined and reproducible encapsulation product suitable for clinical applications.

5.1.1 Physics behind encapsulation droplet formation

Encapsulation of cells within polymer hydrogel systems is a fairly simple process. The cells must be first mixed with a polymer, and then dripped into a gelation bath that solidifies the polymer as a gel. The cells thereby become trapped within the matrix. Depending on the system employed, gel formation can occur through ionic cross-linking with divalent cations in the case of alginate or by poly-electrolyte complexation between a negatively charged polymer and positively charged polymer in the case of membrane core systems [2, 120]. The manufacturing process of spherical hydrogels uses a simple process of extrusion through a narrow opening such as a cylindrical nozzle, yet there are many physical factors that can influence the size of the droplets, and ultimately the size of the spherical hydrogels formed.

During droplet formation of the polymers, there is competition between two main forces. The polymer experiences an attractive force to the nozzle/extrusion orifice material as well as surface tension due to the spherical nature of droplets [121]. For simplification, this will combined as surface tension. Eventually, the droplet on the tip of the nozzle will grow larger and larger until the downward force becomes too great and overcomes the surface tension at the nozzle/polymer interface. This causes the droplet to break from the nozzle and fall into the gelation bath for solidification. In the case of cell encapsulation, it is important to tightly regulate these two opposing forces in order to generate spherical hydrogels with of a homogeneous size, especially if desired in the sub-millimeter range (Figure 5-1).

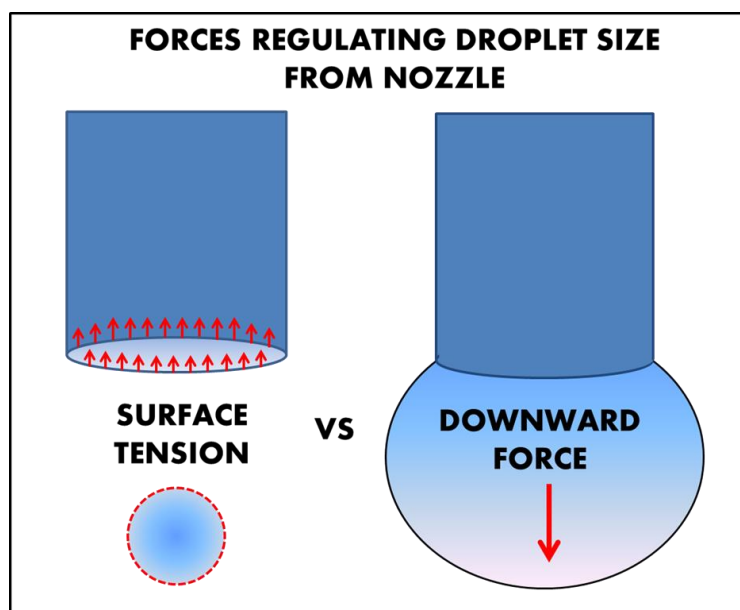


Figure 5-1: Competitive forces regulating droplet size during encapsulation and spherical hydrogel formation



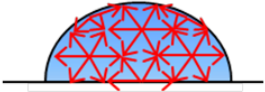

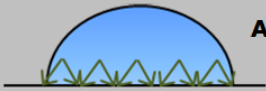

The basic principles of encapsulation systems consist of competition between attractive and downward forces applied to the polymer solution. Droplet formation occurs once a critical magnitude of downward force is reached that breaks the surface tension at the nozzle/polymer interface. Characteristics of both the polymer solution and the encapsulation parameters can affect the attractive forces and magnitude of applied forces, which eventually controls the droplet size and hydrogel sphere diameter.

This is a simple way to describe encapsulation by the opposing forces of surface tension and downward force during droplet formation. However, there are both characteristics of the polymer solution as well as the encapsulator machine parameters that will affect the magnitude of each of the governing forces. By altering these magnitudes, the diameters of the resulting droplets can become either smaller or larger. Thus it is important to understand how each will affect the physics of droplet formation in order to obtain desired sizes.

Polymers are made of repeated molecules that are bonded together often in a strand. Each polymer has unique properties that are defined by the type of repeated molecule and the amount of repeats per strand

[122]. Since these characteristics can vary from polymer to polymer, it is important to classify some of the important polymer characteristics that will affect droplet formation (Table VII). One of the main characteristics of polymers is the viscosity or fluid resistance to movement under an applied force. A viscous polymer solution has a higher degree of surface tension at the tip of the nozzle. This requires a higher magnitude of downward force in order to break the surface tension at the nozzle interface.

Table VII: Polymer characteristics that affect size of droplet formation during encapsulation

Polymer Characteristics		
Physical Property	Description	Affecting Variables
	<p>Fluid resistance of movement under applied force</p> <p>↑ Viscosity = ↑ Surface Tension (γ)</p> <p>↑ Viscosity =  Diameter</p>	<ul style="list-style-type: none">• Polymer Concentration• Molecular Weight• Temperature
Molecular self-interaction		
	<p>Cohesion</p> <p>↑ Cohesion = ↑ Surface Tension (γ)</p> <p>↑ Cohesion =  Diameter</p>	<ul style="list-style-type: none">• Polymer chemical backbone• Molecular side groups
Molecular interaction with materials		
	<p>Adhesion/Friction</p> <p>↑ Adhesion = ↑ Surface Tension (γ)</p> <p>↑ Adhesion =  Diameter</p>	<ul style="list-style-type: none">• Hydrophillic attraction• Hydrophobic repulsion

Cohesion, or how the molecules of the polymer interact with each other, can also affect the degree of surface tension at the tip of the nozzle. If the molecules interact with each other to a great extent, this will require a larger amount of downward force to be applied in order to break the self-interaction and surface tension for droplet formation. Similarly, adhesion or how the polymer molecules interact with the nozzle surface will affect the degree of surface tension at the nozzle interface. If there is a high degree of hydrophilic attraction to the metal nozzle, this will require a larger amount of downward force to be applied in order to break the attraction for droplet formation.

On the other hand, the downward force that is applied to the polymer droplet is largely controlled by parameters of the encapsulation system that is employed during manufacture. The downward force applied to the polymer droplet in a very simple encapsulation system can be gravity. This is the case of a nozzle suspended above the gelation bath. Engineers have also found that other forces can be applied to the polymer as it is extruded through the nozzle, and the magnitudes of the applied forces can tightly regulate the size of the droplets formed. There are various types of forces that have been employed in cell encapsulators (Figure 5-2). These include air stripping, electric potential (electrostatic devices), vibrational, and microfluidics [2, 123-127]. By altering the magnitude of these applied downward forces, the size of the droplets formed can be controlled.

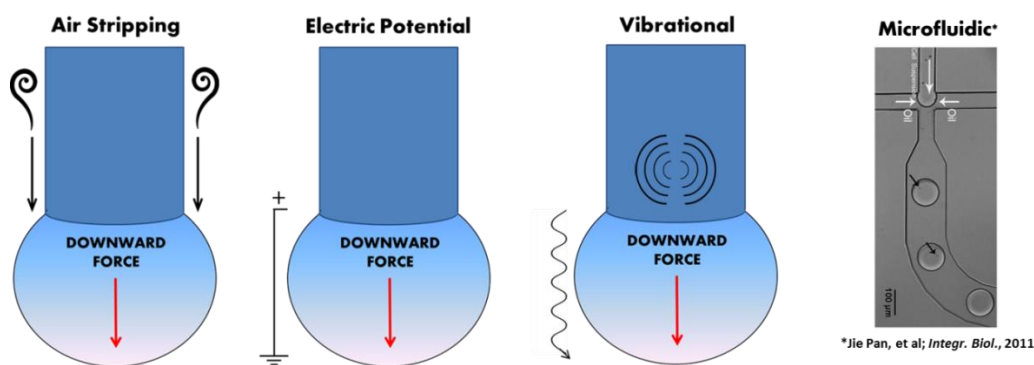


Figure 5-2: Types of encapsulation apparatuses currently available and the downward forces employed to control droplet sizes

Air stripping encapsulation consists of a coaxial nozzle system where pressurized air in the outer nozzle strips polymer droplets from the inner concentric nozzle that feeds the polymer solution.

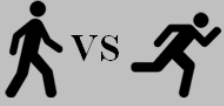
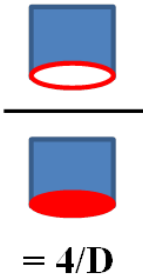
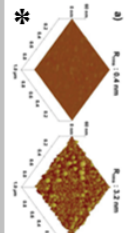
Electrostatic encapsulation applies an electric potential between the tip of the nozzle and the surface of the gelation bath that pulls polymer droplets toward the gelation bath.

Vibrational encapsulation applies frequencies to a steady stream of flowing polymer solution. This creates sine waves through the polymer solution that induces surface tension driven formation of droplets prior to entering the gelation solution.

Microfluidic encapsulation applies device geometry governed fluidic dynamics on immiscible solutions (hydrophilic vs. hydrophobic) to induce droplet formation and gelation.

There are characteristics of the encapsulator and manufacturing process that will also have an effect on the magnitude of force that is applied to the droplets (Table VIII). For instance, the flow rate of the polymer solution used during encapsulation can affect droplet size. The polymer fluid speed limits the time the forces are applied to the droplets [128]. A higher flow rate results in less applied force and thus larger diameter hydrogels [129].

Table VIII: Encapsulator characteristics that affect size of droplet formation during encapsulation

Encapsulator Characteristics		
Physical Property	Description	Affecting Variables
 Flow Rate	<p>Fluid speed limits the magnitude of forces applied to the needle/droplet</p> <p>↑ Flow Rate = ↓ Downward Force</p> <p>↑ Flow Rate = ● Diameter</p>	<ul style="list-style-type: none"> • Syringe pump flow rate (Q) • Pressure driven flow rate (Q)
 Nozzle Inner/Outer Diameter/Gauge	<p>Larger diameter decreases surface area contact to volume ratio for polymer adhesion to nozzle</p> <p>↑ Gauge = ↓ Surface Tension/Volume Ratio</p> <p>↑ Gauge = ● Diameter</p>	<ul style="list-style-type: none"> • Surface area in contact with polymer
 Nozzle Roughness	<p>Rough surfaces increase surface area for polymer adhesion</p> <p>↑ Roughness = ↑ Surface Tension (γ)</p> <p>Inhomogeneous and Satellite Droplet Formation</p>	<ul style="list-style-type: none"> • Roughness (RMS) • Nozzle manufacture

* Shekhar Agnihotri et al, *Nanoscale*, 2013

The inner diameter of the nozzle used during encapsulation will also affect the droplet size. A larger diameter nozzle makes contact with a smaller volume of the polymer. The decreased surface area to volume ratio of the polymer solution for large diameter nozzles decreases the attractive forces of the polymer solution with the nozzle. This reduction in attraction of the polymer with the large diameter nozzle allows for larger diameter hydrogels. The diameter of the inner nozzle also controls what diameters of hydrogels are obtainable [130]. It is not possible to obtain hydrogel diameters smaller than

the inner diameter of the nozzle [127]. It is possible to generate hydrogel diameters slightly larger than diameter of the nozzle, but as a rule of thumb, the inner diameter of the nozzle should be around half the diameter of the desired hydrogels.

The roughness and shape of the nozzle can also affect the diameter and the homogeneity of hydrogels. A very rough inner nozzle or high RMS has a larger molecular surface area for the polymer to interact. This creates a higher surface tension and requires a larger amount of applied force to break into droplets. A rough or imperfect nozzle surface also results in inhomogeneity of the polymer hydrogels [131]. Polymers can also display some innate heterogeneity based on self interaction. Any imperfection in the nozzle surface will compound any heterogeneity in the polymer solution to produce aberrant droplets and heterogeneity in the spherical hydrogel product. Imperfectly manufactured nozzles can also result in satellite droplet formation. These miniscule droplets 20-50 μm in diameter can be generated if the polymer solution is too diluted or exhibits low viscosity. The satellite droplets can then become integrated and gelled on the surface of the larger hydrogel spheres. This can compromise the integrity of the spherical nature of the surface of the hydrogels and may lead to pericapsular fibrotic overgrowth.

Overall, it is important to understand how characteristics of both the polymer solution and the encapsulator machine parameters will affect the physics behind droplet formation and solidification of spherical hydrogels. The operator is then better equipped to fine tune the encapsulation process to manufacture homogeneous spherical hydrogels suitable for transplantation.

5.1.2 Apparatuses available for islet encapsulation and current limitations

Many of the encapsulators currently in practice for single cell encapsulation work very well. However, many the apparatuses do not take into account the unique parameters that must be satisfied when encapsulating islets. Islets are clusters of 1,000-2,000 excitable cells [132]. β -cells, which are the major

cell type that constitutes islets, are responsible for insulin secretion in response to high glucose [14]. These cells are particularly sensitive and their intracellular machinery such as mitochondria, which are required for glucose-sensing and insulin secretion, can become easily damaged [133]. Furthermore, islets are typically isolated from cadaveric donor pancreata. Islet isolation often results in minimal numbers of extracted islets and these clusters of cells do not proliferate substantially [19]. For this reason, encapsulators that apply high shear stresses or encapsulate cells extremely quickly may not be ideal for islet encapsulation.

One such example is the vibrational encapsulator. In order to encapsulate cells, a continuous flow of polymer solution is extruded through the nozzle. The applied vibrational sine waves travel through the continuous stream of polymer solution and induce surface tension to break the stream into polymer droplets [134]. The polymer droplets then become gelled in the gelation solution in individual particles. The Buchi Encapsulator B395 Pro™ is such an encapsulator that works very well to produce large quantities of encapsulated single celled organisms at various sized hydrogels [135]. After testing this machine in Bratislava, Slovakia, it was observed that this encapsulation system may not be ideal for islet clusters (Figure 5-3).



Figure 5-3: Buchi Encapsulator B395 Pro™ testing with PMCG polymer system.

The Buchi Encapsulator B395 Pro™ from Switzerland uses vibration or frequency driven generation of polymer droplets. During testing for future application of this machine with the PMCG microcapsule system, it was discovered that this machine requires high polymer flow rates with potentially high shear stresses that may not be ideal for islet encapsulation. Optimization of encapsulation parameters for polymers with various viscosities may also hinder the application of this machine for islet encapsulation in the future.

The vibrational sine waves through the polymer solution might be impeded by the presence of islets. The inhomogeneous islet/polymer solution may then result in inhomogeneous droplet formation. Most importantly, this encapsulation apparatus requires a continuous stream of polymer extrusion, and consequently, very high flow rates through the nozzle. This high flow rate allows for quick encapsulation of the cells; however, this also means that there is very little room for quality control measures during encapsulation. This reduces the time to make adjustments to achieve homogeneously sized hydrogel spheres. If the parameters of encapsulation are slightly off, all the islets will be

encapsulated without the ability to finely tune the droplet formation. If the resulting hydrogels are not of ideal quality, the entire batch of isolated islets may be wasted. Also, the vibrational system is flexible with various polymer solutions, yet requires testing to determine optimal apparatus parameters for these systems. This includes optimization of frequency and flow rate to obtain homogeneously sized particles of the particular polymer system. Since polymer characteristics such as viscosity may vary from one polymer system to another, and these properties may also be influenced by the presence of islets, the determination of the optimal parameters for the encapsulator may be difficult to attain. This may limit the uniform application of the vibrational system as there are many encapsulation materials currently researched with islets [136].

Another system employed for cell encapsulation is microfluidic based devices [124, 125, 137]. These systems can produce uniform sized hydrogels; however their small geometry, can at times become clogged by debris within the device [81, 138]. This is particularly important considering islets, which range in size from 50-400 μm on average [132]. Furthermore, the microfluidic based systems currently in practice, do not have capacity for large scale production. There is potential to multiplex microfluidic systems and encapsulate large batches of islets in the future, yet no such microfluidic system exists on the market today.

Air stripping is a common method employed for islet encapsulation [2, 139]. The method uses a system of coaxial and concentric nozzles with air jet production of polymer droplets (Figure 5-4:A). Once the ideal distances between nozzle components and the flow rates of polymer/air have been determined, the droplet formation/hydrogels are very homogenous [140]. The difficulty with the air stripping method lies with completely concentric alignment of the coaxial nozzles. Otherwise, the mechanical stripping forces driving the polymer droplet formation will be variable. For this reason, the current air stripping nozzles require the operator to tweak the inner and outer nozzles until they are perfectly aligned. This

can take some time and makes the system heavily dependent on the operator. The operator must be highly trained in order to adapt and finely-tune parameters for ideal homogeneous encapsulation.

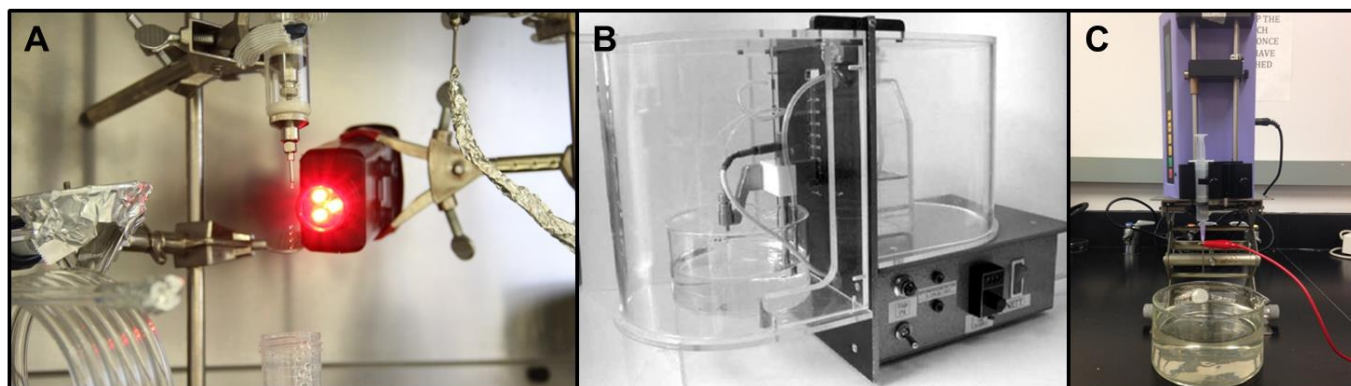


Figure 5-4: Current encapsulation apparatuses available for islet transplantation

A) Air stripping encapsulator with loop reactor for controlled gelation time of hydrogel spheres (Polymer Institute of the Slovak Academy of Sciences, Bratislava, Slovakia). **B)** Electrostatic microbead generator in-house encapsulator (Norwegian University of Science and Technology (NTNU), Trondheim, Norway). **C)** Simplified electrostatic encapsulator (Massachusetts Institute of Technology (MIT), Cambridge, Massachusetts).

The requirement for a technically trained operator is a limitation to the universal application of the current coaxial nozzle system by hindering translation to multiple institutions across the globe. Nonetheless, the air stripping encapsulation system used for the production of PMCG capsules employs the loop reactor apparatus (US patent # 6001312 A). The loop reactor is continually refilled with gelation solution, which allows for controlled gelation of the hydrogel system (Figure 5-5). This is imperative for membrane core polymer encapsulation systems (PMCG) since the time in gelation solution determines the thickness of the membrane that is formed [2]. The loop reactor also permits continuous production of encapsulated cells within spherical hydrogels. This reduces the number of

batches that must be performed in order to encapsulate a large batch of isolated islets. Furthermore, the time the islets spend in the gelation solution can be controlled to minimize the time islets may be exposed to chemicals that may be detrimental to islet functionality [141].

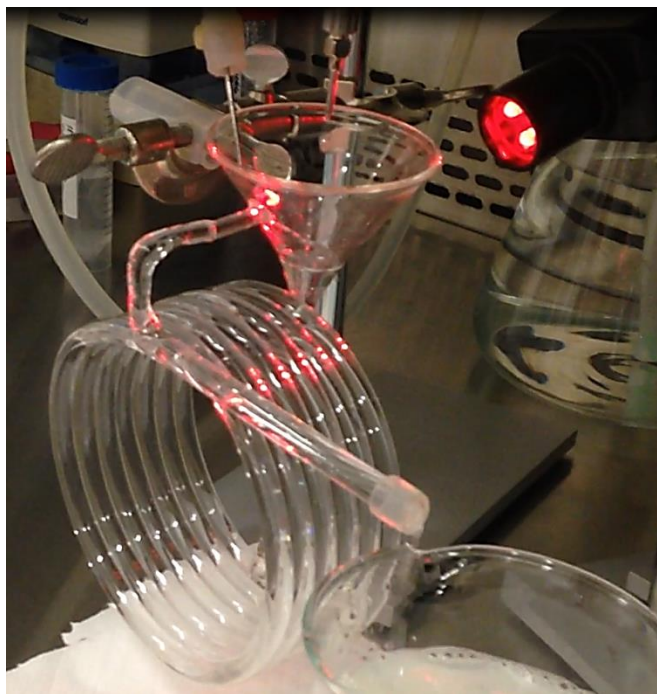


Figure 5-5: Loop reactor for continuous production of hydrogel spheres with controlled gelation time.

Gelation solution is continually circulated through the loop reactor which allows for the continuous production of hydrogel spheres. The flow rate of the gelation solution determines the amount of time the hydrogel spheres are in the gelation solution (gelation time).

The electrostatic system applies a voltage potential between the tip of the nozzle and the surface of the gelation bath. Two versions of the electrostatic system (in-house versions) were employed during studies (Figure 5-2:B/C). The major benefit to electrostatic encapsulation is its simplicity and reproducibility. It can produce homogeneous batches of hydrogel spheres at various sizes simply by altering the applied

voltage potential (Figure 5-6). This is possible with very little operator dependency. Once the ideal voltage for a specific polymer system is determined, very few adjustments must be made in order to produce multiple large batches of homogeneously sized hydrogels. Although there is potential for large batches of encapsulated islets, current electrostatic systems must use multiple batches to limit the time islets are within the gelation bath. Islets are sensitive cells and cannot be left in the high concentration of ions or potentially toxic cross-linkers for too long [141, 142]. Thus it is possible to encapsulate rather large batches of islets using electrostatic systems, but this requires some hours of manufacture to produce repetitive batches of encapsulated islets. Lastly, the two electrostatic systems employed in studies had variable safety precautions for the operator. For one system, the high voltage could only be activated once the housing unit was secured, which is safer for the operator and more appropriate for clinical practice. The other system employed open encapsulation where the operator may be exposed to high voltage. Extreme care was taken when using this system to ensure no operator exposure to high voltage.

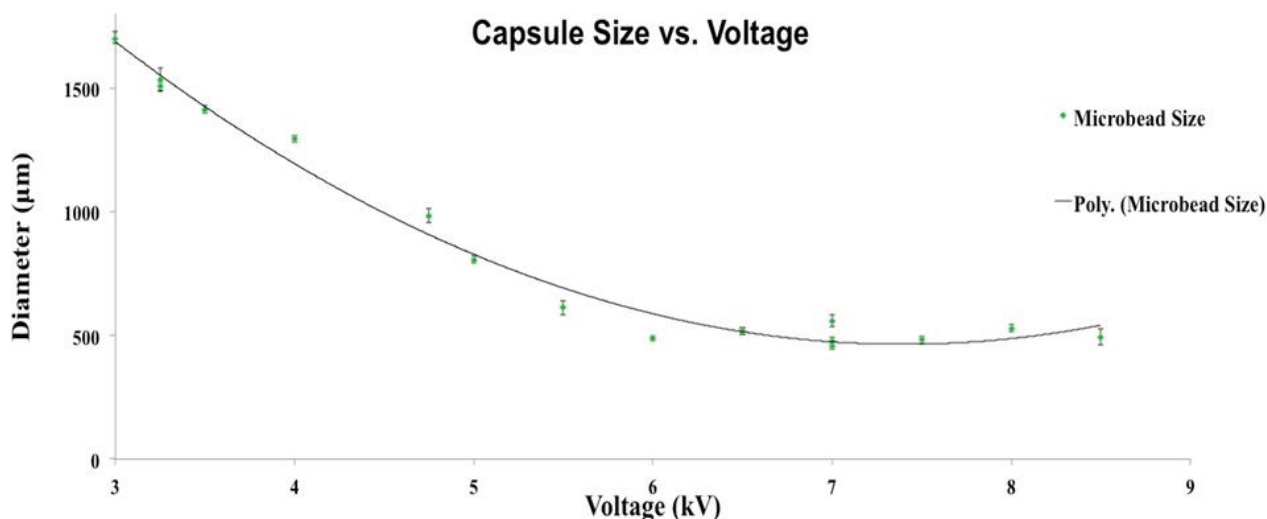


Figure 5-6: Size of Ca²⁺/Ba²⁺ alginate microbeads in response to voltage variation.

Relationship between applied voltage (kV) and size of empty microbeads (μm). Based on the polynomial regression, applied voltage is negatively correlated to microbead size. (n=17 batches; 50 microbeads sized per batch; Mean \pm SD)

5.1.3 Key technologies to implement into a clinically relevant islet encapsulator

Each of the encapsulation systems has its benefits and limitations. Ideally, a combination of the best apparatuses from each encapsulation system may be ideal for encapsulation of islets. Forming the polymer droplets using electrostatic methods would allow for consistently sized hydrogels without the necessity of a highly skilled technician. If the electrostatically formed droplets then fell into the loop reactor, this would allow for controlled gelation of the hydrogels. This will be important for homogeneity of hydrogel formation as well as a reduction in the amount of time islets are exposed to the potentially toxic gelation solutions. Lastly, the continuous production associated with the loop reactor will allow for very large numbers of islets to be encapsulated quickly but slow enough to allow for quality control assurances during encapsulation.

5.1.4 Design criteria for novel encapsulator

An islet encapsulation system should ideally produce uniform, spherical hydrogels, with an integral smooth surface at a defined diameter. The hydrogels should exhibit a low polydispersity and consistent chemical composition throughout the batch. There should be little operator dependency and little batch to batch variation from batches produced on different days and by different technicians. Consistency in the manufactured product is critical to confidently define hydrogel characteristics that lead to success or failure of the technology [39].

The number of islet cells per hydrogel should be defined and tightly regulated. Islets are highly metabolically active and consume large quantities of oxygen to maintain proper functionality [25]. Too many islet cells per hydrogel may exacerbate islet hypoxia in low oxygen environments. Oxygen availability may also be dependent on the transplantation site. The optimal number of islet cells per hydrogel is not clearly defined; nonetheless, strict control over this factor would be highly advantageous. This may prove difficult as batches of encapsulated islets often exhibit empty hydrogels as well as hydrogels with many islets. Islets tend to aggregate during washing steps or are not evenly distributed when mixed with the polymer solution. Empty hydrogels are also undesirable by taking up transplant real estate.

Islets should always be fully encapsulated and not protruding from the hydrogels. This is especially important since exposed islets compromises the overarching goal of immuno-protection, and may initiate a cellular reaction that negatively affects the entire encapsulated islet graft.

Encapsulation processes that cause stress or damage to intracellular machinery important for insulin secretion should be avoided. Physical forces used to control droplet size during islet encapsulation should be mild or shown to be well tolerated by islets. Exposure of islets to harsh chemical/gelation

environments should be kept to a minimum or shown to be inconsequential. The amount of time islets spend out of culture should be kept to a minimum. The hydrogel should also be well tolerated by the islets and biocompatible with the host.

The islet encapsulation system should also have the potential for scalability as up to 500,000 cadaveric human islets may be required to be encapsulated in one batch in the future. This is not an easy feat to produce this large number of encapsulated islets with a consistent chemical composition and size while maintaining gentle manufacture conditions suitable for islets and with a limited time out of culture.

Lastly, if the machine is to be used in clinical applications, the encapsulation system should satisfy GMP standards and regulatory agency specifications. This includes criterion for strict assurance of sterility, safety, and reproducibility of a product with adequate quality control measures during manufacture.

5.2 Apparatus Design: Electrostatic with integrated Loop Reactor (ELR) Encapsulator for continuous production of spherical polymer hydrogels with controlled gelation time

In collaboration with Nisco Engineering, a high precision encapsulation specialty company in Switzerland, the best technologies from multiple encapsulation apparatuses were implemented into the final design of the ELR encapsulator. The ELR encapsulator was designed to continuously manufacture uniform, spherical polymer hydrogels with controlled size and gelation time. Some encapsulators on the market can claim such feats, yet many are not suitable for islet encapsulation due to the high shear stresses placed on the fragile cell clusters or are limited by production capabilities. Most importantly, the ELR encapsulator is designed to be a user friendly device, and once the ideal parameters for encapsulation are established, there is little operator dependency on the final product. This is especially important when submitting to regulatory agencies like the FDA, where a defined cellular/material

product must be thoroughly validated for safety, potency, and reproducibility prior to coming onto the market.

The ELR encapsulator adopts 3 key technologies from previous encapsulation devices. 1) *Electrostatic encapsulation*, which is a user friendly method, reproducible, and requires only minimal adjustments on a voltage dial to finely tune droplets to the desired size. 2) *Loop reactor gelation*, which can be used to control the time of gelation of the polymer droplets, and the process can be made continuous through the use of a circuit design. 3) *Electrostatic ring electrode accelerator*, which is an important component that allows the first two technologies to be combined in a safe and reproducible manner. The ring electrode makes it possible to place the electrostatic potential between the nozzle and accelerator to drive droplet formation. The droplets then pass through the orifice in the ring accelerator and fall into the loop reactor by gravity (Figure 5-7).

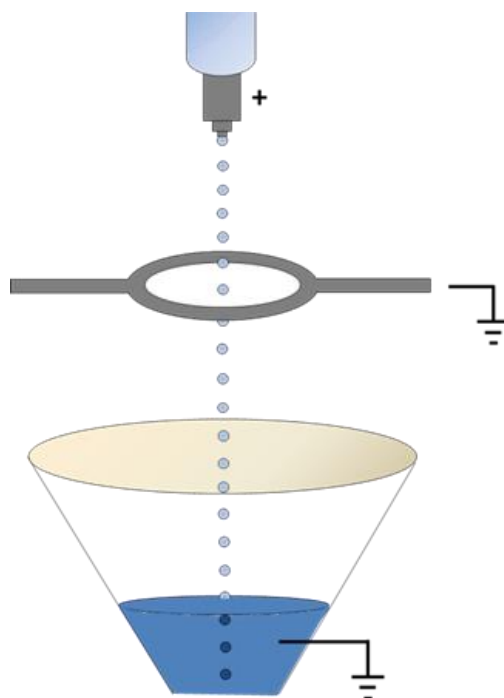


Figure 5-7: General diagram of ELR encapsulation

A voltage potential is placed between the tip of a nozzle and the electrostatic accelerator. The electrostatic force pulls polymer droplets toward the accelerator which can then pass through the opening via gravity. The polymer droplets solidify within the funnel and loop reactor.

In order to integrate all three of these components into one device, a completely novel encapsulation model was created in the ELR Encapsulator (Figure 5-8). The housing unit of the Nisco VAR1 Electrostatic Encapsulator was enlarged and provided the framework as the base model. Safety features were also added to ensure high voltage could only be activated once all openings were secure. The control system is accessible on the left to make any fine adjustments that might be required to tune the droplet formation during production.

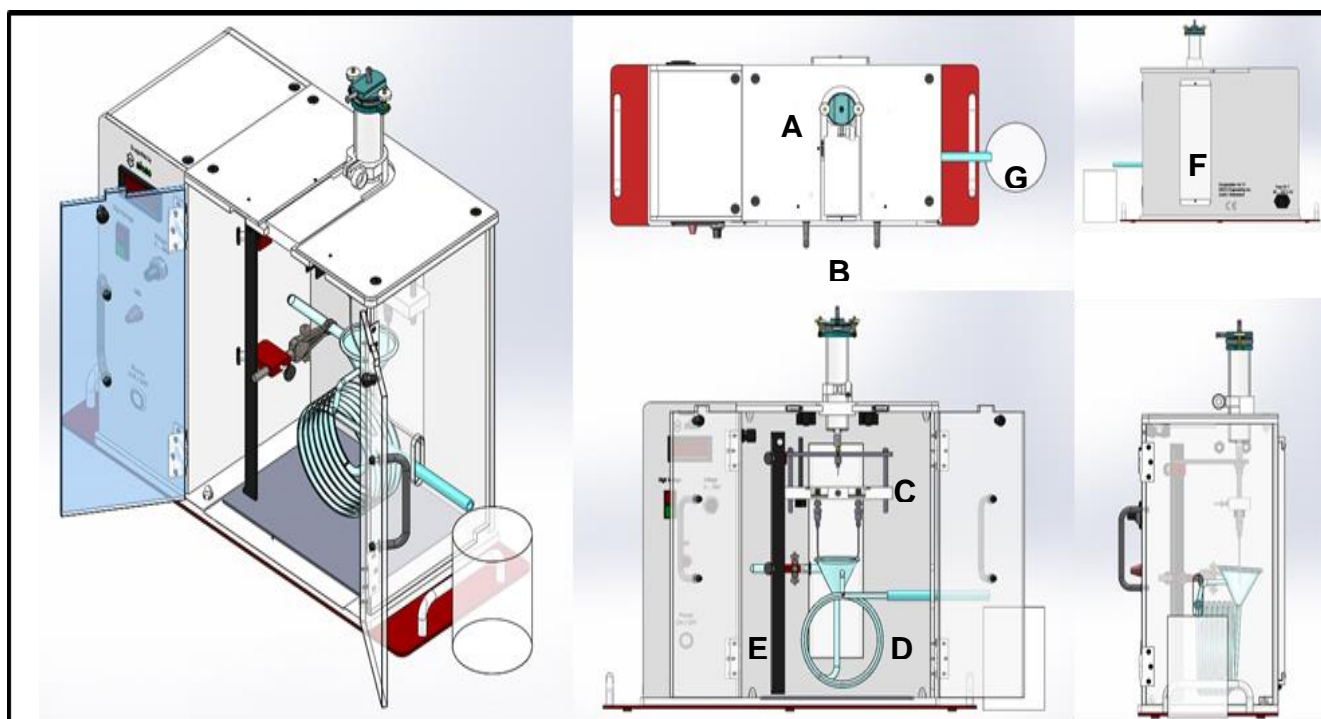


Figure 5-8: 3D rendering of the ELR Encapsulator with integrated Loop Reactor

A) 60 mL glass syringe with customized head for air pressure connection and loading of polymer solution. The syringe connects to a nozzle inside the housing unit for droplet formation.

B) Removable syringe holder with integrated safety switch. High voltage is only applied to the unit once all openings are secured.

C) Electrostatic accelerator and nozzle system for voltage dependent polymer droplet formation.

D) Loop reactor where droplets fall into the funnel to become hardened by the gelation solution. The loop reactor is continually refilled by gelation solution which provides for controlled gelation time as well as continuous production of polymer hydrogel spheres.

E) Customized support bar to hold nozzle components and loop reactor. Each of the supported components can be adjusted vertically and horizontally to a desired distance.

F) Rear window for LED illumination. The encapsulation unit is backlit with light to better visualize droplet sizes as they leave the nozzle.

G) Collection beaker for capsules as they exit the encapsulation unit and loop reactor. This allows for continuous post-processing of capsules and dilution of the gelation solution.

The ELR encapsulator works in the following manner. A polymer solution with or without islets is loaded into a 60 mL glass syringe using a luer lock connection on top of the syringe. The loading port is then attached to a gas regulator which is used to control the flow rate of the polymer solution through the nozzle. The main support holds the nozzle, accelerator, and the funnel of the loop reactor. These can then be positioned above one another and adjusted vertically and horizontally with measureable distances. One adjustable arm branches from the main support to position the nozzle and accelerator. Another adjustable arm positions the loop reactor.

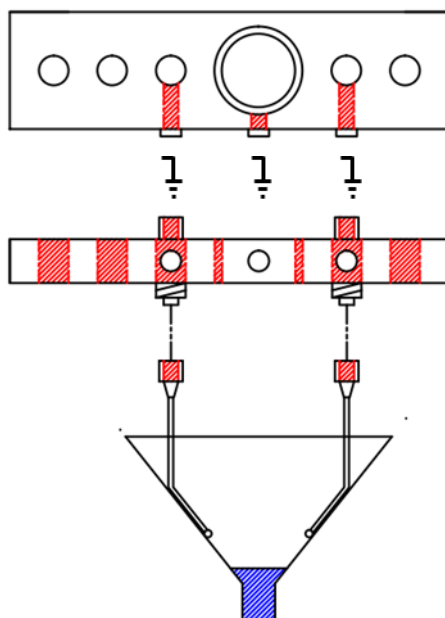


Figure 5-9: Top and side view of Ring Electrode Accelerator

The accelerator is made of non-conductive PEEK. The metal scoped electrode (center) is flanked by two luer lock connectors for the gelation solution. Ports connect the metal pieces and allow the accelerator and gavage needles to be grounded.

Components holding the nozzle and accelerator are made of either electrically conductive stainless steel or non-conductive polyether ether ketone (PEEK). This way a voltage potential can be applied between the nozzle and accelerator since they are spatially separated by a non-conductive screw (PEEK). The accelerator bar is made of PEEK but has a stainless steel orifice (scoped electrode). The polymer droplets are attracted toward the scoped electrode, and then fall through the orifice by gravity. The scoped electrode is flanked on both sides with two stainless steel luer lock connectors that continually feed the loop reactor with gelation solution. All metal components in the accelerator (PEEK) connected to individual metal ports that can be grounded by wires (Figure 5-9). By controlling electrical conductance in the system, a voltage potential can be created between the nozzle and accelerator, and this is independent of the distance to the gelation solution. After the polymer droplet formation is driven by electrostatics, they then fall by gravity into the loop reactor for gelation.

The loop reactor circulates gelation solution at a constant rate. This rate is dependent on the height of the solution in the funnel according to hydrodynamic principles. The height of the solution in the funnel is maintained by continually replenishing with gelation solution. Silicon tubing and a two-way splitter delivers the gelation solution to the housing unit via an air pressure regulator or peristaltic pump. These attach to luer lock connectors on the accelerator bar. The gelation solution is then fed into the funnel using 2 bent gavage needles that attach to the bottom of the accelerator bar (Figure 5-10). These are also made of metal and ground the gelation solution. Ultimately, the time of gelation for polymer droplets is controlled by the flow rate used to feed the loop reactor to an appropriate height.

Once the polymer droplets have hardened in the loop reactor, they exit the encapsulation housing unit into a collection beaker. The collection beaker can be prefilled with a dilution solution to quench gelation. In another variation, the collection beaker can be filled with more gelation solution and the hydrogels can be collected in a sieve. The sieve can then be transferred to another beaker with gelation

solution in order to allow enough time to completely saturate the gel. Once the polymer droplets have been cured to the desired amount, they can be processed and placed in culture in the case of encapsulated islets.

One of the benefits to using the ELR Encapsulator is that the morphology and hydrogel size can be monitored throughout the encapsulation process. This can be accomplished by taking small samples of the hydrogels as they exit the loop reactor, and then evaluating their characteristics under the microscope. On a similar note, the rear of the ELR Encapsulator is backlit by LED illumination to better visualize droplet sizes as they leave the tip of the nozzle. This is especially important during the start of encapsulation to establish the ideal parameters to obtain desired diameters. The LED illumination can also be beneficial during the encapsulation process to quickly discern if the process has changed and adjustments are needed.

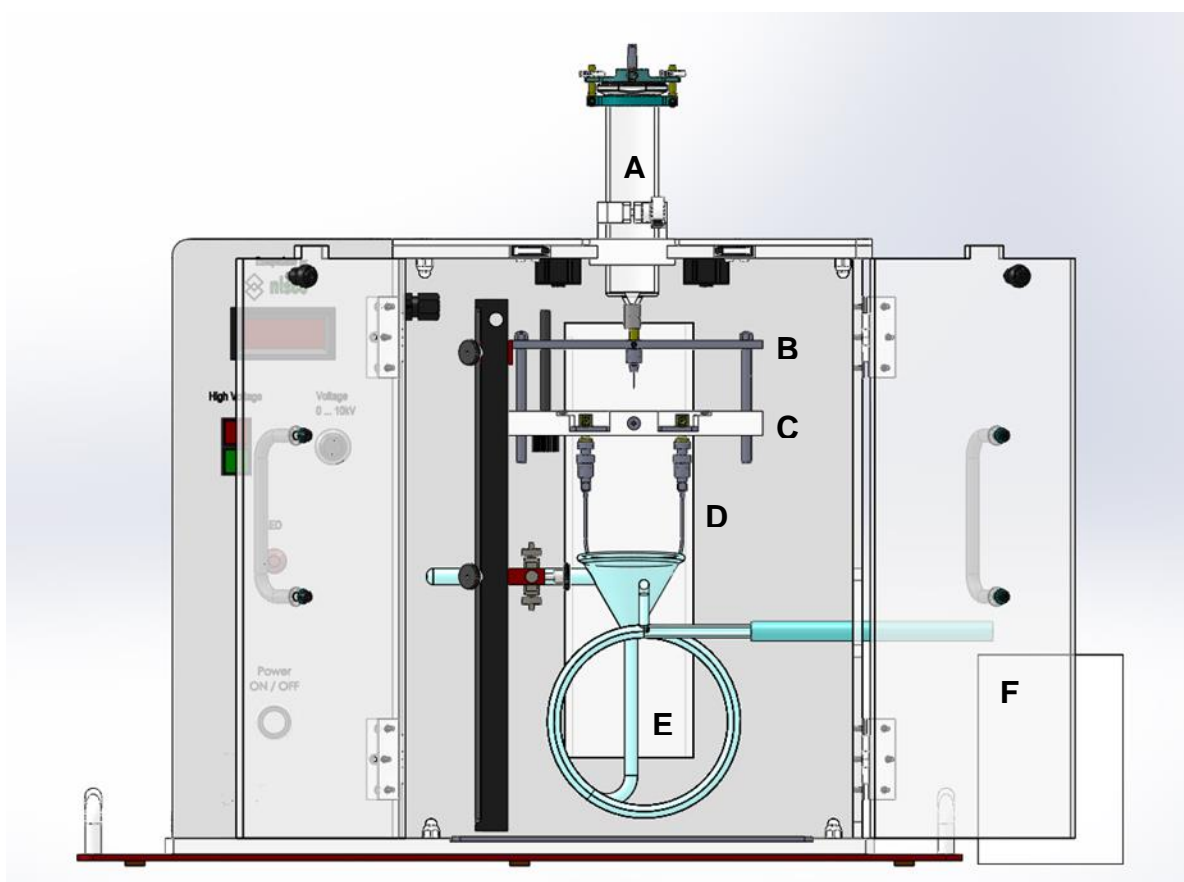


Figure 5-10: Diagram of the internal housing unit of the ELR Encapsulator

A) The 60 mL glass syringe is loaded with the polymer and islet/cell solution and attached to an air pressure regulator to control the flow rate to the nozzle.

B) An adapted arm holds an exchangeable nozzle that extrudes the polymer solution. The arm is made of stainless steel and carries the high voltage to the nozzle tip.

C) Another adapted arm holds the electrostatic accelerator and feeds for the gelation solution. This arm is made of the insulator PEEK with individual ports to ground both the electrostatic accelerator and gelation solution. The electric potential created between the nozzle tip and accelerator drives the polymer droplet formation, which then fall by gravity through the opening in the electrostatic accelerator.

D) Two metal gavage feeding needles supply the loop reactor with a continuous flow of grounded gelation solution.

E) Once the droplets fall into the funnel of the loop reactor, they circulate through the loops by hydrodynamic forces maintained by refilling the gelation solution. The flow rate of gelation solution and can be adjusted to control the time of polymer gelation.

F) After gelation in the loop reactor, the polymer spheres exit the encapsulation unit and are collected in a beaker for post-processing.

The ELR Encapsulator has the potential for continuous manufacture of hydrogel spheres in large batches. This can be accomplished by continually circulating the gelation solution through the use of a peristaltic pump and circuit design (Figure 5-11). The peristaltic pump circulates gelation solution through the gavage needles and into the funnel of the loop reactor. The loop reactor solidifies the hydrogels, which exit into a sieve that is placed on top of the collection beaker. The volume of gelation solution in the collection beaker is large enough to keep hydrogels submerged while in the sieve. Once the hydrogels are collected in the sieve for an allotted amount of time, the sieve can be exchanged with an empty sieve to repeat the process. The sieve containing the hydrogels can be moved to a beaker with fresh gelation solution. The hydrogels can then achieve saturation before undergoing washing and dilution of the gelation solution. Finally, the hydrogels are complete and can be placed into culture in the case of islets. Islets are highly sensitive cells and can withstand only a limited amount of time in the gelation solutions, typically about 20 minutes. Since the process is continuous, very large batches of encapsulated islets can be produced where all the hydrogels have had enough time to fully saturate without overexposure to the gelation solution.

A key component that allows the circulation of the gelation solution is the submerged yankeur tube in the collection beaker. The peristaltic pump pulls up the solution in the collection beaker through the yankeur tube. This is then circulated through a closed vessel reservoir so large volumes of gelation solution can be added to the system. The gelation solution is then circulated from the reservoir to the loop reactor to continue the process. The volume of gelation solution that is added to the circuit may be variable yet solution levels in the collection beaker and reservoir should be closely regulated at the start of encapsulation.

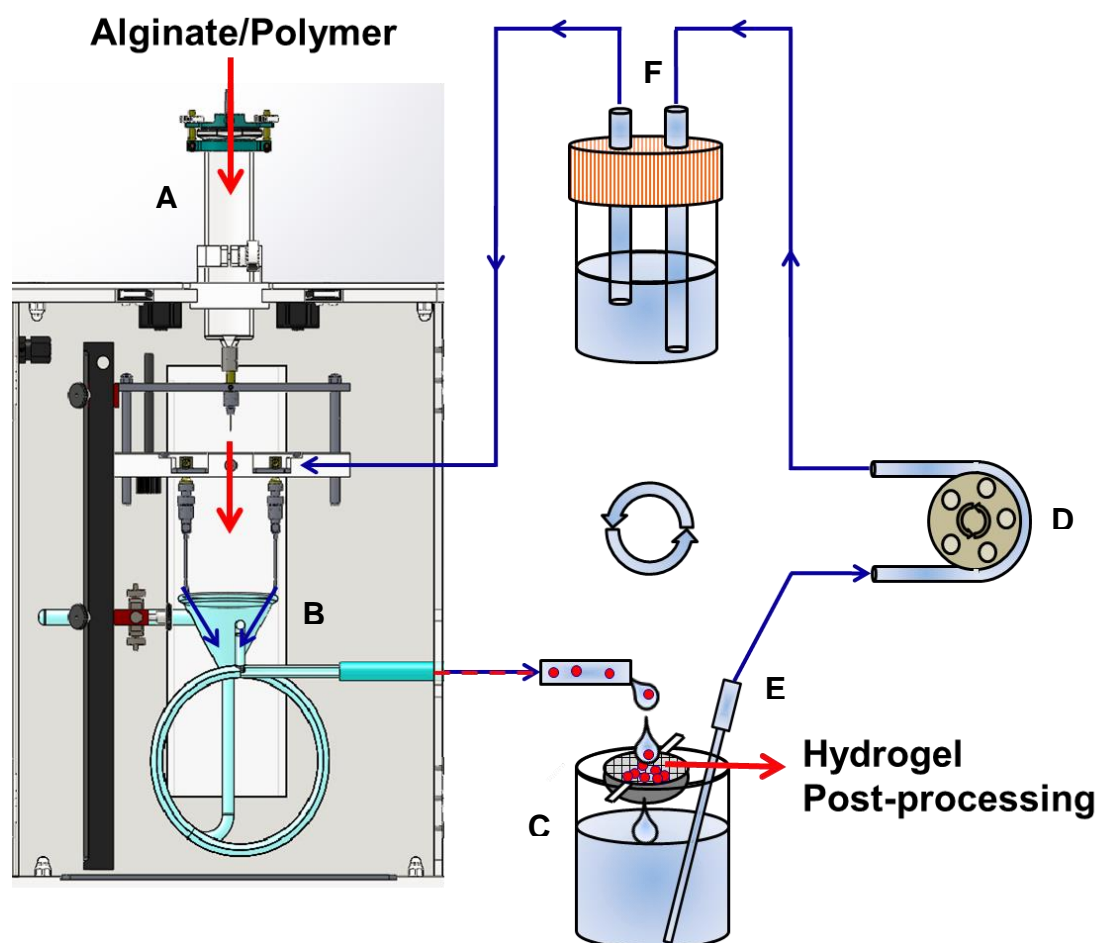


Figure 5-11: Encapsulation Circuit for Continuous Production of Spherical Hydrogels

A) The polymer solution is extruded through the electrostatic nozzle system and droplet size can be monitored by altering the applied voltage using external potentiometers.

B) The polymer droplets then circulate in the loop reactor with controlled gelation time.

C) Once solidified, the hydrogels are collected in a sieve. The sieve can then be transferred to a beaker filled with fresh gelation solution to ensure appropriate gel saturation. Encapsulated cells can then be washed quickly and placed in culture.

D) The gelation solution circulates through the circuit using a peristaltic pump. By controlling the peristaltic circuit flowrate, the flowrate in the loop reactor can also be controlled, and most importantly, the gelation time.

E) It is important to maintain hydrodynamic forces in the circuit in order to circulate the gelation solution. Hydrodynamic forces are maintained in the collection beaker using a sterile yankauer and tubing that connects to the peristaltic pump. Hydrodynamic forces are maintained in the loop reactor by gravity driven circulation.

F) A gelation solution reservoir is contained in a vessel for sterility purposes as well as the maintenance of hydrostatic pressures for large volumes in the circuit. In the case that fresh gelation solution is required to feed the loop reactor, the yankauer can be inserted into bottles of fresh gelation solution and spent gelation solution can be discarded.

There are other important factors that must be considered when using a recirculating gelation solution system. As the hydrogel forms, some of the molecular components in the gelation solution will become depleted since they are used to solidify the gels. A rather small amount of components are consumed per volume of polymer; however, appropriate polymer to gelation solution volume ratios should be defined for each hydrogel system to ensure homogeneity throughout the final product [142]. As a rule of thumb, large volumes of gelation solution should be used if an excess is available. Furthermore, fresh gelation solution can always be introduced into the circuit if needed and the depleted solution discarded.

A problem that often occurs during encapsulation is the formation of tiny satellite hydrogels that then stick/gel to the surface of the larger hydrogel spheres. This is not desirable as these satellites compromise the spherical integrity of the hydrogel surface, and may create a niche for fibrotic cellular attachment. In the case of a recirculating gelation solution system, these satellite hydrogels may pass through the collection sieve and become continually circulated throughout the gelation solution. This might produce more large hydrogels with satellite protrusions. To remedy this, the reservoir may be designed to act as a catch for these satellites by controlling the heights of the inlets and outlets or incorporating additional filtration. Furthermore, surface imperfections in encapsulation nozzles are the leading cause of satellite formation. Nisco has incorporated state-of-the-art nozzles that are precisely polished to eliminate surface imperfections.

Some polymer/hydrogel systems may require the use of fresh gelation solution. In the particular case of membrane/core hydrogels, the time of gelation can be very short (40-50 seconds) and requires immediate dilution [2]. For these systems, the peristaltic pump can still be used and the yankeur tube should be transferred from bottle to bottle of fresh gelation solution. The reservoir can be made into an open container to eliminate bubble formation when transferring the yankeur tube from bottle to bottle. After the fresh gelation solution passes through the loop reactor and solidifies the hydrogels, the

hydrogels can be quenched in the collection beaker filled with dilution solution. The hydrogels can then be collected in a sieve for post-processing, and the spent gelation solution should be discarded.

A major design criterion for the ELR Encapsulator was to build a clinical grade encapsulation unit. This requires the device to satisfy strict sterility standards as well as quality control measures. Quality control measures for encapsulation devices include the reproducibility of homogeneously sized hydrogels with a uniform chemical make-up. There should be little batch to batch variation for hydrogels manufactured on different days. In the case of the ELR encapsulator, components were designed so all distances between parts can be measureable. This is important since polymers behave uniquely to their formula and parameters such as voltage and distance between parts will subsequently have an effect on each individual hydrogel system. However, once the ideal parameters are defined for each hydrogel system, there should be very little batch to batch variation and little dependency on the operator. Furthermore, sterility can be ensured since the ELR encapsulation system is largely a closed loop circuit. As the loop reactor is enclosed within the sterile and closed housing unit, the collection beaker and the yankeur tubing are the only openings for potential contamination of the system. Care should be taken to ensure these areas remain organized and free of possible sources of contamination.

5.3 Conclusion:

The ELR Encapsulator is the first of its kind that can continuously manufacture spherical hydrogels with a specified diameter and controlled gelation time. The high-throughput system is very user friendly and may be well suited to produce GMP grade, large batches of encapsulated cells for clinical transplantation in the future.

6 CITED LITERATURE

1. Kizilel, S., et al., *Encapsulation of pancreatic islets within nano-thin functional polyethylene glycol coatings for enhanced insulin secretion*. Tissue Eng Part A, 2010. **16**(7): p. 2217-28.
2. Wang, T., et al., *An encapsulation system for the immunoisolation of pancreatic islets*. Nat Biotechnol, 1997. **15**(4): p. 358-62.
3. Davis, N.E., et al., *Enhanced function of pancreatic islets co-encapsulated with ECM proteins and mesenchymal stromal cells in a silk hydrogel*. Biomaterials, 2012. **33**(28): p. 6691-7.
4. Yang, H., A. Al-Jazaeri, and J.R. Wright, Jr., *The immunoprotective effect of Sertoli cells coencapsulated with islet xenografts is not dependent upon Fas ligand expression*. Cell Transplant, 2002. **11**(8): p. 799-801.
5. Dang, T.T., et al., *Enhanced function of immuno-isolated islets in diabetes therapy by co-encapsulation with an anti-inflammatory drug*. Biomaterials, 2013. **34**(23): p. 5792-801.
6. Pedraza, E., et al., *Preventing hypoxia-induced cell death in beta cells and islets via hydrolytically activated, oxygen-generating biomaterials*. Proc Natl Acad Sci U S A, 2012. **109**(11): p. 4245-50.
7. Johnson, A.S., et al., *Quantitative assessment of islets of Langerhans encapsulated in alginate*. Tissue Eng Part C Methods, 2011. **17**(4): p. 435-49.
8. Ludwig, B., et al., *Transplantation of human islets without immunosuppression*. Proc Natl Acad Sci U S A, 2013. **110**(47): p. 19054-8.
9. Kim, S. and Y.H. Bae, *Long-term insulinitropic activity of glucagon-like peptide-1/polymer conjugate on islet microcapsules*. Tissue Eng, 2004. **10**(11-12): p. 1607-16.
10. Jourdan, G., et al., *Co-encapsulation of bioengineered IGF-II-producing cells and pancreatic islets: effect on beta-cell survival*. Gene Ther, 2011. **18**(6): p. 539-45.
11. Adewola, A.F., et al., *Microfluidic perfusion and imaging device for multi-parametric islet function assessment*. Biomed Microdevices, 2010. **12**(3): p. 409-17.

12. King, A., *Microencapsulation of islets of Langerhans: impact of cellular overgrowth*. Ups J Med Sci, 2001. **106**(3): p. 161-74.
13. King, A., S. Sandler, and A. Andersson, *The effect of host factors and capsule composition on the cellular overgrowth on implanted alginate capsules*. Journal of Biomedical Materials Research, 2001. **57**(3): p. 374-383.
14. Keizer, J. and G. Magnus, *ATP-sensitive potassium channel and bursting in the pancreatic beta cell. A theoretical study*. Biophys J, 1989. **56**(2): p. 229-42.
15. Shapiro, A.M., et al., *Islet transplantation in seven patients with type 1 diabetes mellitus using a glucocorticoid-free immunosuppressive regimen*. N Engl J Med, 2000. **343**(4): p. 230-8.
16. Turgeon, N.A., et al., *Experience with a novel efalizumab-based immunosuppressive regimen to facilitate single donor islet cell transplantation*. Am J Transplant, 2010. **10**(9): p. 2082-91.
17. Hopkins, K.D., *Update on islet-cell transplantation for type 1 diabetes*. Lancet, 2002. **359**(9324): p. 2172.
18. Sakata, N., et al., *Encapsulated islets transplantation: Past, present and future*. World J Gastrointest Pathophysiol, 2012. **3**(1): p. 19-26.
19. Socha, K., M. Socha, and P. Fiedor, *Proliferation of transplanted allogeneic pancreatic islets*. Transplant Proc, 2003. **35**(6): p. 2341-2.
20. Pagliuca, F.W., et al., *Generation of functional human pancreatic beta cells in vitro*. Cell, 2014. **159**(2): p. 428-39.
21. Dufrane, D., R.M. Goebbels, and P. Gianello, *Alginate macroencapsulation of pig islets allows correction of streptozotocin-induced diabetes in primates up to 6 months without immunosuppression*. Transplantation, 2010. **90**(10): p. 1054-62.
22. Lim, F. and A.M. Sun, *Microencapsulated islets as bioartificial endocrine pancreas*. Science, 1980. **210**(4472): p. 908-10.
23. Qi, M., et al., *PVA hydrogel sheet macroencapsulation for the bioartificial pancreas*. Biomaterials, 2004. **25**(27): p. 5885-92.

24. Dionne, K.E., C.K. Colton, and M.L. Yarmush, *Effect of hypoxia on insulin secretion by isolated rat and canine islets of Langerhans*. Diabetes, 1993. **42**(1): p. 12-21.
25. Papas, K.K., et al., *High-density culture of human islets on top of silicone rubber membranes*. Transplant Proc, 2005. **37**(8): p. 3412-4.
26. de Groot, M., et al., *Response of encapsulated rat pancreatic islets to hypoxia*. Cell Transplant, 2003. **12**(8): p. 867-75.
27. Toso, C., et al., *Effect of microcapsule composition and short-term immunosuppression on intraportal biocompatibility*. Cell Transplantation, 2005. **14**(2-3): p. 159-167.
28. Dufrane, D., et al., *The influence of implantation site on the biocompatibility and survival of alginate encapsulated pig islets in rats*. Biomaterials, 2006. **27**(17): p. 3201-3208.
29. Veriter, S., et al., *In Vivo Selection of Biocompatible Alginates for Islet Encapsulation and Subcutaneous Transplantation*. Tissue Engineering Part A, 2010. **16**(5): p. 1503-1513.
30. Liu, X.Y., et al., *Biocompatibility Investigation of Polyethylene Glycol and Alginate-Poly-L-Lysine for Islet Encapsulation*. Asaio Journal, 2010. **56**(3): p. 241-245.
31. Yang, K.C., et al., *Comparison of Bioartificial Pancreas Performance in the Bone Marrow Cavity and Intramuscular Space*. Archives of Medical Research, 2010. **41**(3): p. 151-153.
32. Duvivier-Kali, V.F., et al., *Complete protection of islets against allorejection and autoimmunity by a simple barium-alginate membrane*. Diabetes, 2001. **50**(8): p. 1698-1705.
33. Omer, A., et al., *Long-term normoglycemia in rats receiving transplants with encapsulated islets*. Transplantation, 2005. **79**(1): p. 52-58.
34. Wang, T., et al., *Successful allotransplantation of encapsulated islets in pancreatectomized canines for diabetic management without the use of immunosuppression*. Transplantation, 2008. **85**(3): p. 331-337.
35. Basta, G., et al., *Long-Term Metabolic and Immunological Follow-Up of Nonimmunosuppressed Patients With Type 1 Diabetes Treated With Microencapsulated Islet Allografts*. Diabetes Care, 2011. **34**(11): p. 2406-2409.

36. Tuch, B.E., et al., *Safety and Viability of Microencapsulated Human Islets Transplanted Into Diabetic Humans*. Diabetes Care, 2009. **32**(10): p. 1887-1889.
37. Jacobs-Tulleneers-Thevissen, D., et al., *Sustained function of alginate-encapsulated human islet cell implants in the peritoneal cavity of mice leading to a pilot study in a type 1 diabetic patient*. Diabetologia, 2013. **56**(7): p. 1605-1614.
38. Calafiore, R., et al., *Microencapsulated pancreatic islet allografts into nonimmunosuppressed patients with type 1 diabetes - First two cases*. Diabetes Care, 2006. **29**(1): p. 137-138.
39. Rokstad, A.M., et al., *Advances in biocompatibility and physico-chemical characterization of microspheres for cell encapsulation*. Adv Drug Deliv Rev, 2014. **67-68**: p. 111-30.
40. Anderson, J.M., A. Rodriguez, and D.T. Chang, *Foreign body reaction to biomaterials*. Semin Immunol, 2008. **20**(2): p. 86-100.
41. Graham, M.L., et al., *The streptozotocin-induced diabetic nude mouse model: differences between animals from different sources*. Comp Med, 2011. **61**(4): p. 356-60.
42. Avila, J.G., et al., *Improved outcomes in islet isolation and transplantation by the use of a novel hemoglobin-based O-2 carrier*. American Journal of Transplantation, 2006. **6**(12): p. 2861-2870.
43. Gai, W., et al., *Differential target molecules for toxicity induced by streptozotocin and alloxan in pancreatic islets of mice in vitro*. Exp Clin Endocrinol Diabetes, 2004. **112**(1): p. 29-37.
44. Boyd, V., O.M. Cholewa, and K.K. Papas, *Limitations in the Use of Fluorescein Diacetate/Propidium Iodide (FDA/PI) and Cell Permeable Nucleic Acid Stains for Viability Measurements of Isolated Islets of Langerhans*. Curr Trends Biotechnol Pharm, 2008. **2**(2): p. 66-84.
45. de Vos, P., A.F. Hamel, and K. Tatarkiewicz, *Considerations for successful transplantation of encapsulated pancreatic islets*. Diabetologia, 2002. **45**(2): p. 159-173.
46. Kulseng, B., et al., *Alginate polylysine microcapsules as immune barrier: Permeability of cytokines and immunoglobulins over the capsule membrane*. Cell Transplantation, 1997. **6**(4): p. 387-394.
47. Hals, I.K., et al., *Alginate Microencapsulation of Human Islets Does Not Increase Susceptibility to Acute Hypoxia*. Journal of Diabetes Research, 2013.

48. Velho, G., P. Froguel, and G. Reach, *Determination of Peritoneal Glucose Kinetics in Rats - Implications for the Peritoneal Implantation of Closed-Loop Insulin Delivery Systems*. Diabetologia, 1989. **32**(6): p. 331-336.
49. DeVos, P., et al., *Kinetics of intraperitoneally infused insulin in rats - Functional implications for the bioartificial pancreas*. Diabetes, 1996. **45**(8): p. 1102-1107.
50. Schrezenmeir, J., et al., *Effect of Microencapsulation on Oxygen Distribution in Islets Organs*. Transplantation, 1994. **57**(9): p. 1308-1314.
51. Colton, C.K. and E.S. Avgoustiniatos, *Bioengineering in Development of the Hybrid Artificial Pancreas*. Journal of Biomechanical Engineering-Transactions of the Asme, 1991. **113**(2): p. 152-170.
52. Renvall, S. and J. Niinikoski, *Intraperitoneal Oxygen and Carbon-Dioxide Tensions in Experimental Adhesion Disease and Peritonitis*. American Journal of Surgery, 1975. **130**(3): p. 286-292.
53. Schrezenmeir, J., F. Velten, and J. Beyer, *Immobilized Hemoglobin Improves Islet Function and Viability in the Bioartificial Pancreas in-Vitro and in-Vivo (Vol 26, Pg 792, 1994)*. Transplantation Proceedings, 1994. **26**(3): p. 1834-1834.
54. Hsu, B.R.S., et al., *Prolonged Postprandial Hyperglycemia in Streptozotocin-Induced Diabetic Mice after Intraperitoneal Treatment with Microencapsulated Islets*. Transplantation Proceedings, 1994. **26**(6): p. 3706-3708.
55. Williams, J.C., et al., *Increased Hematopoietic Cells in the merck(-/-) Mouse Peritoneal Cavity: A Result of Augmented Migration*. Journal of Immunology, 2010. **184**(12): p. 6637-6648.
56. Veriter, S., P. Gianello, and D. Dufrane, *Bioengineered Sites for Islet Cell Transplantation*. Current Diabetes Reports, 2013. **13**(5): p. 745-755.
57. Svensson, J., et al., *High Vascular Density and Oxygenation of Pancreatic Islets Transplanted in Clusters Into Striated Muscle*. Cell Transplantation, 2011. **20**(5): p. 783-788.
58. Christoffersson, G., et al., *Clinical and Experimental Pancreatic Islet Transplantation to Striated Muscle Establishment of a Vascular System Similar to That in Native Islets*. Diabetes, 2010. **59**(10): p. 2569-2578.

59. *Skeletal Muscle: Pathology, Diagnosis, and Management of Disease*. 2002, London: Greenwich Medical Media.
60. Rafael, E., et al., *Intramuscular autotransplantation of pancreatic islets in a 7-year-old child: A 2-year follow-up*. American Journal of Transplantation, 2008. **8**(2): p. 458-462.
61. Sterkers, A., et al., *Islet survival and function following intramuscular autotransplantation in the minipig*. Am J Transplant, 2013. **13**(4): p. 891-8.
62. Qi, M., et al., *Encapsulation of Human Islets in Novel Inhomogeneous Alginate-Ca(2+)/Ba(2+) Microbeads: In Vitro and In Vivo Function*. Artificial Cells Blood Substitutes and Biotechnology, 2008. **36**(5): p. 403-420.
63. Qi, M.R.G., et al., *Survival of human islets in microbeads containing high guluronic acid alginate crosslinked with Ca²⁺ and Ba²⁺*. Xenotransplantation, 2012. **19**(6): p. 355-364.
64. Vaithilingam, V., et al., *Beneficial Effects of Coating Alginate Microcapsules with Macromolecular Heparin Conjugates-In Vitro and In Vivo Study*. Tissue Engineering Part A, 2014. **20**(1-2): p. 324-334.
65. Siebers, U., et al., *Time course of the cellular reaction toward microencapsulated xenogeneic islets in the rat*. Transplant Proc, 1998. **30**(2): p. 494-5.
66. Yi, S., et al., *T cell-activated macrophages are capable of both recognition and rejection of pancreatic islet xenografts*. J Immunol, 2003. **170**(5): p. 2750-8.
67. Schroppel, B., et al., *Role of donor-derived monocyte chemoattractant protein-1 in murine islet transplantation*. J Am Soc Nephrol, 2005. **16**(2): p. 444-51.
68. Milani, B.Y., et al., *Rapamycin inhibits the production of myofibroblasts and reduces corneal scarring after photorefractive keratectomy*. Invest Ophthalmol Vis Sci, 2013. **54**(12): p. 7424-30.
69. Veiseh, O., et al., *Size- and shape-dependent foreign body immune response to materials implanted in rodents and non-human primates*. Nat Mater, 2015. **14**(6): p. 643-51.
70. Burkholder, T.J., et al., *Relationship between muscle fiber types and sizes and muscle architectural properties in the mouse hindlimb*. J Morphol, 1994. **221**(2): p. 177-90.

71. Weiler, U., et al., *Consequences of selection on muscle composition. A comparative study on gracilis muscle in wild and domestic pigs*. Anat Histol Embryol, 1995. **24**(2): p. 77-80.
72. Bloemberg, D. and J. Quadrilatero, *Rapid determination of myosin heavy chain expression in rat, mouse, and human skeletal muscle using multicolor immunofluorescence analysis*. PLoS One, 2012. **7**(4): p. e35273.
73. Tanaka, M., et al., *Abnormalities in three-dimensional capillary architecture and imbalance between vascular endothelial growth factor-A and thrombospondin-1 in soleus muscle of ovariectomized rat*. Acta Histochem, 2015.
74. Soon-Shiong, P., et al., *Insulin independence in a type 1 diabetic patient after encapsulated islet transplantation*. Lancet, 1994. **343**(8903): p. 950-1.
75. Sun, Y., et al., *Normalization of diabetes in spontaneously diabetic cynomolgus monkeys by xenografts of microencapsulated porcine islets without immunosuppression*. J Clin Invest, 1996. **98**(6): p. 1417-22.
76. O'Sullivan, E.S., et al., *Islets transplanted in immunoisolation devices: a review of the progress and the challenges that remain*. Endocr Rev, 2011. **32**(6): p. 827-44.
77. Qi, M., *Transplantation of Encapsulated Pancreatic Islets as a Treatment for Patients with Type 1 Diabetes Mellitus*. Advances in Medicine, 2014. **2014**: p. 15.
78. Chicheportiche, D. and G. Reach, *In vitro kinetics of insulin release by microencapsulated rat islets: effect of the size of the microcapsules*. Diabetologia, 1988. **31**(1): p. 54-7.
79. Duvivier-Kali, V.F., et al., *Survival of microencapsulated adult pig islets in mice in spite of an antibody response*. Am J Transplant, 2004. **4**(12): p. 1991-2000.
80. Omer, A., et al., *Long-term normoglycemia in rats receiving transplants with encapsulated islets*. Transplantation, 2005. **79**(1): p. 52-8.
81. Nourmohammadzadeh, M., et al., *Microfluidic array with integrated oxygenation control for real-time live-cell imaging: effect of hypoxia on physiology of microencapsulated pancreatic islets*. Anal Chem, 2013. **85**(23): p. 11240-9.
82. Van Schravendijk, C.F., R. Kiekens, and D.G. Pipeleers, *Pancreatic beta cell heterogeneity in glucose-induced insulin secretion*. J Biol Chem, 1992. **267**(30): p. 21344-8.

83. Gembal, M., P. Gilon, and J.C. Henquin, *Evidence that glucose can control insulin release independently from its action on ATP-sensitive K⁺ channels in mouse B cells*. J Clin Invest, 1992. **89**(4): p. 1288-95.
84. Marigliano, M., et al., *Pig-to-nonhuman primates pancreatic islet xenotransplantation: an overview*. Curr Diab Rep, 2011. **11**(5): p. 402-12.
85. Qi, M., et al., *Implementation of a simplified method of islet isolation for allogeneic islet transplantation in cynomolgus monkeys*. Pancreas, 2014. **43**(2): p. 226-35.
86. Schneider, S., et al., *Long-term graft function of adult rat and human islets encapsulated in novel alginate-based microcapsules after transplantation in immunocompetent diabetic mice*. Diabetes, 2005. **54**(3): p. 687-93.
87. King, A.J.F., *The use of animal models in diabetes research*. British Journal of Pharmacology, 2012. **166**(3): p. 877-894.
88. Gazda, L.S., et al., *Encapsulation of porcine islets permits extended culture time and insulin independence in spontaneously diabetic BB rats*. Cell Transplant, 2007. **16**(6): p. 609-20.
89. Duvivier, V., et al., *Long-term culture of free or encapsulated islets isolated from specific pathogen-free (SPF) pigs*. Diabetes Metab, 1998. **24**(6): p. 517-22.
90. Ao, Z., et al., *Microencapsulation enhances canine islet survival during long-term culture*. Transplant Proc, 1995. **27**(6): p. 3350.
91. Noguchi, H., et al., *Fresh islets are more effective for islet transplantation than cultured islets*. Cell Transplant, 2012. **21**(2-3): p. 517-23.
92. Kin, T., et al., *Risk factors for islet loss during culture prior to transplantation*. Transpl Int, 2008. **21**(11): p. 1029-35.
93. Ono, J., et al., *Long-term culture of pancreatic islet cells with special reference to the beta-cell function*. In Vitro, 1979. **15**(2): p. 95-102.
94. Lehmann, R., et al., *Superiority of small islets in human islet transplantation*. Diabetes, 2007. **56**(3): p. 594-603.


95. Jamiolkowski, R.M., et al., *Islet transplantation in type I diabetes mellitus*. Yale J Biol Med, 2012. **85**(1): p. 37-43.
96. Li, N., et al., *Transient oxidative stress damages mitochondrial machinery inducing persistent beta-cell dysfunction*. J Biol Chem, 2009. **284**(35): p. 23602-12.
97. Saadeh, M., et al., *Reactive oxygen species stimulate insulin secretion in rat pancreatic islets: studies using mono-oleoyl-glycerol*. PLoS One, 2012. **7**(1): p. e30200.
98. Meda, P., *Protein-mediated interactions of pancreatic islet cells*. Scientifica (Cairo), 2013. **2013**: p. 621249.
99. Goto, M., et al., *The ADP/ATP ratio: A novel predictive assay for quality assessment of isolated pancreatic islets*. Am J Transplant, 2006. **6**(10): p. 2483-7.
100. Sakata, N., et al., *Optimization of glucose level to determine the stimulation index of isolated rat islets*. Pancreas, 2008. **36**(4): p. 417-23.
101. Ihm, S.H., et al., *Effect of donor age on function of isolated human islets*. Diabetes, 2006. **55**(5): p. 1361-8.
102. Marcelli-Tourvieille, S., et al., *In vivo and in vitro effect of sirolimus on insulin secretion*. Transplantation, 2007. **83**(5): p. 532-8.
103. Marigliano, M., et al., *Hemoglobin A1C Percentage in Nonhuman Primates: A Useful Tool to Monitor Diabetes before and after Porcine Pancreatic Islet Xenotransplantation*. J Transplant, 2011. **2011**: p. 965605.
104. Mueller, K.R., et al., *Differences in glucose-stimulated insulin secretion in vitro of islets from human, nonhuman primate, and porcine origin*. Xenotransplantation, 2013. **20**(2): p. 75-81.
105. Keding, M., et al., *In vitro culture reduces immunogenicity of pancreatic endocrine islets*. Nature, 1977. **270**(5639): p. 736-8.
106. Takahashi, A., et al., *Measurement of intracellular calcium*. Physiol Rev, 1999. **79**(4): p. 1089-125.
107. Lodish H, B.A., Zupursky SL, et al., *Molecular Cell Biology*. 4th edition. 2000, New York: W.H. Freeman.

108. Grynkiewicz, G., M. Poenie, and R.Y. Tsien, *A new generation of Ca^{2+} indicators with greatly improved fluorescence properties*. J Biol Chem, 1985. **260**(6): p. 3440-50.
109. Gee, K.R., et al., *Chemical and physiological characterization of fluo-4 Ca^{2+} -indicator dyes*. Cell Calcium, 2000. **27**(2): p. 97-106.
110. Somers, G., et al., *Calcium-antagonists and islet function. VI. Effects of barium*. Pflugers Arch, 1976. **365**(1): p. 21-8.
111. Howell, S.L. and M. Tyhurst, *Barium accumulation in rat pancreatic B cells*. J Cell Sci, 1976. **22**(2): p. 455-65.
112. MacDonald, P.E., J.W. Joseph, and P. Rorsman, *Glucose-sensing mechanisms in pancreatic beta-cells*. Philos Trans R Soc Lond B Biol Sci, 2005. **360**(1464): p. 2211-25.
113. Takahashi, N., et al., *Two-photon excitation imaging of pancreatic islets with various fluorescent probes*. Diabetes, 2002. **51 Suppl 1**: p. S25-8.
114. Song, S.H., et al., *Diazoxide attenuates glucose-induced defects in first-phase insulin release and pulsatile insulin secretion in human islets*. Endocrinology, 2003. **144**(8): p. 3399-405.
115. Siegel, E.G., D. Janjic, and C.B. Wollheim, *Phenytoin inhibition of insulin release. Studies on the involvement of Ca^{2+} fluxes in rat pancreatic islets*. Diabetes, 1982. **31**(3): p. 265-9.
116. Dolgin, E., *Encapsulate this*. Nat Med, 2014. **20**(1): p. 9-11.
117. Dufrane, D., et al., *Parameters favouring successful adult pig islet isolations for xenotransplantation in pig-to-primate models*. Xenotransplantation, 2006. **13**(3): p. 204-14.
118. Dufrane, D. and P. Gianello, *Pig islet xenotransplantation into non-human primate model*. Transplantation, 2008. **86**(6): p. 753-60.
119. Susan Safley, e.a. *Microencapsulated non-human primate (NHP) islet allografts and porcine islet xenografts in streptozotocin-diabetic NHPs: islet survival, function, and host responses in IPITA*. 2015. Melbourne.
120. Lee, K.Y. and D.J. Mooney, *Alginate: properties and biomedical applications*. Prog Polym Sci, 2012. **37**(1): p. 106-126.

121. Grubelnik, V., *Drop formation in a falling stream of liquid*. American Journal of Physics, 2005. **73**(5): p. 415-419.
122. Cowie, J.M.G.A., Valeria, *Polymers: Chemistry and Physics of Modern Materials, Third Edition 3rd Edition* 2007: CRC Press.
123. Steele, J.A., et al., *Therapeutic cell encapsulation techniques and applications in diabetes*. Adv Drug Deliv Rev, 2014. **67-68**: p. 74-83.
124. Tendulkar, S., et al., *A scalable microfluidic device for the mass production of microencapsulated islets*. Transplant Proc, 2011. **43**(9): p. 3184-7.
125. Tendulkar, S., et al., *A three-dimensional microfluidic approach to scaling up microencapsulation of cells*. Biomed Microdevices, 2012. **14**(3): p. 461-9.
126. Rabanel, J.M., et al., *Progress technology in microencapsulation methods for cell therapy*. Biotechnol Prog, 2009. **25**(4): p. 946-63.
127. Strand, B.L., et al., *Alginate-polylysine-alginate microcapsules: effect of size reduction on capsule properties*. J Microencapsul, 2002. **19**(5): p. 615-30.
128. Klok, T.I. and J.E. Melvik, *Controlling the size of alginate gel beads by use of a high electrostatic potential*. J Microencapsul, 2002. **19**(4): p. 415-24.
129. Poncelet D, B.V., Neufeld RJ, et al., *Theory of electrostatic dispersion of polymer solution in the production of microgel beds containing biocatalyst*. ;. Adv Colloid Interface Sci., 1999(79): p. 213-28.
130. Brian Chang, G.N., Sunghwan Jung, *Drop formation from a wettable nozzle*. Commun Nonlinear Sci Numer Simulat, 2012. **17**: p. 2045-2051.
131. Hunter, H., *Formation and break up of microscale liquid jets*. 2009.
132. McClenaghan, N.H., *Physiological regulation of the pancreatic {beta}-cell: functional insights for understanding and therapy of diabetes*. Exp Physiol, 2007. **92**(3): p. 481-96.
133. Wang, Y., et al., *Implication of mitochondrial cytoprotection in human islet isolation and transplantation*. Biochem Res Int, 2012. **2012**: p. 395974.


134. Buchi. *Encapsulator B-395 Pro*. 2015; Available from:
<http://www.buchi.com/en/products/spray-drying-and-encapsulation/encapsulator-b-395-pro>.
135. Penolazzi, L., et al., *Encapsulation of mesenchymal stem cells from Wharton's jelly in alginate microbeads*. Tissue Eng Part C Methods, 2010. **16**(1): p. 141-55.
136. Nemethova V, L.I., Razga F *Vibration Technology for Microencapsulation: The Restrictive Role of Viscosity*. J Bioprocess Biotech, 2015(5).
137. Jun, Y., et al., *Microfluidics-generated pancreatic islet microfibers for enhanced immunoprotection*. Biomaterials, 2013. **34**(33): p. 8122-30.
138. Tran, T.M., S. Cater, and A.R. Abate, *Coaxial flow focusing in poly(dimethylsiloxane) microfluidic devices*. Biomicrofluidics, 2014. **8**(1): p. 016502.
139. Beck, J., et al., *Islet encapsulation: strategies to enhance islet cell functions*. Tissue Eng, 2007. **13**(3): p. 589-99.
140. Matsumoto, S., H. Kobayashi, and Y. Takashima, *Production of monodispersed capsules*. J Microencapsul, 1986. **3**(1): p. 25-31.
141. Williams, C.G., et al., *Variable cytocompatibility of six cell lines with photoinitiators used for polymerizing hydrogels and cell encapsulation*. Biomaterials, 2005. **26**(11): p. 1211-8.
142. Morch, Y.A., et al., *Binding and leakage of barium in alginate microbeads*. J Biomed Mater Res A, 2012. **100**(11): p. 2939-47.

7 APPENDIX




RightsLink®

[Home](#)
[Create Account](#)
[Help](#)



Live Chat



Title: Size- and shape-dependent foreign body immune response to materials implanted in rodents and non-human primates

Author: Omid Veisheh, Joshua C. Doloff, Minglin Ma, Arturo J. Vegas, Hok Hei Tam, Andrew R. Bader

Publication: Nature Materials

Publisher: Nature Publishing Group

Date: May 18, 2015

Copyright © 2015, Rights Managed by Nature Publishing Group

LOGIN

If you're a copyright.com user, you can login to RightsLink using your copyright.com credentials. Already a **RightsLink user** or want to [learn more?](#)

Author Request

If you are the author of this content (or his/her designated agent) please read the following. If you are not the author of this content, please click the Back button and select an alternative [Requestor Type](#) to obtain a quick price or to place an order.

Ownership of copyright in the article remains with the Authors, and provided that, when reproducing the Contribution or extracts from it, the Authors acknowledge first and reference publication in the Journal, the Authors retain the following non-exclusive rights:

- a) To reproduce the Contribution in whole or in part in any printed volume (book or thesis) of which they are the author(s).
- b) They and any academic institution where they work at the time may reproduce the Contribution for the purpose of course teaching.
- c) To reuse figures or tables created by them and contained in the Contribution in other works created by them.
- d) To post a copy of the Contribution as accepted for publication after peer review (in Word or Text format) on the Author's own web site, or the Author's institutional repository, or the Author's funding body's archive, six months after publication of the printed or online edition of the Journal, provided that they also link to the Journal article on NPG's web site (eg through the DOI).

NPG encourages the self-archiving of the accepted version of your manuscript in your funding agency's or institution's repository, six months after publication. This policy complements the recently announced policies of the US National Institutes of Health, Wellcome Trust and other research funding bodies around the world. NPG recognises the efforts of funding bodies to increase access to the research they fund, and we strongly encourage authors to participate in such efforts.

Authors wishing to use the published version of their article for promotional use or on a web site must request in the normal way.

If you require further assistance please read NPG's online [author reuse guidelines](#).

For full paper portion: Authors of original research papers published by NPG are encouraged to submit the author's version of the accepted, peer-reviewed manuscript to their relevant funding body's archive, for release six months after publication. In addition, authors are encouraged to archive their version of the manuscript in their institution's repositories (as well as their personal Web sites), also six months after original publication.

v2.0

Authorization by Nature Publishing Group for authors to use published figures for thesis purposes.

8 VITA

EDUCATION:

University of Illinois at Chicago (UIC), PhD 2015

Doctor of Philosophy in Bioengineering

- Cell and Tissue Engineering

University of Illinois at Urbana-Champaign (UIUC), BS 2009

Bachelor of Science in General Engineering

- Mechanical Engineering, Component Design and Control Systems
- Secondary Field: Bioengineering
- James Scholar Honors Engineering Program

Universidad Pontificia Comillas de Madrid, Spain (UPC)

- International Minor in Engineering in Spanish Studies

Universidad Politécnica de Madrid, Spain (UPM)

- Finite element research project for matrix analysis of 3D trusses

AWARDS:

- UIC Dean's Scholar Fellow 2014
- BRG Bioencapsulation Conference Bratislava, SK Travel Grant 2014
 - Best Student Oral Contribution
- Kosciuszko Foundation Tuition Scholarship 2013, 2014

RESEARCH EXPERIENCE:

- Rodent islet transplantation (kidney capsule, intraportal, IP and IM)
- *In vitro* and *in vivo* characterization of encapsulated islet functionality
- Encapsulation apparatus use and design (air-stripping, electrostatic)
- Encapsulation technologies ((Ca²⁺)(Ca²⁺/Ba²⁺)(Ba²⁺)-alginate beads, PMCG capsule)
- GMP human islet isolation and transplantation fully qualified team member
- Diabetic and immunosuppressed NHP studies
- Rodent and NHP animal protocols
- Chemical modifications of islets and alginate microbeads

LEADERSHIP:

Encapsulation Project Manager (UIC)

- Assumed managerial responsibilities of encapsulation group once supervisor Dr. Qi took a position at City of Hope in 2013.
- Includes simultaneous management and execution of two JDRF collaborative encapsulation grants with MIT and Slovakia.
- Management of NHP work completed at UIC.

Mentoring (UIC)

- One undergraduate student
- Two high-school students

PEER REVIEWED PUBLICATIONS:

Accepted Manuscripts

1. ****Matthew A Bochenek**, Meirigeng Qi, Enza Marchese, Yong Wang, Maureen Davis, Berit L. Strand, Igor Lacik, and Jose Oberholzer. Skeletal muscle tissue as a potential transplantation site for pancreatic islets encapsulated in Ca²⁺/Ba²⁺ alginate microbeads. *Transplantation*. **Manuscript Submitted, October 2015
2. Arturo Vegas*, Omid Veisheh*, Mads Gurtler, Jeffrey Millman, Felicia Pagliuca, Andrew Bader, Joshua Doloff, Jie Li, Michael Chen, Karsten Olejnik, Hok Hei Tam, Siddharth Jhunjhunwala, Erin Langan, Stephanie Aresta-Dasilva, Srujan Gandham, James McGarrigle, **Matthew Bochenek**, Jennifer Hollister-Lock, Jose Oberholzer, Dale Greiner, Gordon Weir, Douglas Melton, Robert Langer, and Daniel Anderson. Long term Glycemic Control Using Polymer Encapsulated, Human Stem-Cell Derived β -cells in Immune Competent Rodents. *Nature Medicine*, Final Revisions, 2015
3. Arturo Vegas, Omid Veisheh, Joshua Doloff, Minglin Ma, Hok Hei Tam, Katlin Bratlie, Jie Li, Andrew Bader, Erin Langan, Karsten Olejnik, Patrick Fenton, Jeon Woong Kang, Jennifer Hollister-Locke, **Matthew Bochenek**, Alan Chiu, Sean Siebert, Katherine Tang, Siddharth Jhunjhunwala, Stephanie Aresta-Dasilva, Nimit Dholakia, Raj Thakrar, Thema Vietti, Michael Chen, Josh Cohen, Karolina Siniakowicz, Meirigeng Qi, James McGarrigle, Stephen Lyle, David Harlan, Dale Greiner, Jose Oberholzer, Gordon Weir, Robert Langer, and Daniel Anderson. Combinatorial Development of Hydrogels that Mitigate the Foreign Body Response in Primates. *Nature Biotechnology*, In Press, 2015
4. Omid Veisheh*, Joshua C. Doloff*, Minglin Ma*, Arturo J. Vegas, Hok Hei Tam, Andrew Bader, Jie Li, Erin Langan, Jeffrey Wyckoff, Whitney S. Loo, Siddharth Jhunjhunwala, Alan Chiu, Sean Siebert, Katherine Tang, Jennifer Hollister-Lock, Stephanie Aresta-Dasilva, **Matthew Bochenek**, Joshua Mendoza-Elias, Yong Wang, Merigeng Qi, Danya M. Lavin, Nimit Dholakia, Raj Thakrar, Gordon C. Weir, Jose Oberholzer, Dale L. Greiner, Robert Langer, and Daniel G. Anderson. Size- and shape-dependent foreign body immune response to materials implanted in rodents and non-human primates. *Nature Materials*, 2015 Jun;14(6):643-51

5. Meirigeng Qi, Yong Wang, Kjetil Formo, Enza Marchese, Shusen Wang, James McGarrigle, **Matthew A. Bochenek**, Katie Kinzer, Pilar V Sanchez, Maureen Davis, Sang Joon Ahn, Amelia Bartholomew, Enrico Benedetti, and Jose Oberholzer. Implementation of a Simplified Method of Islet Isolation to Facilitate Allogeneic Islet Transplantation in Cynomolgus Monkeys. *Pancreas*, 2014 Mar;43(2):226-35
6. Nourmohammadzadeh, Mohammad; Lo, Joe; **Bochenek, Matt**; Mendoza-Elias, Joshua; Wang, Qain; Li, Ze; Feng, Feng; Qi, Merigeng; Eddington, David; Oberholzer, Jose; Wang, Yong. Microfluidic Array with Integrated Oxygenation Control for Real-Time Live-Cell Imaging: Effect of Hypoxia on Physiology of Microencapsulated Pancreatic Islets. *Analytical Chemistry*, Oct. 1, 2013
7. Meirigeng Qi, Yong Wang, Enza Marchese, **Matthew A. Bochenek**, Pilar Vaca, Maureen E. Davis, Sang Joon Ahn, Alexander Schwartz, Berit Strand, Igor Lacík and José Oberholzer. Transplantation of Pancreatic Islets Immobilized in Alginate-Based Microcapsules: From Animal Studies to Clinical Trials. *Micro and Nanosystems*, 2013, 5, 186-193

Manuscripts in preparation:

1. M. Qi, E. Marchese, **M. A Bochenek**, J. McGarrigle, S J. Ahn, K. K Danielson, P. V Sanchez, M. Davis, D. Gutierrez, E. Benedetti, Y. Wang, I. lacik, B. L Strand and J. Oberholzer. Effect of Short-term Immunosuppressive Medications on the Biocompatibility of Alginate Microbeads Implanted into the Peritoneal Cavity of Cynomolgus Monkeys. In preparation, (Biomaterials).
2. Meirigeng Qi, Gabriela Kolláriková, Kjetil Formo, Enza Marchese, Yong Wang, Barbara Barbaro, **Matthew A Bochenek**, Berit L Strand, Igor Lacik, and Jose Oberholzer. Laparoscopic transplantation of allogeneic islets encapsulated in microcapsules made of sodium alginate, cellulose sulfate and poly(methylene-co-guanidine) in baboons. In preparation, (Biomaterials)

SCIENTIFIC PRESENTATIONS:

Peer Reviewed:

International Pancreas and Islet Transplantation Association (IPITA)

15th World Congress – Melbourne, Australia

**November 17, 2015

- Oral presentation, abstract # 538, “*In vivo and in vitro characterization of 1.5 mm Ba2+-alginate macro-encapsulated cynomolgus monkey islets.*”

XXII International Conference on Bioencapsulation

Bratislava, Slovakia

September 17, 2014

- Oral presentation, abstract #O2-, “*Skeletal Muscle as a Potential Transplantation Site for Microencapsulated Islets.*” *Best student oral contribution
- Poster presentation, abstract #P-27, “*Lab on a Chip for Microencapsulated Islet Assessment Under Hypoxic Conditions.*”

International Pancreas and Islet Transplantation Association (IPITA)

14th World Congress – Monterey, California

September 27, 2013

- Oral presentation, abstract # 367, “*Skeletal Muscle Tissue as a Potential Transplantation Site for Pancreatic Islets Encapsulated in Ca²⁺/Ba²⁺ Alginate Microbeads.*”
- Oral presentation, abstract #447, “*Effect of Minimal Immunomodulation on the Biocompatibility of Alginate Microbeads Implanted into the Peritoneal Cavity of Cynomolgus Monkeys.*”

Other:

Diabetes and Metabolism Research Seminar-UIC

May 1, 2014

- Oral presentation of chemical modifications of alginate for microencapsulation technologies to endocrinologists and diabetes experts.

UIC Diabetes and Obesity Research Day

October 9, 2013

- Poster presentation of intramuscular transplantation of encapsulated islets.

Diabetes and Metabolism Research Seminar-UIC

February 19, 2013

- Oral presentation on encapsulation results in NHP to endocrinologist and diabetes experts.

UIC College of Medicine Research Forum 2012

November 16, 2012

- Poster presentation of intramuscular transplantation of encapsulated islets.

Chicago Diabetes Project

September 12, 2012

- Oral presentation on encapsulation in C57 mice and intramuscular transplantation results.

Chicago Diabetes Day – University of Chicago

May 19th 2012

- Poster presentation of intramuscular transplantation of encapsulated islets.

Biologic Resources Laboratories – University of Illinois at Chicago

March 1, 2012

- Oral presentation on encapsulation in NHP to veterinary staff of animal care department.